NASA CR-136079

ANNUAL REPORT

THEORETICAL INVESTIGATIONS OF PLASMA PROCESSES

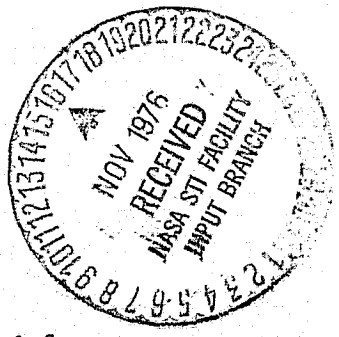

Prepared for

LEWIS RESEARCH CENTER

NATIONAL AERONAUTICS AND SPACE ADMINISTRATION

Grant NGR-06-002-147

(NASA-CR-136079) THEORETICAL INVESTIGATIONS OF PLASMA PROCESSES Annual Report, Oct. 1975 - Oct. 1976 (Colorado State Univ.) 86 p HC A05/MF A01 CSCL 20I

N77-10910

Unclas
G3/75 09004

October 1976

Department of Electrical Engineering

Colorado State University

Fort Collins, Colorado

1. Report No.	2. Government Accession No.	3. Recipient's Catalog No.
NASA CR-135079		

4. Title and Subtitle	5. Report Date
Theoretical Investigation of Plasma Processes	15 October 1976
	6. Performing Organization Code

7. Author(s)	8. Performing Organization Report No.
H. E. Wilhelm and S. H. Hong	
	10. Work Unit No.
	YOS-5260

9. Performing Organization Name and Address	11. Contract or Grant No.
Department of Electrical Engineering Colorado State University Fort Collins, CO 80523	NGR-06-002-147
	13. Type of Report and Period Covered
12. Sponsoring Agency Name and Address	1 Oct. '75 - 31 Oct. '76
National Aeronautics and Space Administration Washington, DC 20546	14. Sponsoring Agency Code

15. Supplementary Notes

Grant Manager, Maris Mantenieks
NASA Lewis Research Center
Cleveland, OH 44135

16. Abstract

System analyses are presented for electrically sustained, collision-dominated plasma centrifuges, in which the plasma rotates under the influence of the Lorentz forces resulting from the interaction of the current density fields with an external magnetic field. It is shown that gas discharge centrifuges are technically feasible in which the plasma rotates at speeds up to 10^6 cm/sec. The associated centrifugal forces produce a significant spatial isotope separation, which is somewhat perturbed in the viscous boundary layers at the centrifuge walls. The isotope separation effect is the more pronounced, the larger the Hartmann number H and Hall coefficient $\omega\tau$ are. The induced magnetic fields have negligible influence on the plasma rotation if the Hall coefficient is small, $\omega\tau << 1$. In the technical realization of collision dominated plasma centrifuges, a trade-off has to be made between power density (large particle density) and speeds of rotation (large H and/or $\omega\tau$). The diffusion of sputtered atoms to system surfaces of ion propulsion systems and the deposition of the atoms is treated theoretically by means of a simple model which permits an analytical solution. The problem leads to an inhomogeneous integral equation.

17. Key Words (Suggested by Author(s))	18. Distribution Statement
Plasma Centrifuge Analysis Isotope Separation Gas Discharge Theory Atom Deposition Analysis	Unclassified - Unlimited

19. Security Classif. (of this report)	20. Security Classif. (of this page)	21. No. of Pages	22. Price*
Unclassified	Unclassified		na

* For sale by the National Technical Information Service, Springfield, Virginia 22161

CONTENTS

INTRODUCTION

The Grant NGR-06-002-147, "Theoretical Investigations on Plasma Processes," is concerned with i) the system analysis of plasma centrifuges for isotope separation, and ii) the deposition of the sputtered atoms on system components such as the solar energy collectors of ion propulsion systems. The progress made on these subjects in the period from 9.1.75 to 11.1.76 is communicated herein.

The present report consists of three papers, two of which have been accepted for publication. By means of system analyses, it is shown that plasma centrifuges at high plasma and power densities are technically promising for isotope separation. The largest spatial isotope separation is obtained by maximizing the Hartmann number and the Hall coefficient of the isotope mixture plasma of the centrifuge discharge. Furthermore, it is shown that induced magnetic fields have no effect for small Hall-coefficients and little effect for large Hall-coefficients on the plasma rotation and the isotope separation efficiency. A new approach to the deposition problem of sputtered atoms is given. Its solution leads to a simpler, but still mathematically difficult integral equation.

BOUNDARY-VALUE PROBLEM FOR PLASMA CENTRIFUGE AT ARBITRARY MAGNETIC REYNOLDS NUMBERS*)

H. E. Wilhelm and S. H. Hong

Department of Electrical Engineering
Colorado State University
Fort Collins, CO 80523

ABSTRACT

The boundary-value problem for the partial differential equations, which describe the (azimuthal) rotation velocity and induced magnetic fields in a cylindrical plasma centrifuge with ring electrodes of different radii and an external, axial magnetic field, is solved in closed form. The electric field, current density, and velocity distributions are discussed in terms of the Hartmann number H and the magnetic Reynolds number R. For small Hall-coefficients, $\omega\tau << 1$, the induced magnetic field does not affect the plasma rotation. As a result of the Lorentz forces, the plasma rotates with speeds as high as 10^5 cm/sec around its axis of symmetry at typical conditions, so that the lighter (heavier) ion and atom components are enriched at (off) the center of the discharge cylinder.

*) Supported in part by NASA.

On principle, electromagnetic forces allow to rotate plasmas up to relativistic speeds. Theta pinch experiments show that the plasma rotates during the discharge pulse at such high speeds that the energy distribution of the emitted neutrons is shifted.[1] From the theoretical point of view, the basic mechanism for plasma rotation by means of crossed electric and magnetic fields and Lorentz forces in rarefied[1-15] and dense[16-17] plasmas is understood qualitatively. Experimental evidence on isotope separation in rotating plasmas has been reported among others by Bonnevier,[10-11] Guilloud,[20] Heller and Simon,[21] James and Simpson,[22] and Ban and Sekiguchi[23-24]. Exact solutions for the boundary-value problems describing plasma centrifuge systems are not known, neither for collision-dominated[25-26] nor for collisionless[2-4] plasmas.

A simple model for an electrical discharge centrifuge with an axial, external magnetic field $\vec{B}_o$ is shown in Fig. 1. This plasma centrifuge employs electrodes of different radii R_+ and R_- ($R_+ >> R_-$) in the end plates $z = \pm c$ of an electrically isolating discharge chamber of radius R_o so that the field lines of the current density $\vec{j}$ and of the external axial magnetic field $\vec{B}_o$ cross under a nonvanishing angle (except at the chamber axis). The resultant Lorentz force $\vec{j} \times \vec{B}_o$ rotates the discharge around its axis of symmetry. In steady state, the magnetic body forces in the azimuthal direction are balanced by the viscous forces (boundary layers at the chamber walls). As opposed to the centrifuge with radial electric current flow between an inner and outer cylinder electrode, the centrifuge scheme in Fig. 1 avoids the boundary layer

and losses at the inner cylinder surface. In the following, the boundary-value problem for this centrifuge is solved in closed form based on the magnetogasdynamic equations for dense isotope plasmas with negligible Hall effect.

THEORETICAL FORMULATION

For a purely azimuthal flow field, $\vec{v} = \{0, v(r,z), 0\}$, the plasma behaves incompressible, $\nabla \cdot \vec{v} = 0$. From the continuity equation, $\nabla \cdot (\rho\vec{v}) = \vec{v} \cdot \nabla\rho = 0$, it follows then that the density gradient $\nabla\rho$ is everywhere perpendicular to the flow field $\vec{v}$. In accordance with the magnetogasdynamic equations,[27] Maxwells equations and Ohms' law[27] [which imply $\nabla^2\vec{B} = -\mu_o\sigma\nabla\times(\vec{v}\times\vec{B})$], the plasma in the centrifuge with homogeneous magnetic field $\vec{B}_o$ (Fig. 1) is described by the boundary-value problem for the azimuthal velocity $V_\theta(r,z)$ and azimuthal induction $B_\theta(r,z)$ fields (r,θ,z = cylindrical coordinates):

$$\frac{1}{r}\frac{\partial}{\partial r}\left(r\frac{\partial V_\theta}{\partial r}\right) - \frac{V_\theta}{r^2} + \frac{\partial^2 V_\theta}{\partial z^2} = -\frac{B_o}{\mu\mu_o}\frac{\partial B_\theta}{\partial z} \quad , \qquad (1)$$

$$\frac{1}{r}\frac{\partial}{\partial r}\left(r\frac{\partial B_\theta}{\partial r}\right) - \frac{B_\theta}{r^2} + \frac{\partial^2 B_\theta}{\partial z^2} = -\mu_o\sigma B_o\frac{\partial V_\theta}{\partial z} \quad , \qquad (2)$$

where

$$V_\theta(r,z)_{r=R_o} = 0, \quad -c \le z \le +c \quad , \qquad (3)$$

$$V_\theta(r,z)_{z=\pm c} = 0, \quad 0 \le r \le R_o \quad , \qquad (4)$$

and

$$B_\theta(r,z)_{r=R_o} = \frac{\mu_o I}{2\pi R_o} \quad , \quad -c \le z \le +c \quad , \qquad (5)$$

$$\frac{1}{r}\frac{\partial}{\partial r}\left[rB_\theta(r,z)\right]_{z=\pm c} = \frac{\mu_o I}{2\pi}\frac{\delta(r-R_\pm)}{r} \quad , \quad 0 \le r \le R_o \quad . \qquad (6)$$

Eqs. (1) and (2) are the azimuthal components of the equations of plasma motion and magnetic induction, respectively (μ = viscosity, μ_o = magnetic permeability, σ = electrical conductivity). The

boundary conditions (3) and (4) consider that the plasma does not slip at the walls $r = R_o$ and $z = \pm c$. The boundary conditions (5) and (6) follow from Maxwell's equations for a total discharge current of $|I|$ amps flowing from the ring "anode" ($r=R_+$) to the ring "cathode" ($r=R_-$) of vanishing radial width [$\delta(r-R_\pm)$ = Dirac function] if $I < 0$ (Fig. 1). According to Eq. (6), the net current sustaining the discharge is $2\pi\int_0^{R_o} j_z(r,z=\pm c)\, r dr = I\int_0^{R_o} \delta(r-R_\pm)dr = I$. The pressure distribution $p=p(r,z)$ in the rotating plasma is determined by the r- and z-components of the equation of motion,

$$-\rho_p \frac{V_\theta^2}{r} = -\frac{\partial p}{\partial r} - j_z B_\theta, \quad 0 = -\frac{\partial p}{\partial z} + j_r B_\theta \quad , \qquad (7\text{-}8)$$

where

$$\frac{1}{r}\frac{\partial}{\partial r}(rB_\theta) = \mu_o j_z, \quad -\frac{\partial B_\theta}{\partial z} = \mu_o j_r \quad , \qquad (9\text{-}10)$$

in accordance with Maxwell's equations. In absence of the Hall effect, $\omega\tau<<1$, it is $\nabla\times\vec{B} = \mu_o(j_r, 0, j_z)$. Hence, $B_r = 0$ and $B_z = 0$ because of the homogeneity of the boundary conditions for B_r and B_z, whereas $B_\theta \neq 0$ since $j_{r,z} \neq 0[B_\theta(r,z = \pm c) = (\mu_o I/2\pi r)H(r-R_\pm)]$. Since the induced magnetic field is azimuthal, $\vec{B} = \{0, B_\theta, B_o\}$, the induced electric field is independent of B_θ, i.e. $\vec{V}\times\vec{B} = V_\theta B_o \vec{e}_r$.

NONDIMENSIONAL BOUNDARY-VALUE PROBLEM

The characteristic nondimensional parameters of the magnetogas-dynamic centrifuge under consideration are obtained by introducing the nondimensional independent and dependent variables,

$$\rho = r/R_o \ , \ 0 \leq \rho \leq 1 \quad , \tag{11}$$

$$\zeta = z/c \ , \ -1 \leq \zeta \leq +1 \quad , \tag{12}$$

and

$$V(\rho,\zeta) = V_\theta(r,z)/V_o, \ B(\rho,\zeta) = B_\theta(r,z)/B_o \quad , \tag{13}$$

where

$$V_o \equiv I/2\pi R_o B_o \sigma c, \quad B_o \equiv B_o \quad . \tag{14}$$

In terms of the nondimensional space variables and fields, the boundary-value problem defined in Eqs. (1) - (6) assumes for $V(\rho,\zeta)$ and $B(\rho,\zeta)$ the form:

$$\frac{1}{\rho}\frac{\partial}{\partial\rho}\left(\rho\frac{\partial V}{\partial\rho}\right) - \frac{V}{\rho^2} + N^{-2}\frac{\partial^2 V}{\partial\zeta^2} = -\frac{H^2}{R}\frac{\partial B}{\partial\zeta} \quad , \tag{15}$$

$$\frac{1}{\rho}\frac{\partial}{\partial\rho}\left(\rho\frac{\partial B}{\partial\rho}\right) - \frac{B}{\rho^2} + N^{-2}\frac{\partial^2 B}{\partial\zeta^2} = -\frac{R}{N^2}\frac{\partial V}{\partial\zeta} \quad , \tag{16}$$

where

$$V(\rho,\zeta)_{\rho=1} = 0, \qquad -1 \leq \zeta \leq +1 \quad , \tag{17}$$

$$V(\rho,\zeta)_{\zeta=\pm1} = 0, \qquad 0 \leq \rho \leq 1 \quad , \tag{18}$$

and

$$B(\rho,\zeta)_{\rho=1} = R, \qquad -1 \leq \zeta \leq +1 \quad , \tag{19}$$

$$\frac{1}{\rho}\frac{\partial}{\partial\rho}\left[\rho B(\rho,\zeta)\right]_{\zeta=\pm1} = R\,\delta(\rho-\rho_\pm)/\rho, \quad 0 \leq \rho \leq 1, \tag{20}$$

with

$$H \equiv (\sigma/\mu)^{\frac{1}{2}} B_o R_o, \quad N \equiv c/R_o, \quad R \equiv \mu_o I/2\pi R_o B_o \equiv \mu_o \sigma V_o c \gtrless 0. \tag{21}$$

The Hartmann number H, N, and the magnetic Reynolds number R characterize the ratio of Lorentz to viscous forces, the geometry of the centrifuge, and the intensity ratio of the induced and external magnetic fields, respectively.

The linear statement,

$$B(\rho,\zeta) = R\rho + \Psi(\rho,\zeta) \quad , \tag{22}$$

reduces the Eqs. (16), (19), and (20) for $B(\rho,\zeta)$ to equations with a homogeneous boundary condition (24) for $\Psi(\rho,\zeta)$:

$$\frac{1}{\rho}\frac{\partial}{\partial\rho}\left(\rho\frac{\partial\Psi}{\partial\rho}\right) - \frac{\Psi}{\rho^2} + N^{-2}\frac{\partial^2\Psi}{\partial\zeta^2} = -\frac{R}{N^2}\frac{\partial V}{\partial\zeta} \quad , \tag{23}$$

where

$$\Psi(\rho,\zeta)_{\rho=1} = 0, \qquad -1 \leq \zeta \leq +1 \quad , \tag{24}$$

$$\frac{1}{\rho}\frac{\partial}{\partial\rho}[\rho\Psi(\rho,\zeta)]_{\zeta=\pm1} = R\left[\frac{\delta(\rho-\rho_{\pm})}{\rho} - 2\right], \quad 0 \leq \rho \leq 1 \quad . \tag{25}$$

In view of Bessel's differential equation, $Z_m'' + \rho^{-1}Z_m' + (k_n^2 - \rho^{-2}m^2)Z_m = 0$, for cylinder functions $Z_m(k_n\rho)$, partial solutions of the coupled inhomogeneous Eqs. (15) and (23) are sought in the form,

$$V_n(\rho,\zeta) = J_1(k_n\rho)\, f_n(\zeta) \quad , \tag{26}$$

$$\Psi_n(\rho,\zeta) = J_1(k_n\rho)\, g_n(\zeta) \quad , \tag{27}$$

where the eigen-values $k_n > 0$ are determined by the homogeneous boundary conditions (17) and (24) as the real roots of the transcendental equation,

$$J_1(k_n) = 0 \ , \ n = 1,2,3,.... \quad . \tag{28}$$

Thus, the general solution of the coupled Eqs. (15) and (23) obtains by linear superposition as the Fourier-Bessel series:[28]

$$V(\rho,\zeta) = \sum_{n=1}^{\infty} J_1(k_n\rho)\, f_n(\zeta) \quad , \tag{29}$$

$$\Psi(\rho,\zeta) = \sum_{n=1}^{\infty} J_1(k_n\rho)\, g_n(\zeta) \quad . \tag{30}$$

Substitution of Eqs. (26) - (27) into Eqs. (15) and (23) yields ordinary coupled differential equations of second order for $f_n(\zeta)$ and $g_n(\zeta)$:

$$f_n'' - k_n^2 N^2 f_n = -H^2 N^2 R^{-1} g_n' \quad , \tag{31}$$

$$g_n'' - k_n^2 N^2 g_n = -R f_n' \quad . \tag{32}$$

By elimination, Eqs. (31) - (32) are reduced to decoupled differentail equations of fourth order,

$$f_n'''' - (2k_n^2 + H^2) N^2 f_n'' + k_n^4 N^4 f_n = 0 \quad , \tag{33}$$

$$g_n'''' - (2k_n^2 + H^2) N^2 g_n'' + k_n^4 N^4 g_n = 0 \quad , \tag{34}$$

with

$$f_n(\zeta)_{\zeta=\pm 1} = 0 \quad , \tag{35}$$

$$g_n(\zeta)_{\zeta=\pm 1} = 2Rk_n^{-1} J_o(k_n\rho_\pm)/J_o^2(k_n) \quad , \tag{36}$$

as boundary conditions, by Eqs. (18) and (25), respectively. In deriving Eq. (36), the Dirac function in Eq. (25) has been expanded in the Fourier-Dini series,[28]

$$\delta(\rho - \rho_\pm)/\rho = 2 + 2 \sum_{n=1}^{\infty} [J_o(k_n\rho_\pm)/J_o^2(k_n)] J_o(k_n\rho) \quad . \tag{37}$$

In addition to Eqs. (35) - (36), $f_n(\zeta)$ and $g_n(\zeta)$ have to satisfy also the coupled Eqs. (31) - (32). With the four real roots of Eqs. (33) - (34) [f_n, $g_n \propto \exp(\omega\zeta)$],

$$\omega_{1n} = \omega_n^+ \ , \ \omega_{2n} = \omega_n^- , \omega_{3n} = -\omega_n^+ \ , \ \omega_{4n} = -\omega_n^- \qquad , \tag{38}$$

where

$$\omega_n^{\pm} \equiv 2^{-\frac{1}{2}} N\{(2k_n^2 + H^2) \pm [(2k_n^2 + H^2)^2 - 4k_n^4]^{\frac{1}{2}}\}^{\frac{1}{2}} \qquad , \tag{39}$$

the general solutions for $f_n(\zeta)$ and $g_n(\zeta)$ of Eqs. (33) - (34) can be written as:

$$f_n(\zeta) = A_n^+ \frac{\sinh \omega_n^+ \zeta}{\sinh \omega_n^+} + B_n^+ \frac{\cosh \omega_n^+ \zeta}{\cosh \omega_n^+} + A_n^- \frac{\sinh \omega_n^- \zeta}{\sinh \omega_n^-} + B_n^- \frac{\cosh \omega_n^- \zeta}{\cosh \omega_n^-} \qquad , \tag{40}$$

$$g_n(\zeta) = C_n^+ \frac{\sinh \omega_n^+ \zeta}{\sinh \omega_n^+} + D_n^+ \frac{\cosh \omega_n^+ \zeta}{\cosh \omega_n^+} + C_n^- \frac{\sinh \omega_n^- \zeta}{\sinh \omega_n^-} + D_n^- \frac{\cosh \omega_n^- \zeta}{\cosh \omega_n^-} \qquad . \tag{41}$$

Only four of the eight integration constants $A_n^{\pm}$, ... $D_n^{\pm}$ are independent. Substitution of Eqs. (40) - (41) into Eq. (31) and Eq. (32) yields

$$A_n^{\pm} [(\omega_n^{\pm})^2 - k_n^2 N^2]/\omega_n^{\pm} = -H^2 N^2 R^{-1} \ \mathrm{tgh}\omega_n^{\pm} \cdot D_n^{\pm} \qquad , \tag{42}$$

$$B_n^{\pm} [(\omega_n^{\pm})^2 - k_n^2 N^2]/\omega_n^{\pm} = -H^2 N^2 R^{-1} \ \mathrm{cth} \ \omega_n^{\pm} \cdot C_n^{\pm} \qquad , \tag{43}$$

and

$$C_n^{\pm} [(\omega_n^{\pm})^2 - k_n^2 N^2]/\omega_n^{\pm} = - R \ \mathrm{tgh} \ \omega_n^{\pm} \cdot B_n^{\pm} \qquad , \tag{44}$$

$$D_n^{\pm} [(\omega_n^{\pm})^2 - k_n^2 N^2]/\omega_n^{\pm} = - R \ \mathrm{cth} \ \omega_n^{\pm} \cdot A_n^{\pm} \qquad , \tag{45}$$

respectively. The coefficient determinant of Eqs. (42) and (45) or Eqs. (43) and (44) vanishes (condition for existence of nontrivial solution),

$$\Delta^{\pm} \equiv [(\omega_n^{\pm})^2 - k_n^2 N^2]^2 - H^2 N^2 (\omega_n^{\pm})^2 = 0 \qquad , \tag{46}$$

in agreement with Eq. (39). From the latter or Eq. (46) one deduces the relations,

$$[(\omega_n^{\pm})^2 - k_n^2 N^2]/\omega_n^{\pm} = \pm NH \quad , \tag{47}$$

which simplify the left sides of Eqs. (42) - (45).

Application of the boundary conditions (35) to Eq. (40) shows that

$$-A_n^- = +A_n^+ \equiv A_n \quad , \quad -B_n^- = +B_n^+ \equiv B_n \quad . \tag{48}$$

Substitution of Eq. (48) into Eqs. (40) and (41) gives

$$f_n(\zeta) = A_n\left[\frac{\sinh \omega_n^+ \zeta}{\sinh \omega_n^+} - \frac{\sinh \omega_n^- \zeta}{\sinh \omega_n^-}\right] + B_n\left[\frac{\cosh \omega_n^+ \zeta}{\cosh \omega_n^+} - \frac{\cosh \omega_n^- \zeta}{\cosh \omega_n^-}\right] \quad , \tag{49}$$

and

$$g_n(\zeta) = -A_n \frac{R}{NH}\left[\frac{\cosh \omega_n^+ \zeta}{\sinh \omega_n^+} + \frac{\cosh \omega_n^- \zeta}{\sinh \omega_n^-}\right] - B_n \frac{R}{NH}\left[\frac{\sinh \omega_n^+ \zeta}{\cosh \omega_n^+} + \frac{\sinh \omega_n^- \zeta}{\cosh \omega_n^-}\right] \quad , \tag{50}$$

the latter under consideration of Eqs. (44) - (45) and Eq. (47). Application of the boundary conditions (36) to Eq. (50) yields, upon elimination,

$$A_n = -\frac{NH}{k_n} \frac{J_o(k_n \rho_-) + J_o(k_n \rho_+)}{(\operatorname{cth} \omega_n^+ + \operatorname{cth} \omega_n^-)\, J_o^2(k_n)} \quad , \tag{51}$$

$$B_n = +\frac{NH}{k_n} \frac{J_o(k_n \rho_-) - J_o(k_n \rho_+)}{(\operatorname{tgh} \omega_n^+ + \operatorname{tgh} \omega_n^-)\, J_o^2(k_n)} \quad . \tag{52}$$

By combining Eqs. (49) - (52), we obtain the solutions for $f_n(\zeta)$ and $g_n(\zeta)$ in final form:

$$f_n(\zeta)/NH = - \frac{J_o(k_n\rho_-) + J_o(k_n\rho_+)}{(\text{cth}\ \omega_n^+ + \text{cth}\ \omega_n^-)k_n\ J_o^2(k_n)} \left[\frac{\sinh\ \omega_n^+\zeta}{\sinh\ \omega_n^+} - \frac{\sinh\ \omega_n^-\zeta}{\sinh\ \omega_n^-}\right]$$

$$+ \frac{J_o(k_n\rho_-) - J_o(k_n\rho_+)}{(\text{tgh}\ \omega_n^+ + \text{tgh}\ \omega_n^-)k_n\ J_o^2(k_n)} \left[\frac{\cosh\ \omega_n^+\zeta}{\cosh\ \omega_n^+} - \frac{\cosh\ \omega_n^-\zeta}{\cosh\ \omega_n^-}\right] \quad , \tag{53}$$

and

$$g_n(\zeta)/R = + \frac{J_o(k_n\rho_-) + J_o(k_n\rho_+)}{(\text{cth}\ \omega_n^+ + \text{cth}\ \omega_n^-)k_n\ J_o^2(k_n)} \left[\frac{\cosh\ \omega_n^+\zeta}{\sinh\ \omega_n^+} + \frac{\cosh\ \omega_n^-\zeta}{\sinh\ \omega_n^-}\right]$$

$$- \frac{J_o(k_n\rho_-) - J_o(k_n\rho_+)}{(\text{tgh}\ \omega_n^+ + \text{tgh}\ \omega_n^-)k_n\ J_o^2(k_n)} \left[\frac{\sinh\ \omega_n^+\zeta}{\cosh\ \omega_n^+} + \frac{\sinh\ \omega_n^-\zeta}{\cosh\ \omega_n^-}\right] \quad . \tag{54}$$

Below, also the ζ-derivative of $g_n(\zeta)$ is required, which is given by

$$g_n'(\zeta)/R = + \frac{J_o(k_n\rho_-) + J_o(k_n\rho_+)}{(\text{cth}\ \omega_n^+ + \text{cth}\ \omega_n^-)k_n\ J_o^2(k_n)} \left[\omega_n^+ \frac{\sinh\ \omega_n^+\zeta}{\sinh\ \omega_n^+} + \omega_n^- \frac{\sinh\ \omega_n^-\zeta}{\sinh\ \omega_n^-}\right]$$

$$- \frac{J_o(K_n\rho_-) - J_o(k_n\rho_+)}{(\text{tgh}\ \omega_n^+ + \text{tgh}\ \omega_n^-)k_n\ J_o^2(k_n)} \left[\omega_n^+ \frac{\cosh\ \omega_n^+\zeta}{\cosh\ \omega_n^+} + \omega_n^- \frac{\cosh\ \omega_n^-\zeta}{\cosh\ \omega_n^-}\right] \quad . \tag{55}$$

In terms of $f_n(\zeta)$, $g_n(\zeta)$, and $g_n'(\zeta)$, the solutions for the non-dimensional fields $\vec{V} = \{0,V,0\}$, $\vec{B} = \{0,B,1\}$, $\vec{J} = \{J_\rho,0,J_\zeta\}$ and $\vec{E} = \{E_\rho,0,E_\zeta\}$ of the plasma centrifuge are by Eqs. (22), and (29) - (30):

$$V(\rho,\zeta) = \sum_{n=1}^{\infty} J_1(k_n\rho) f_n(\zeta) \quad , \tag{56}$$

$$B(\rho,\zeta) = R\rho + \sum_{n=1}^{\infty} J_1(k_n\rho) g_n(\zeta) \quad , \tag{57}$$

$$J_\rho(\rho,\zeta) = - R^{-1}N^{-1} \sum_{n=1}^{\infty} J_1(k_n\rho) g_n'(\zeta) \quad , \tag{58}$$

$$J_\zeta(\rho,\zeta) = 2 + R^{-1} \sum_{n=1}^{\infty} k_n\ J_o(k_n\rho) g_n(\zeta) \quad , \tag{59}$$

and

$$E_\rho(\rho,\zeta) = - V(\rho,\zeta) + N\, J_\rho(\rho,\zeta), \quad E_\zeta(\rho,\zeta) = N J_\zeta(\rho,\zeta) \quad . \tag{60}$$

The reference values V_o and B_o for $V(\rho,\zeta)$ and $B(\rho,\zeta)$ are defined in Eq. (14). The non-dimensional fields $J_{\rho,\zeta}(\rho,\zeta)$ and $E_{\rho,\zeta}(\rho,\zeta)$ are normalized with respect to

$$j_o = I/2\pi R_o^2, \quad E_o \equiv V_o B_o = I/2\pi R_o \sigma c \quad . \tag{61}$$

If the cathode is in the plane $z = -c(\zeta = -1)$ and the anode is in the plane $z = +c(\zeta = +1)$, then the reference fields V_o, j_o, and E_o [Eqs. (14), (61)] are negative, since $I < 0$. The results are also applicable to the case where the anode is in the plane $z = -c(\zeta = -1)$ and the cathode is in the plane $z = +c(\zeta = +1)$. In the latter situation, the reference fields V_o, j_o, and E_o [Eqs. (14), (61)] are positive, since $I > 0$. These explanations hold for magnetic fields pointing in the positive z- direction, $B_o > 0$; V_o changes its sign with the sign of B_o [Eq. (14)]. Note that the magnetic Reynolds number R in Eq. (21) is defined to change its sign with the sign of V_o.

APPLICATIONS

As an illustration, the radial (ρ) dependence of the nondimensional discharge fields $V(\rho,\zeta)$, $B(\rho,\zeta)$, $E_\rho(\rho,\zeta)$, $J_\rho(\rho,\zeta)$, and $J_\zeta(\rho,\zeta)$ has been computed for $I < 0$ in the cross-sectional planes $\zeta = -0.99$ (cathode region), $\zeta = 0$ (central region), and $\zeta = +0.99$ (anode region) based on Eqs. (56)-(60). The remaining field $E_\zeta(\rho,\zeta)$ is proportional to $J_\zeta(\rho,\zeta)$ [Eq. (60)]. The characteristic (nondimensional) magnetic interaction number H is treated as a parameter: H = 1, 10, 100. The geometry parameter $N = c/R_o$ is taken to be N = 1 corresponding to $R_o = c$ [Eq. (21)]. The radial positions of the cathode and anode are assumed to be:

$$\rho_- = 0.01 \ (R_- = 0.01\ R_o) \ ; \ \rho_+ = 0.9 \ (R_+ = 0.9\ R_o).$$

With the exception of $B_\theta = B_o B$, the dimensional fields are negative everywhere where the nondimensional fields are positive, and vice-versa since $V_o < 0$, $j_o < 0$ and $E_o < 0$ for $I < 0$ [Eqs. (14),(61)].

The Eqs. (56)-(60) indicate that the velocity field $V(\rho,\zeta)$, the current density field $J_{\rho,\zeta}(\rho,\zeta)$, and the electric field $E_{\rho,\zeta}(\rho,\zeta)$ are independent of the magnetic Reynolds number R, whereas the induced magnetic field $B(\rho,\zeta)$ is proportional to R. This is due to the azimuthal direction of the induced magnetic field $B(\rho,\zeta)$, which is parallel to the velocity field $V(\rho,\zeta)$ of rotation [Eqs. (9)-(10)]. Accordingly, the plasma fields $V(\rho,\zeta)$, $B(\rho,\zeta)/R$, $J_{\rho,\zeta}(\rho,\zeta)$, and $E_{\rho,\zeta}(\rho,\zeta)$ depend only on the Hartmann number H, presumed that the Hall effect is negligible ($\omega \equiv |e\vec{B}|/m$ and τ are the gyration frequency and collision frequency of the electrons),

$$\omega\tau << 1$$

Central Region, $\zeta = 0$. In Figs. 2-6, $V(\rho,0)$, $[B(\rho,0) - R\rho]/R$, $E_\rho(\rho,0)$, $J_\rho(\rho,0)$, and $J_\zeta(\rho,0) \propto E_\zeta(\rho,0)$ are shown versus $0 \leq \rho \leq 1$ with H = 1, 10, 100 as a parameter. It is seen that $|V|$ increases considerably at any point $0 < \rho < 1$ as H is increased. Similarly, $(B - R\rho)/R$ and the sources $J_{\rho,\zeta}$ of the magnetic induction increase in intensity within the main central region $0 < \rho < 1 - \Delta\rho$ as H is increased. For large values $H \gtrsim 10$, B and $J_{\rho,\zeta}$ decrease in the wall region $\Delta\rho = \Delta\rho(H)$, so that the electrical discharge becomes more concentrated in the center $0 < \rho < 1 - \Delta\rho$ of the centrifuge. The intensity of E_ρ increases uniformly in the region $0 < \rho < 1$ as H is increased, while $E_\zeta \propto J_\zeta$.

Cathode Region, $\zeta = -0.99$: The Figs. 7-11 show $V(\rho,-0.99)$, $[B(\rho,-0.99) - R\rho]/R$, $E_\rho(\rho,-0.99)$, $J_\rho(\rho,-0.99)$, and $J_\zeta(\rho,-0.99) \propto E_\zeta(\rho,-0.99)$ versus $0 \leq \rho \leq 1$ for H = 1, 10, 100. The fields V, $E_{\rho,\zeta}$, and $J_{\rho,\zeta}$ increase in intensity at any point $0 < \rho < 1$ with increasing H, whereas B/R decreases in $0 < \rho < 1$ with increasing H. Since the ring cathode is at $\rho_- = 0.01$ ($\zeta = -1$), the field distributions are closer concentrated at the axis $\rho \tilde{=} 0$ than those in the plane $\zeta = 0$ (Figs. 2-6). Note that the plasma rotates only in the region $\rho \tilde{=} 0.1$ with a significant velocity, since the Lorentz force $-j_r B_o$ decreases rapidly with increasing $\rho \to 1$.

Anode Region, $\zeta = +0.99$: The Figs. 12-16 present $V(\rho,+0.99)$, $[B(\rho,+0.99) - R\rho]/R$, $E_\rho(\rho,+0.99)$, $J_\rho(\rho,+0.99)$, $J_\zeta(\rho,+0.99) \propto E_\zeta(\rho,+0.99)$ versus $0 \leq \rho \leq 1$ for H = 1, 10, 100. The velocity field is fully developed nearly through the entire centrifuge across section $0 < \rho \lesssim 0.9$, since the Lorentz force $-j_r B_o$ is strongest in the vicinity $\rho \tilde{=} 0.9$ of the ring anode $\rho = 0.9(\zeta = +1)$. As a result, a thin and steep boundary

layer exists close to the cylinder wall ($\rho = 1$) with plasma counter-rotation at sufficiently small H-values. The radial distributions of B, $E_{\rho,\zeta}$, $J_{\rho,\zeta}$ clearly indicate that, in the plane $\zeta = +0.99$, the electrical discharge has shifted to the region $\rho \tilde{=} 0.9$ due to the influence of the (nearby) ring anode at $\rho = 0.9(\zeta = +1)$.

In the graphical illustrations, the cathode radius R_- was chosen to be small compared to the anode radius R_+ to ensure a large angle between the current field lines $\vec{j}(\vec{r})$ and the external magnetic field $\vec{B}_o$, i.e. a significant Lorentz force. A comparison of the Figs. 2 and 7 with Fig. 12 indicates that this choice of electrode radii results in a radial boundary layer of large width and low velocity in the lower half $-c \leq z \leq 0$ of the centrifuge. Hence, $R_- << R_+$ (or $R_- >> R_+$) is not the best choice for a centrifuge of maximum efficiency. Fig. 12 demonstrates that a velocity profile raising uniformly with radius r and decreasing rapidly in a steep boundary layer of narrow width Δr, is obtained by using a cathode and an anode of the same radius $R_- = R_+ \tilde{<} R_o$, which is nearly as large as the centrifuge radius R_o. Although it is $R_- = R_+$ in this case, the current field lines $\vec{j}(\vec{r})$ intersect with $\vec{B}_o$ under a sufficiently large angle $\sphericalangle(\vec{j},\vec{B}_o) \neq 0$ due to the repulsion of the current filaments. As a result, a net Lorentz torque results for a centrifuge with $R_- = R_+$ which is still of the same order of magnitude as for a centrifuge with $R_- << R_+$ (presumed that I, and B_o, c, and R_o are the same).

The accuracy of the Figs. 2-16 is determined by the number of terms considered in the Fourier series on the computer and the accuracy of the eigenvalues k_n. The Fourier series solutions were summed numerically up to n = 100, and the eigenvalues k_n, n = 1,2,3,...100, were computed up to the 10th decimal point.

The centrifuge analysis presented indicates that extremely high speeds of plasma rotation are obtainable already at moderate discharge currents I and magnetic inductions B_o, presumed the Hartmann number H is not small, $H > 1$. As an example, consider a centrifuge discharge with:

$$|I| = 10^2 \text{ amp} \quad , \quad |B_o| = 10^0 \text{ Tesla},$$

$$\sigma = 10^2 \text{ mho m}^{-1}, \; R_o = c = 10^{-1}\text{m}.$$

Hence, by Eq. (14)

$$V_o = I/2\pi R_o B_o \sigma c = (5/\pi) \times 10^1 \text{ m sec}^{-1},$$

and, by Fig. 2,

$$O[V_\theta] = O[V_o V] = 10^3 \text{ m sec}^{-1}, \text{ for } H = 100.$$

If the working gas of the centrifuge discharge consists of two isotope gases, then the centrifugal forces would concentrate the lighter isotope ions and atoms in the central region and enrich the heavier isotope atoms and ions in the peripheral region of the discharge. According to the equations of motion for two isotopes of masses m_i and m_j, the isotope density ratio at distances $0 < r < R_o - \Delta r$, where Δr is the viscous boundary layer thickness, is approximately (T_o = temperature of the isotope ions)

$$\frac{\bar{n}_i(r)}{\bar{n}_j(r)} \simeq \frac{\bar{n}_i(0)}{\bar{n}_j(0)} e^{+\frac{1}{2}\Delta m_{ij} \bar{v}(r)^2/kT_o}, \quad \Delta m_{ij} = m_i - m_j \quad ,$$

where the bar designates a spatial average over the region $|z| < c$. As a specific example, consider an uranium plasma centrifuge containing the isotope ions (i) U^{237} and (j) U^{235} at a temperature $T_o = 10^3$ °K (and electrons at a temperature $T_e > T_o$). In this case, one has $\Delta m_{ij} = m(237) - m(235) = 3.320 \times 10^{-27}$kg, $kT = 1.381 \times 10^{-20}$ Joule. Hence,

the isotope separation ratio is:

$$\frac{\bar{n}_{237}(r)}{\bar{n}_{235}(r)} \Big/ \frac{\bar{n}_{237}(0)}{\bar{n}_{235}(0)} \tilde{=} 1.128 \times 10^{0} \text{ for } \bar{v}(r) = 1 \times 10^{3} \text{ m sec}^{-1} ,$$

$$\tilde{=} 1.617 \times 10^{0} \text{ for } \bar{v}(r) = 2 \times 10^{3} \text{ m sec}^{-1} ,$$

$$\tilde{=} 2.950 \times 10^{0} \text{ for } \bar{v}(r) = 3 \times 10^{3} \text{ m sec}^{-1} .$$

Based on these examples, one can assume with some confidence that high-power plasma centrifuges are technically realizable employing dense, collision-dominated isotope plasmas. The separation of isotopes by centrifugal forces in low density plasmas has been established experimentally.[10-11,20-24.]

References

1. G. Lehner, Reactions under Plasma Conditions, Ed. M. Venugopalan (Wiley-Interscience, New York, 1971).
2. N. N. Komarov and V. M. Fodeev, Sov. Phys. JETP 14, 378 (1962).
3. M. V. Samakhin, Doklady Akad. Nauk SSSR, Fizika, 155, 72 (1964).
4. E. M. Dobryshevskii, Sov. Phys. Techn. Phys. 8, 903 (1964).
5. B. Bonnevier and B. Lehnert, Ark. Fysik 16, 231, (1959).
6. J. Bergstroem, S. Holmberg, and B. Lehnert, Ark. Fysik 23, 543 (1962).
7. J. Bergstroem, S. Holmberg, and B. Lehnert, Ark. Fysik 25, 49 (1963).
8. B. Lehnert, Ark. Fysik 28, 205, (1964).
9. B. Lehnert, Y. Bergstroem, and S. Holmberg, Nuclear Fusion 6, 231 (1966).
10. B. Bonnevier, Ark. Fysik 33, 255 (1966).
11. B. Bonnevier, Plasma Phys. 13, 763 (1970).
12. B. Lehnert, Physica Scripta 2, 106 (1970).
13. B. Lehnert, Nuclear Fusion 11, 485 (1971).
14. B. Lehnert, Physica Scripta 7, 102 (1973).
15. B. Lehnert, Physica Scripta 9, 229 (1974).
16. E. A. Witalis, Plasma Phys. 10, 747. (1968).
17. E. A. Witalis, Z. Naturforschg, 29a, 1138 (1974).
18. H. Mahn, H. Ringler, and G. Zankel, Z. Naturforschg, 23a, 868 (1968).
19. R. Schwenn, Z. Naturforschg, 25a, 1601 (1970).
20. J. C. Guilloud, Entropie 34, 23 (1970).
21. H. Heller and M. Simon, Phys. Letters 50A, 139 (1974).
22. B. N. James and S. W. Simpson, Physics Letters 64A, 347 (1974).
23. T. Ban and T. Sekiguchi, Japan J. Appl. Phys. 14, 1411 (1975).
24. T. Ban and T. Sekiguchi, Japan J. Appl. Phys. 15, 115 (1976).

25. C. C. Chang and T. S. Lundgren, Phys. Fluids 2, 627 (1959).

26. O. Okada and T. Dodo, J. Nucl. Sci. Technol. 10, 626 (1973).

27. L. E. Kalikhman, Magnetogasdynamics (W. B. Saunders, Philadelphia, 1967).

28. G. P. Tolstov, Fourier Series (Prentice-Hall, Englewood-Cliffs, NJ, 1962).

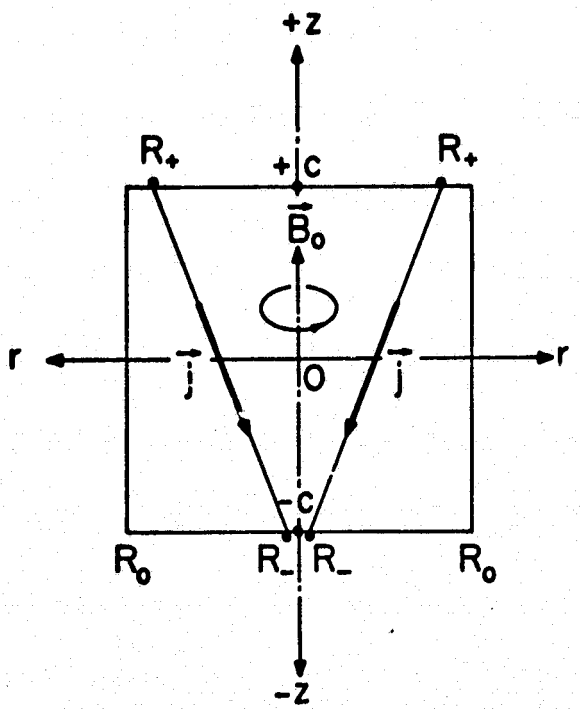

FIG. 1: Scheme of plasma centrifuge of radius R_o and heighth 2c with cathode (R_-), anode (R_+), and axial magnetic field $\vec{B}_o$ ($R_+ >> R_-$).

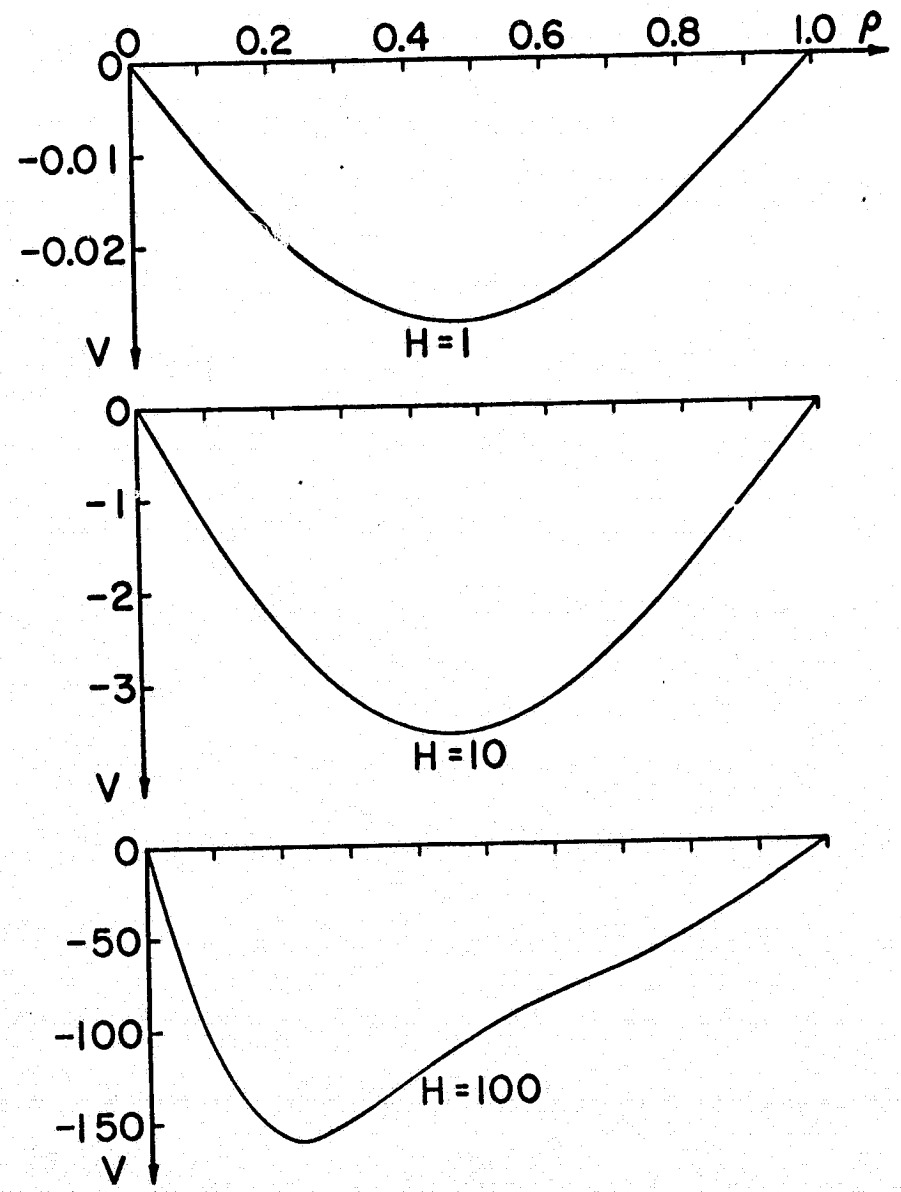

FIG. 2: $V(\rho,\zeta)$ versus ρ for $\zeta = 0$, and $H = 1, 10, 100$.

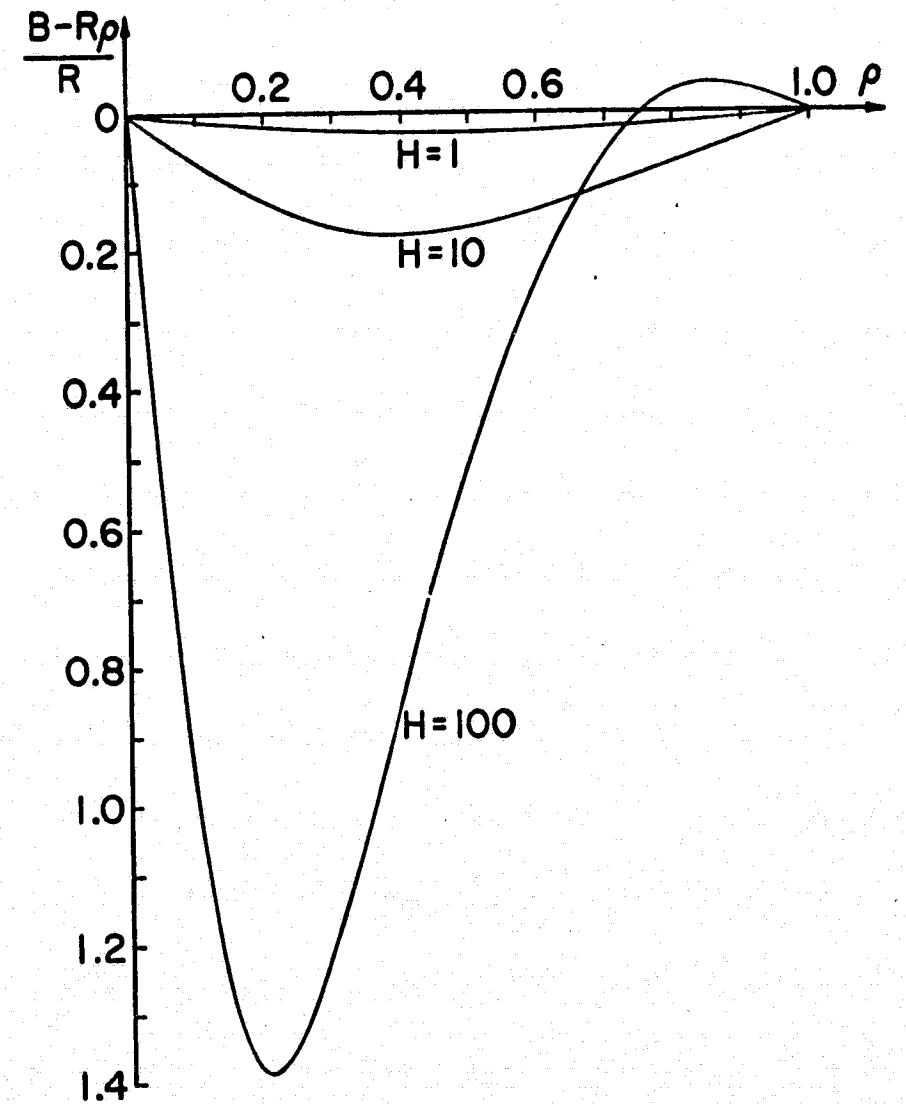

FIG. 3: $[B(\rho,\zeta)-R\rho]/R$ versus ρ for $\zeta = 0$, and $H = 1, 10, 100$.

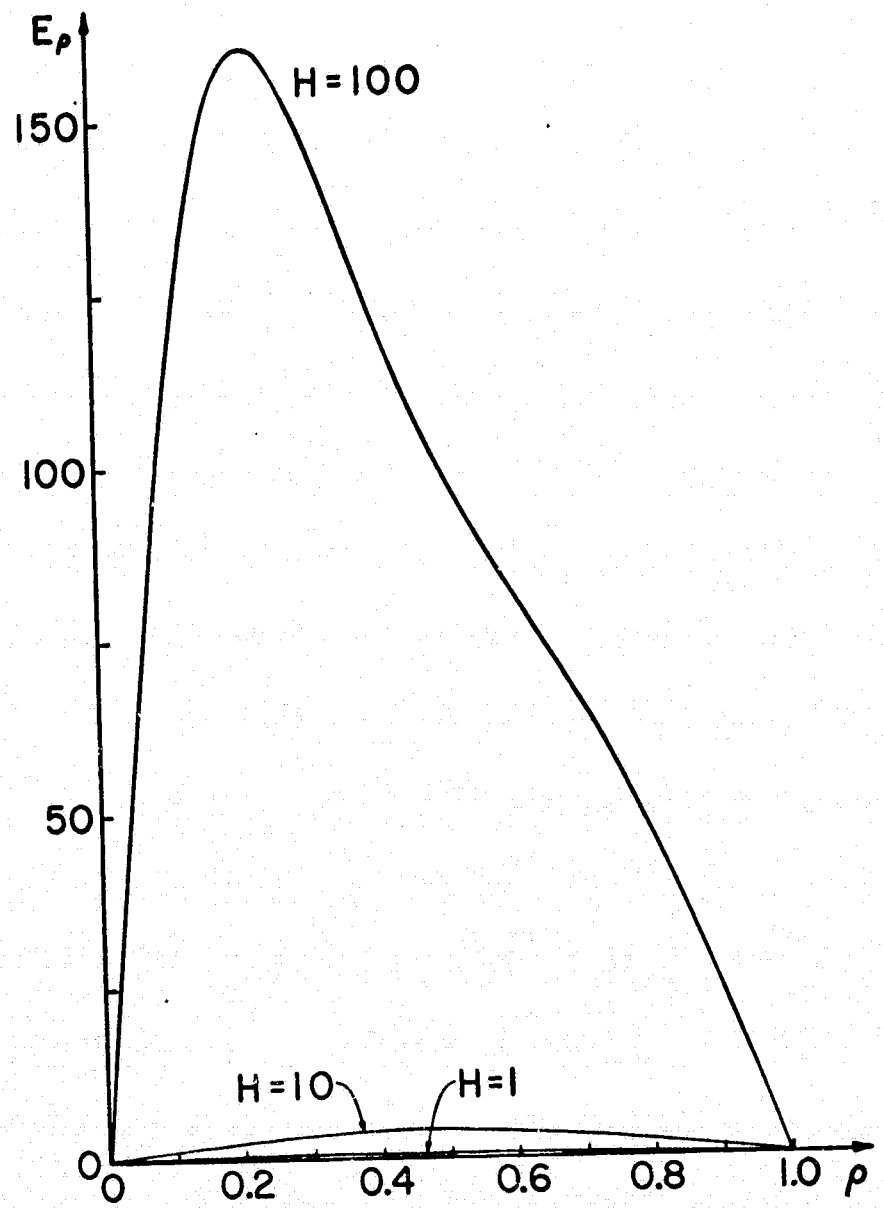

FIG. 4: $E_\rho(\rho,\zeta)$ versus ρ for $\zeta = 0$, and H = 1, 10, 100.

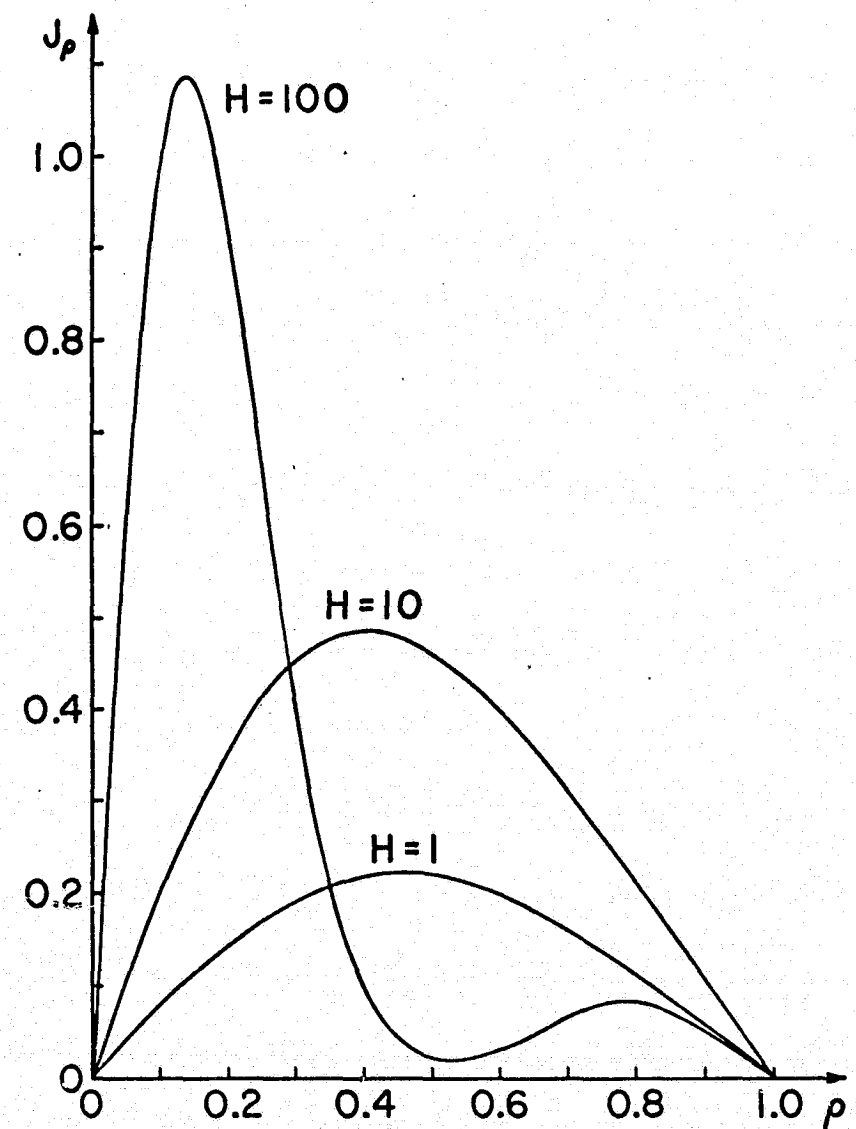

FIG. 5: $J_\rho(\rho,\zeta)$ versus ρ for $\zeta = 0$, and H = 1, 10, 100.

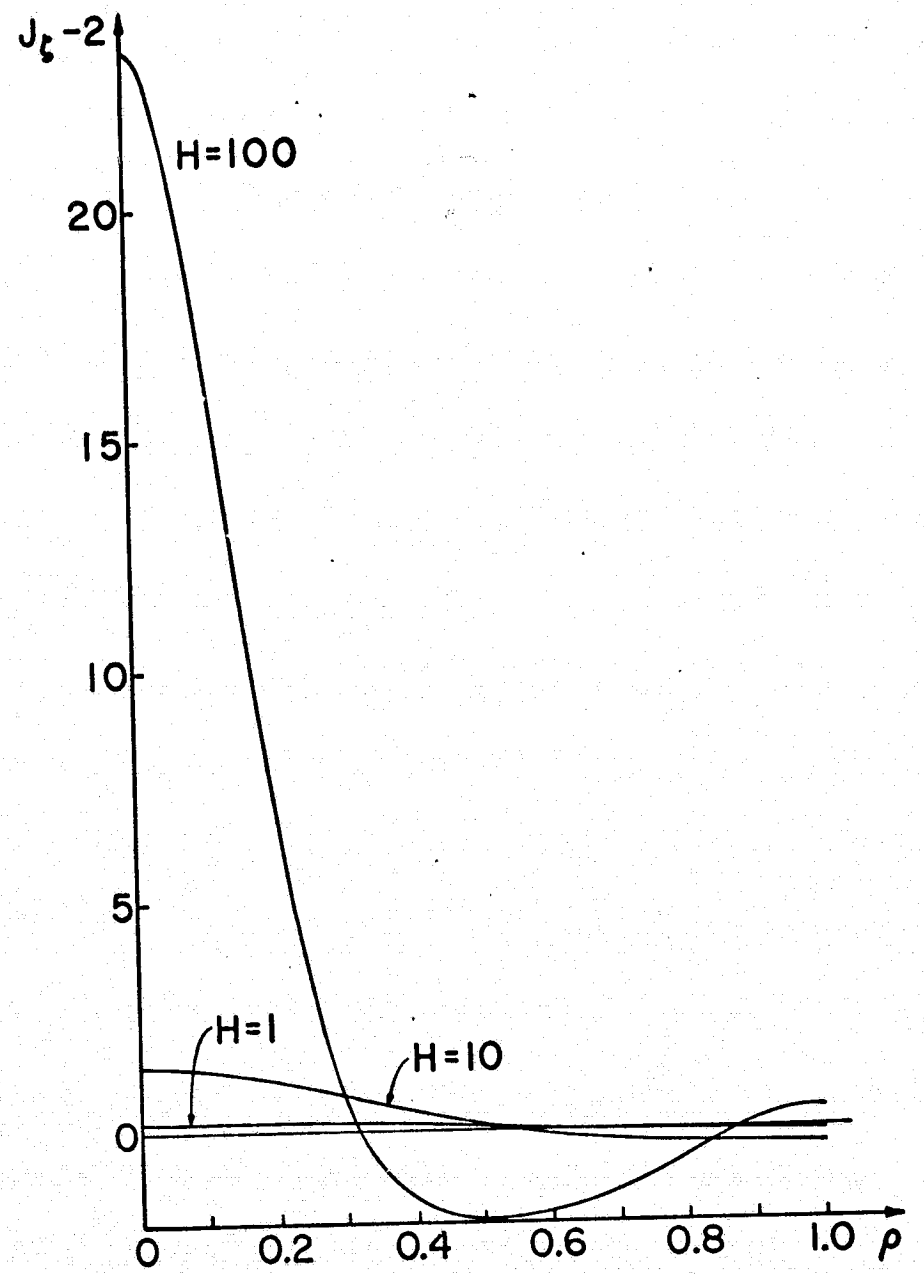

FIG. 6: $J_\zeta(\rho,\zeta)$-2 versus ρ for $\zeta = 0$, and H = 1, 10, 100.

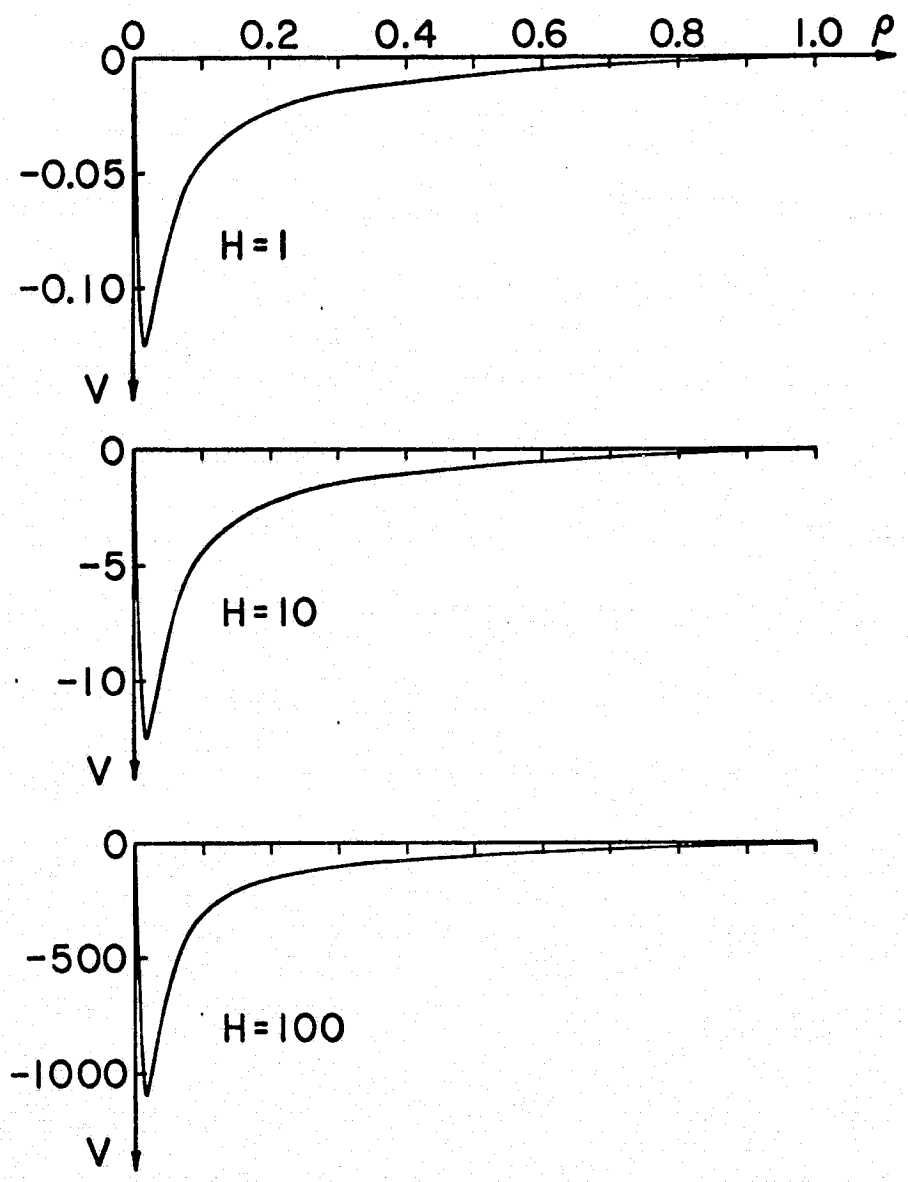

FIG. 7: $V(\rho,\zeta)$ versus ρ for $\zeta = -0.99$, and $H = 1, 10, 100$.

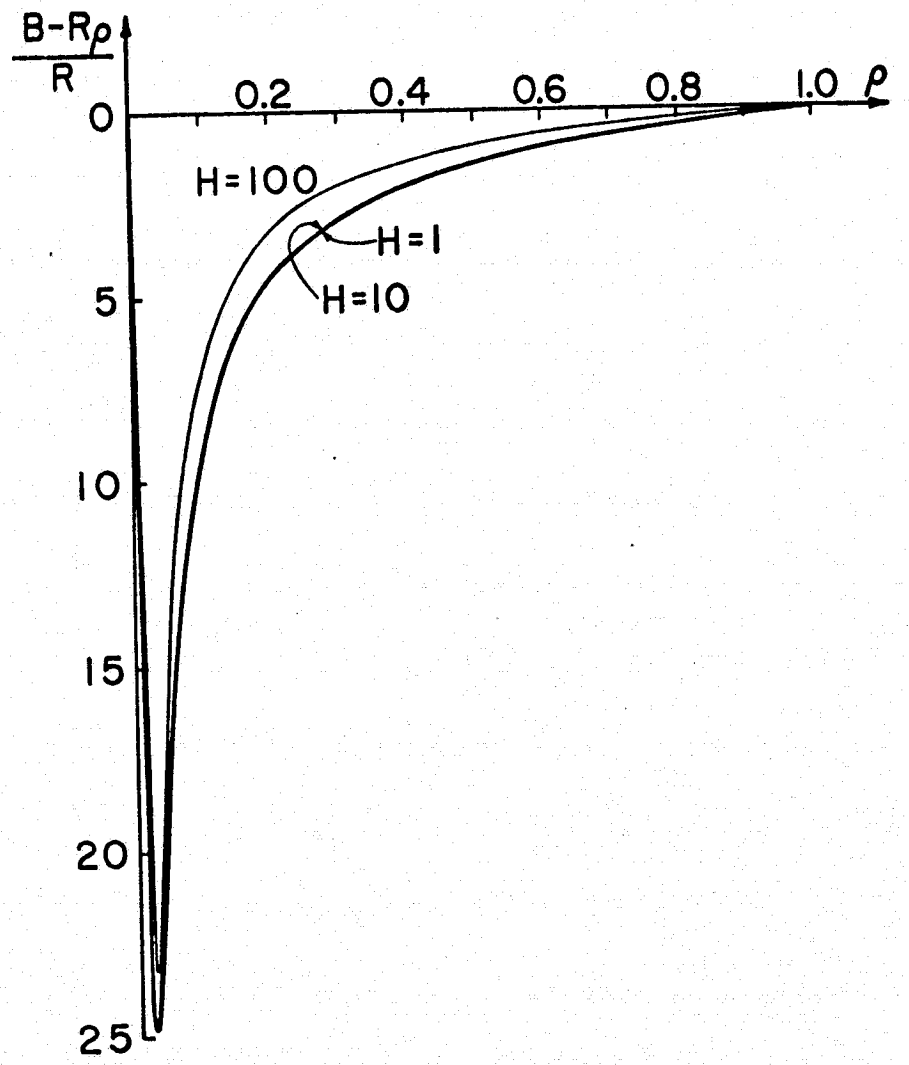

FIG. 8: $[B(\rho,\zeta)-R\rho]/R$ versus ρ for $\zeta = -0.99$, and $H = 1, 10, 100$.

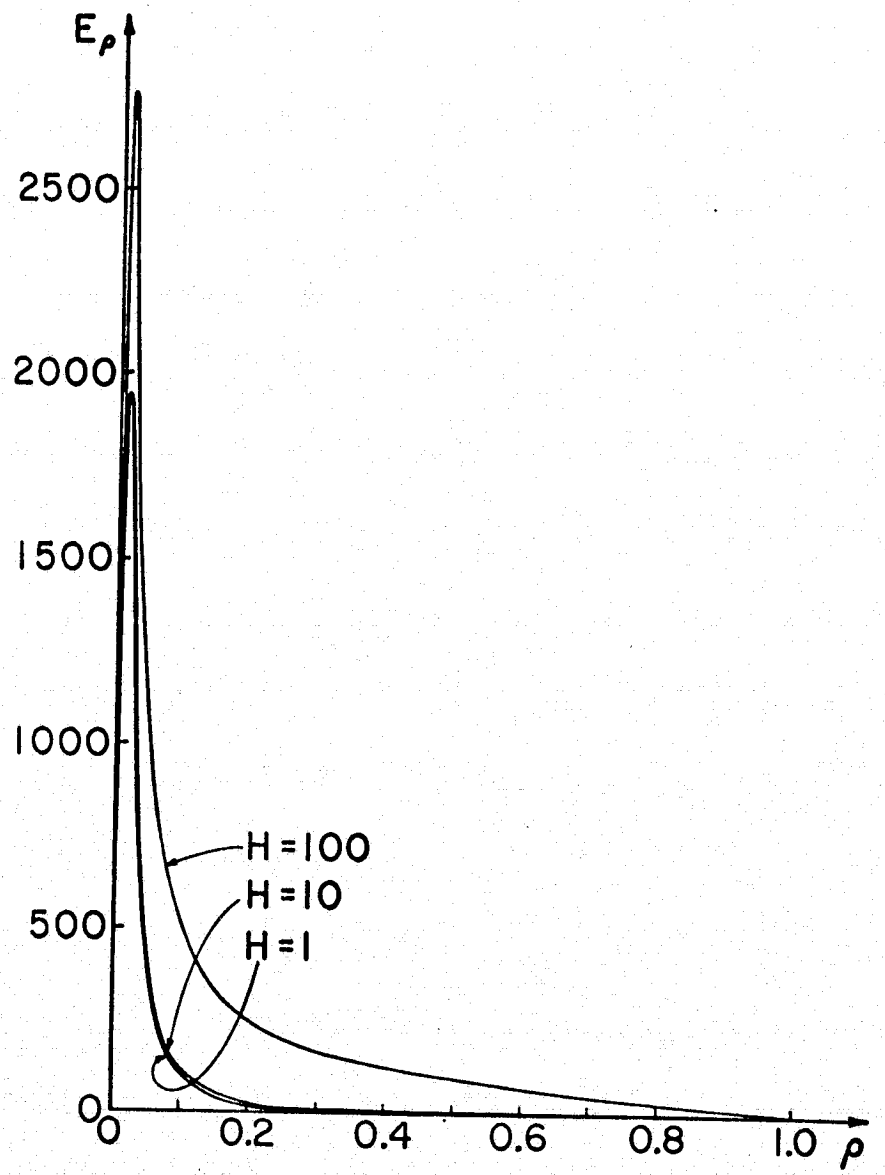

Fig. 9: $E_\rho(\rho,\zeta)$ versus ρ for $\zeta = -0.99$, and H = 1, 10, 100.

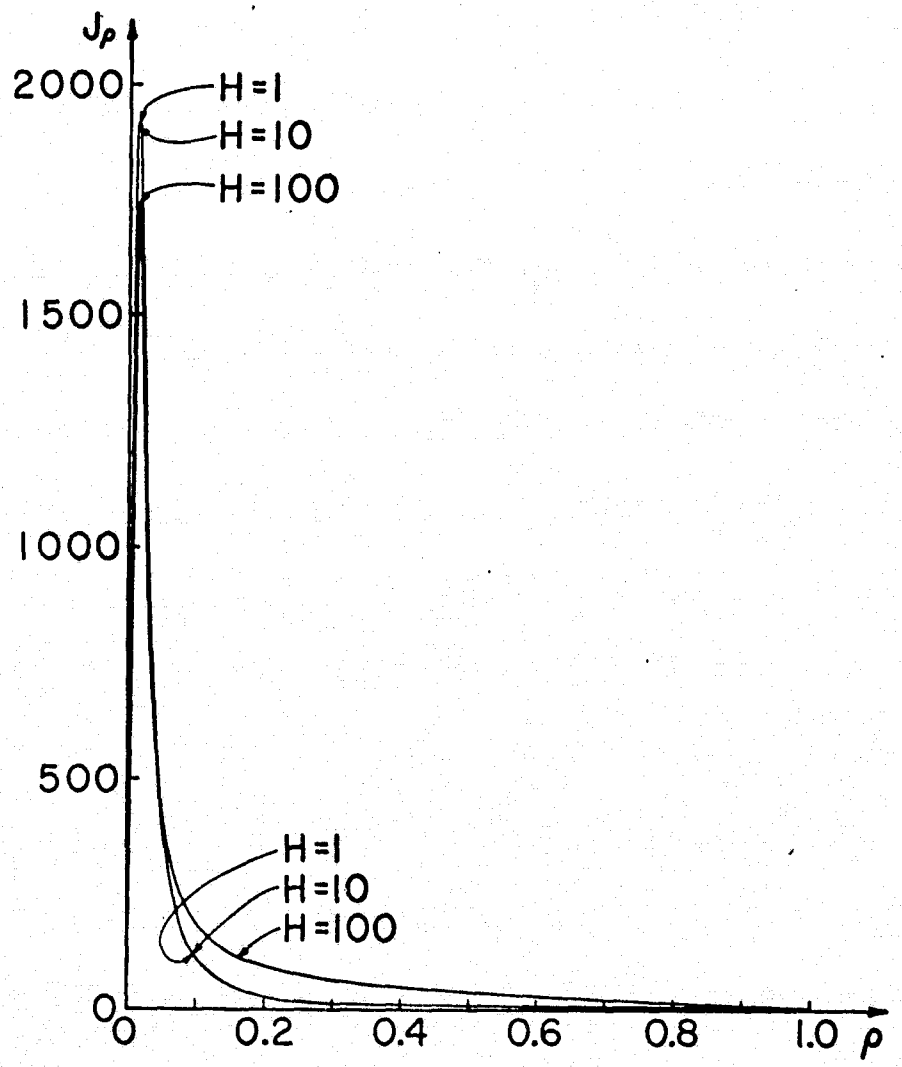

FIG. 10: $J_\rho(\rho,\zeta)$ versus ρ for $\zeta = -0.99$, and H = 1, 10, 100.

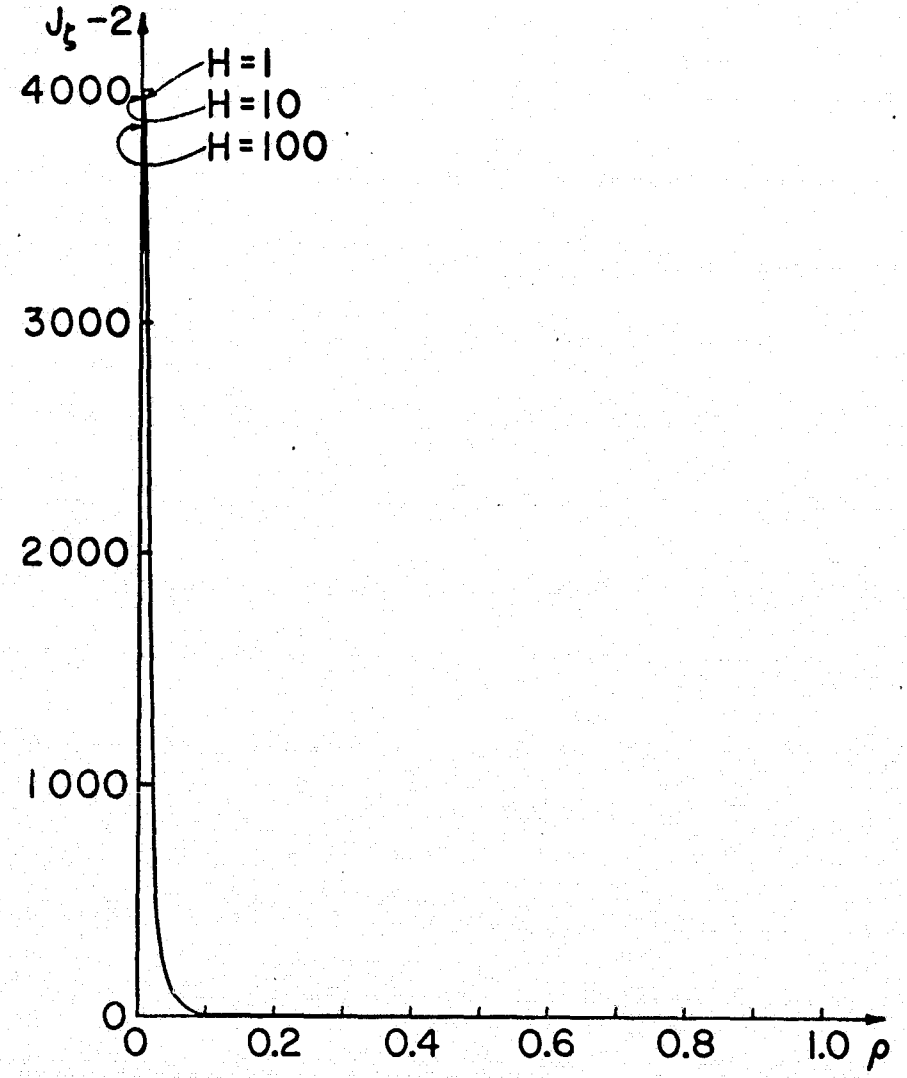

FIG. 11: $J_\zeta(\rho,\zeta)-2$ versus ρ for $\zeta = -0.99$, and H = 1, 10, 100.

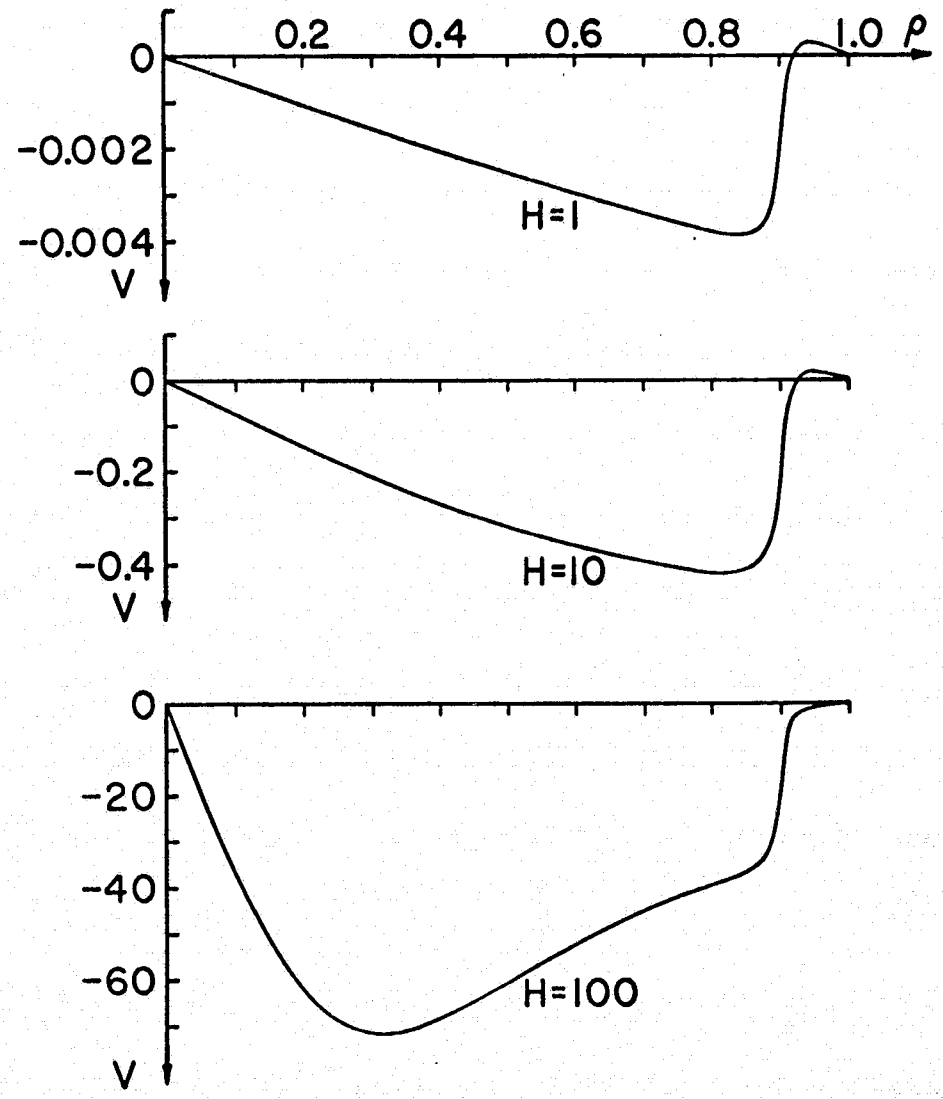

FIG. 12: $V(\rho,\zeta)$ versus ρ for $\zeta = +0.99$, and $H = 1, 10, 100$.

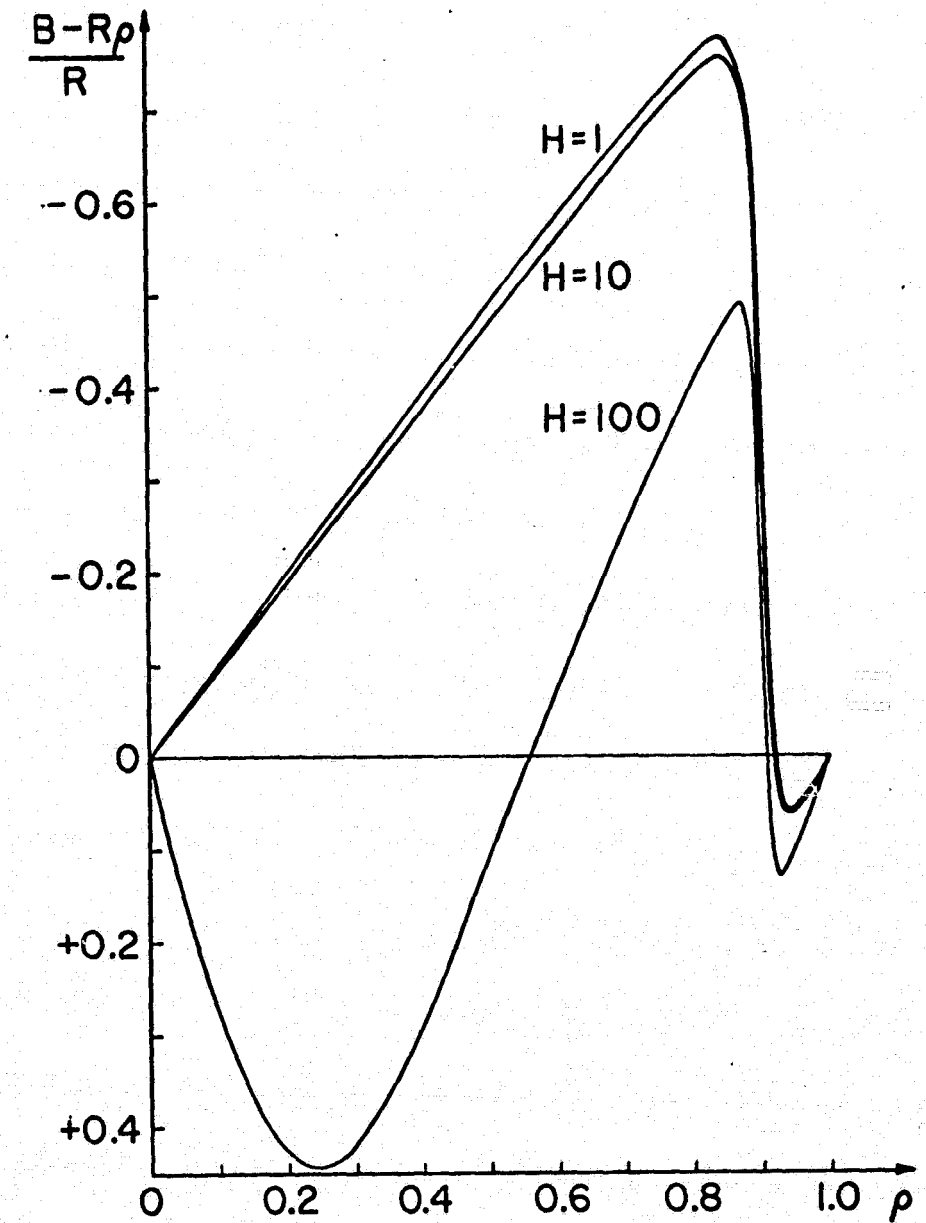

FIG. 13: $[B(\rho,\zeta)-R\rho]/R$ versus ρ for $\zeta = +0.99$, and $H = 1, 10, 100$.

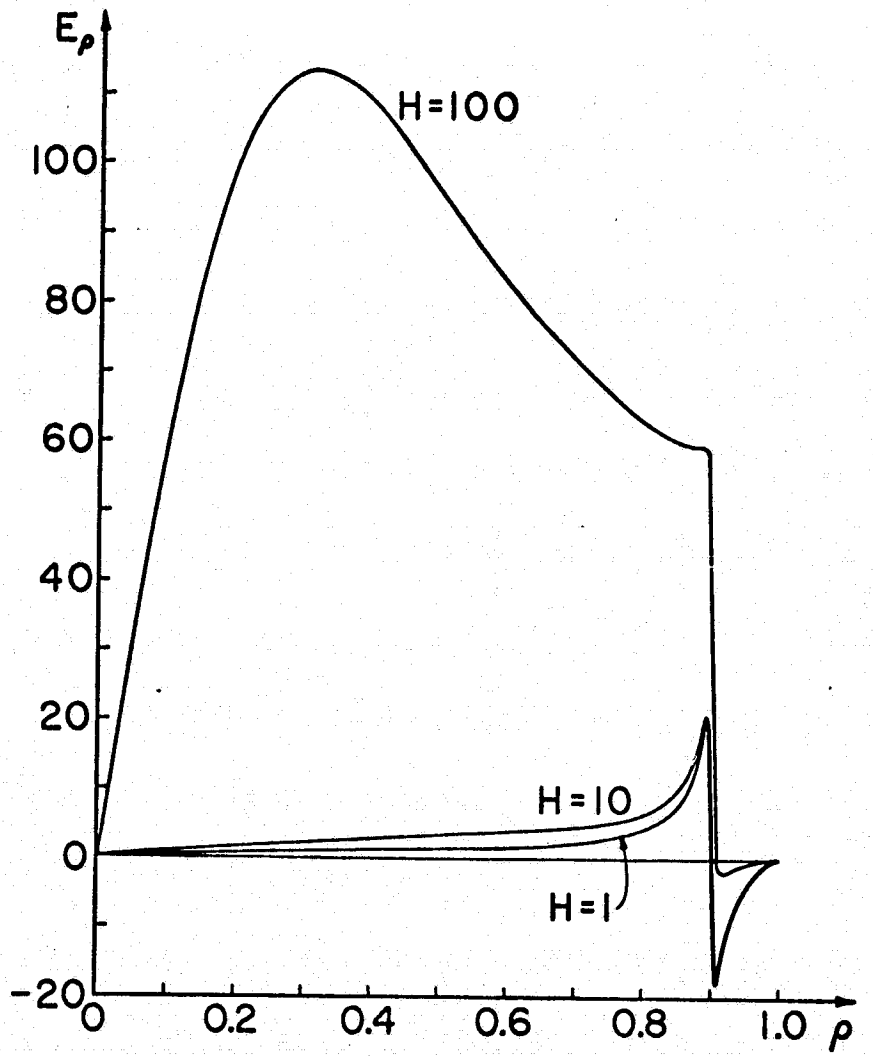

FIG. 14: $E_\rho(\rho,\zeta)$ versus ρ for $\zeta = +0.99$, and H = 1, 10, 100.

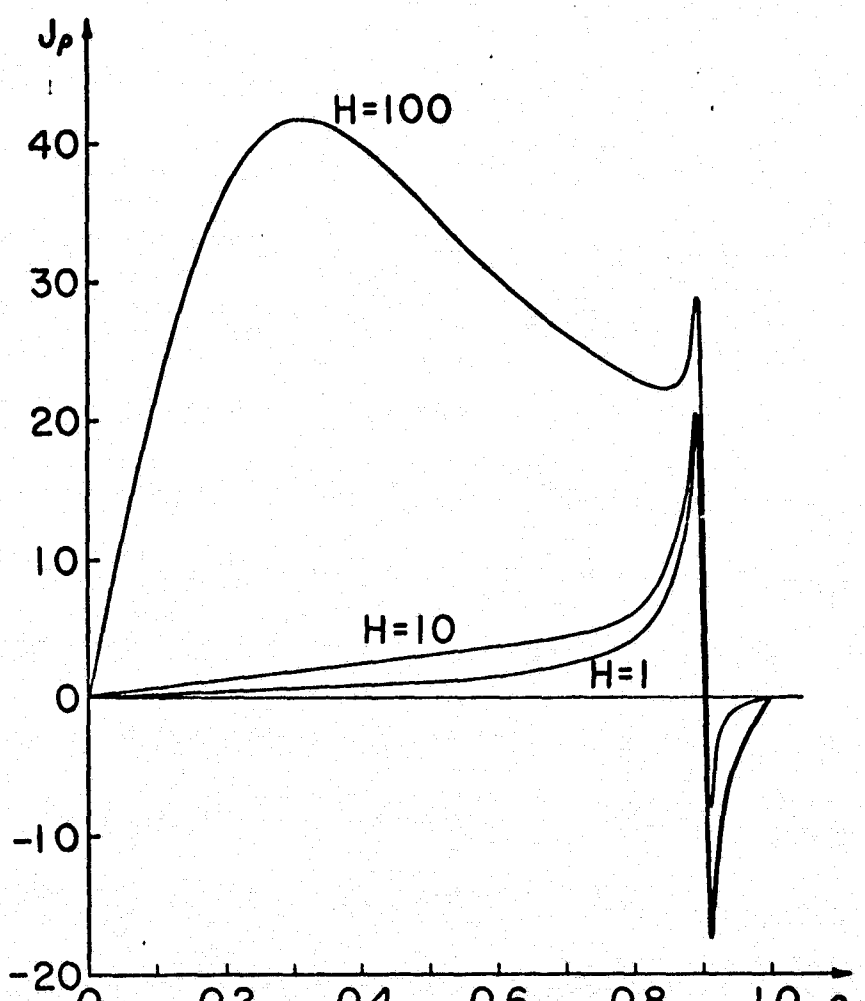

FIG. 15: $J_\rho(\rho,\zeta)$ versus ρ for $\zeta = +0.99$, and H = 1, 10, 100.

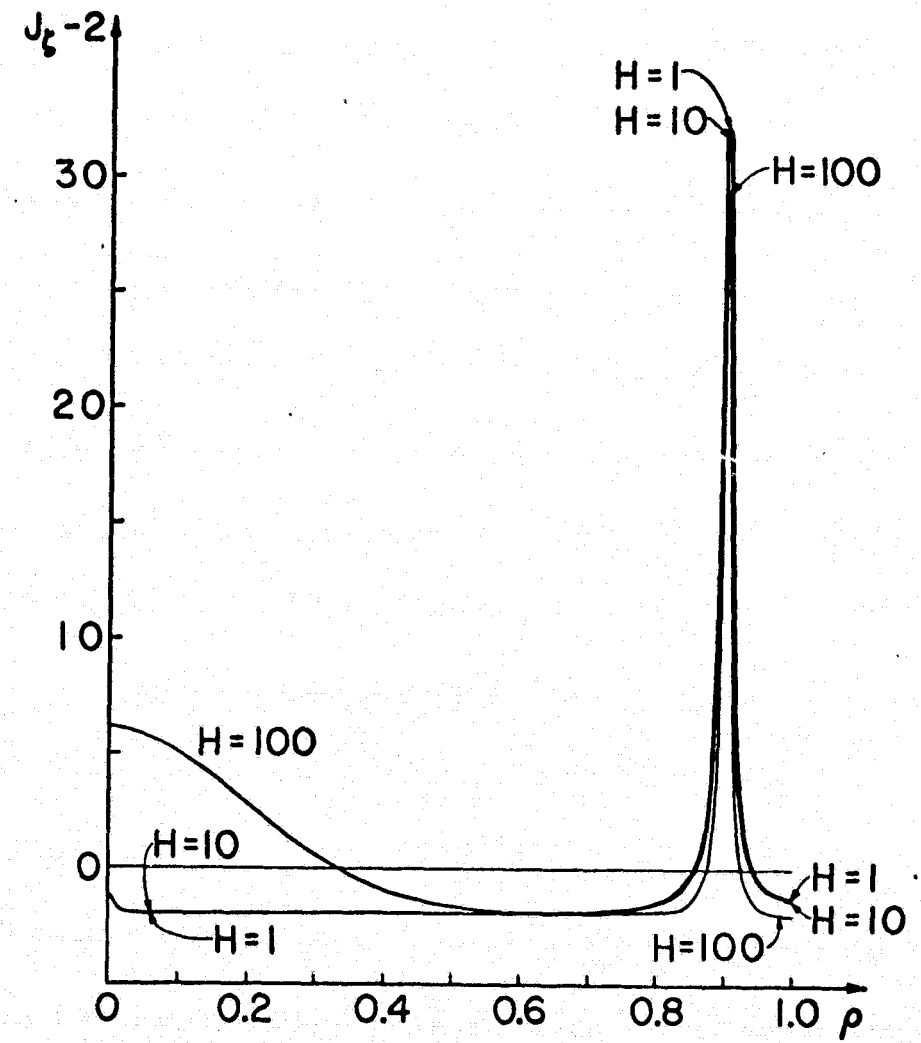

FIG. 16: $J_\zeta(\rho,\zeta)-2$ versus ρ for $\zeta = +0.99$, and $H = 1, 10, 100$.

PLASMA ROTATION BY LORENTZ FORCES IN AN ELECTRICAL DISCHARGE CENTRIFUGE WITH HALL EFFECT*

H. E. Wilhelm and S. H. Hong

Department of Electrical Engineering
Colorado State University
Fort Collins, Colorado 80523

A system analysis for an electrical discharge centrifuge is presented in which the plasma rotates under the influence of the Lorentz forces due to the interaction of the nonuniform current density fields with an axial external magnetic field. The associated boundary-value problem for the coupled partial differential equations, which describe the electric potential and the plasma velocity fields, is solved in closed form. The electric field, current density, and velocity distributions are discussed in terms of the Hartmann number H and the Hall coefficient $\omega\tau$. As a result of the Lorentz forces, the plasma rotates with speeds as high as 10^6 cm/sec around its axis of symmetry at sufficiently large values of H and $\omega\tau$. It is remarkable that the Hall effect supports the plasma rotation. As a result of the centrifugal forces (in the system of reference rotating with the plasma), the heavier (lighter) atom and ion components are enriched in the peripheral (central) region of the discharge centrifuge.

*Supported in part by NASA.

An electrical discharge in a cylindrical container rotates if the Lorentz force has a nonvanishing component in the azimuthal direction. For example, arc experiments in an acial external magnetic field B_z indicate that the discharge plasma rotates[1,2] since the current field lines $\vec{j}$ have a nonvanishing radial component j_r so that $(\vec{j} \times \vec{B})_\theta = -j_r B_z \neq 0$. In a stable arc dishcarge, the j_r-component is caused by the concentration of field lines $(\vec{j})$ at the electrodes and a dilatation (repulsion of currents in the same direction) of the field lines $\vec{j}$ in the interelectrode space.[1] In an unstable arc discharge, significant radial current components j_r are associated with the $m = 0$ and higher order ($m \geq 1$) instabilities.[2]

A simple model for the production of an electrical discharge centrifuge, which has a radial current density j_r which is in magnitude comparable with the axial current density j_z, is shown in Fig. 1. The radial spreading of the current field lines $\vec{j}$ is forced by means of electrodes of considerably different radii R_1 and R_2 ($R_2 >> R_1$) in the end plates $z = \pm c$ of an electrically isolating discharge chamber of radius R_o. The field lines of the current density $\vec{j}$ and of the external axial magnetic field $\vec{B}_o$ cross under a nonvanishing angle (except at the chamber axis) so that the resultant Lorentz force $\vec{j} \times \vec{B}_o$ rotates the discharge around its axis of symmetry. In steady state, the magnetic body forces in the azimuthal direction are balanced by the viscous forces (boundary layers at the chamber walls).

In the literature, the observed rotation of various electrical discharges in axial magnetic fields appears to be understood qualitatively in simple cases.[1,2] Exact solutions for plasma centrifuges are apparently not known either in the case of collisionless or collision-dominated[5,6] plasmas.

In the following, the steady state rotation of the spatially diverging discharge contained by an insulating cylinder in the external axial magnetic field $\vec{B}_o$ (Fig. 1) is treated theoretically. The analysis is based on the magnetogasdynamic approximation, in which two characteristic nondimensional parameters occur, the Hartman number H and the Hall coefficient $\omega\tau$,

$$H = (\sigma/\mu)^{\frac{1}{2}} B_o R_o, \quad \omega\tau = (|e|B_o/m)\tau.$$

The symbols designate the electrical conductivity (σ), the viscosity (μ), the electron gyration frequency (ω), and the electron momentum relaxation time (τ). H and $\omega\tau$ are a measure for the strength of the Lorentz force relative to the viscous force and for the reduction of the current flow $\vec{j}_\perp$ transverse to the magnetic field $\vec{B}_o$, respectively. The magnetic fields associated with the discharge currents $\vec{j} = \{j_r, j_\theta, j_z\}$ are neglected for small magnetic Reynolds numbers [$\sigma_\perp = \sigma/(1 + \omega^2\tau^2)$],

$$\begin{aligned} R_r &= O[B_r/B_o] = \mu_o \omega\tau\sigma_\perp \bar{v} r << 1 \quad , \\ R_\theta &= O[B_\theta/B_o] = |\mu_o I/2\pi R_o|/B_o << 1 \quad , \\ R_z &= O[B_z/B_o] = \mu_o \omega\tau\sigma_\perp \bar{v} R_o << 1 \quad , \end{aligned} \tag{1}$$

where $\bar{v}$ is the characteristic velocity of rotation and I the discharge current. These inequalities are satisfied in many cases, e.g., if $R_\theta << 1$ for i) $\omega\tau >> 1$ and $R \lesssim 1$ or ii) $R << 1$ and $0 \leq \omega\tau < \infty$, where $R \equiv \mu_o \sigma \bar{v}$ max $(R_o; c)$.

THEORETICAL FORMULATION

For a purely azimuthal flow field, $\vec{v} = \{0, v(r,z), 0\}$, the plasma behaves incompressible, $\nabla \cdot \vec{v} = 0$. From the continuity equation, $\nabla \cdot (\rho\vec{v}) = \vec{v} \cdot \nabla\rho = 0$, it follows then that the density gradient $\nabla\rho$ is everywhere perpendicular to the flow field $\vec{v}$. These ideal conditions are realized if secondary flows are absent or at least negligible.[7] In accordance with the magnetogasdynamic equations,[8] Ohm's law with Hall effect,[8] and the conservation equation for the electric charge density ($\nabla \cdot \vec{j} = 0$), the rotating discharge in a homogeneous magnetic field $\vec{B}_o$ (Fig. 1) is described by the following boundary-value problem for the azimuthal velocity $v(r,z)$ and electric potential $\phi(r,z)$ fields [induced magnetic fields neglected, Eq. (1)]:

$$0 = \mu\{\frac{\partial}{\partial r}\left[\frac{1}{r}\frac{\partial}{\partial r}(rv)\right] + \frac{\partial^2 v}{\partial z^2}\} - \sigma_\perp B_o\left(-\frac{\partial\phi}{\partial r} + v\,B_o\right), \tag{2}$$

$$\frac{1}{r}\frac{\partial}{\partial r}\left(r\frac{\partial\phi}{\partial r}\right) + \frac{\sigma}{\sigma_\perp}\frac{\partial^2\phi}{\partial z^2} = B_o\frac{1}{r}\frac{\partial}{\partial r}(r\,v) \quad , \tag{3}$$

where

$$v(r,z)_{r=R_o} = 0 \ , \ -c \leq z \leq +c \quad , \tag{4}$$

$$v(r,z)_{z=\pm c} = 0 \ , \ 0 \leq r \leq R_o \quad , \tag{5}$$

and

$$-\sigma[\partial\phi(r,z)/\partial z]_{z=\pm c} = I\,\delta(r - R_{1,2})/2\pi r \quad , \quad 0 \leq r \leq R_o \quad , \tag{6}$$

$$[\partial\phi(r,z)/\partial r]_{r=R_o} = 0 \ , \ -c \leq z \leq +c \quad . \tag{7}$$

The boundary conditions (4), (5), and (7) consider that the plasma does not slip at the walls $r = R_o$ and $z = \pm c$, and that no current flows into the cylinder wall $r = R_o$, respectively. The boundary conditions in Eq. (6) imply that the cathode (R_1) and anode (R_2) are ring electrodes of vanishing radial width, $\Delta r \to 0[\delta(r - R_{1,2})/2\pi r$ = radial Dirac function]. The net current flowing through the discharge is by Eq. (6)

$$-2\pi\sigma \int_0^{R_o} \frac{\partial\phi(r,z=\pm c)}{\partial z}\, r\,dr = I \int_0^{R_o} \delta(r-R_{1,2})\, dr = I < 0 \quad ,$$

since the positive current ($I < 0$) flows from the anode to the cathode (Fig. 1). The pressure distribution $p = p(r,z)$ is determined by the r- and z-components of the equation of motion,

$$-\rho_M \frac{v^2}{r} = -\frac{\partial p}{\partial r} + \omega\tau\, \sigma_\perp B_o\left(-\frac{\partial\phi}{\partial r} + v\, B_o\right) \quad , \qquad (8r)$$

$$\frac{\partial p}{\partial z} = j_r B_\theta - j_\theta B_r \to 0,\ B_{r,\theta} \to 0 \quad . \qquad (8z)$$

According to Eq. (8z), it is $\partial p/\partial z = 0$ if the induced fields B_r and B_θ are neglected [Eq. (1)]. This means that momentum cannot be exactly balanced in the axial direction if induced magnetic fields are neglected (in absence of secondary flows).[7] Eq. (8z) is in accord with the boundary-layer approximation[7] according to which the normal pressure gradient is $\partial p/\partial z \doteq 0$ at the electrode plates $z = \pm c$, $0 \leq r \leq R_o$.

In absence of the Hall effect, $\omega\tau \ll 1$, it is $\nabla\times\vec{B} = \mu_o(j_r, 0, j_z)$. Hence, $B_r = 0$ and $B_z = 0$ because of the homogeneity of the boundary conditions for B_r and B_z, whereas $B_\theta \neq 0$ since $j_{r,z} \neq 0 [B_\theta(r,z=\pm c) = (\mu_o I/2\pi r)H(r-R_{2,1})]$. Consideration of the induced field $\vec{B} = \{0,B_\theta,0\}$ leaves Eqs. (2)-(3) unchanged. This means that the boundary value problem in Eqs. (2)-(7) and the solutions $v(r,z)$ and $\phi(r,z)$ derived from it remain valid even in presence of a significant induced field $\vec{B} = \{0,B_\theta,0\}$, $R_\theta \geq 1$, as long as the Hall effect is negligible, $\omega\tau \ll 1$.

ANALYTICAL SOLUTION

The characteristic nondimensional parameters of the magnetogasdynamic discharge problem under consideration are obtained by introducing the nondimensional independent and dependent variables,

$$\rho = r/R_o \ , \quad 0 \leq \rho \leq 1 \ , \tag{9}$$

$$\zeta = z/c \ , \quad -1 \leq \zeta \leq +1 \ , \tag{10}$$

and

$$V(\rho,\zeta) = v(r,z)/v_o, \quad \Phi(\rho,\zeta) = \phi(r,z)/\phi_o \ , \tag{11}$$

where

$$v_o \equiv \phi_o/R_o B_o \ , \quad \phi_o \equiv Ic/2\pi\sigma R_o^2 \ . \tag{12}$$

In terms of the nondimensional space variables and fields, the boundary-value problem defined in Eqs. (2) - (7) assumes for $V(\rho,\zeta)$ and $\Phi(\rho,\zeta)$ the form:

$$\frac{1}{\rho}\frac{\partial}{\partial\rho}\left(\rho\frac{\partial\Phi}{\partial\rho}\right) + M^{-2}\frac{\partial^2\Phi}{\partial\zeta^2} = \frac{1}{\rho}\frac{\partial}{\partial\rho}(\rho V) \ , \tag{13}$$

$$\frac{\partial}{\partial\rho}\left[\frac{1}{\rho}\frac{\partial}{\partial\rho}(\rho V)\right] + N^{-2}\frac{\partial^2 V}{\partial\zeta^2} - H_\perp^2 V = -H_\perp^2\frac{\partial\Phi}{\partial\rho} \ , \tag{14}$$

where

$$V(\rho,\zeta)_{\rho=1} = 0 \ , \quad -1 \leq \zeta \leq +1 \ , \tag{15}$$

$$V(\rho,\zeta)_{\zeta=\pm1} = 0 \ , \quad 0 \leq \rho \leq 1 \ , \tag{16}$$

and

$$-[\partial\Phi(\rho,\zeta)/\partial\zeta]_{\zeta=\pm1} = \delta(\rho-\rho_{2,1})/\rho \ , \quad 0 \leq \rho \leq 1 \ , \tag{17}$$

$$[\partial\Phi(\rho,\zeta)/\partial\rho]_{\rho=1} = 0 \ , \quad -1 \leq \zeta \leq 1 \ , \tag{18}$$

with $\rho_{2,1} \equiv R_{2,1}/R_o$. The nondimensional constants M, N, and $H_\perp$ are defined by

$$M^{-2} = (1 + \omega^2\tau^2)(R_o/c)^2 \ , \quad N^{-2} = (R_o/c)^2 \ , \tag{19}$$

$$H_\perp^2 = (\sigma_\perp/\mu)B_o^2R_o^2 = H^2/(1 + \omega^2\tau^2) \ . \tag{20}$$

In view of the similarity of the left sides of Eqs. (13) - (14) with Bessel's differential equation, $Z_m'' + \rho^{-1}Z_m' + (k_\nu^2 - \rho^{-2}m^2)Z_m = 0$, for cylinder functions $Z_m(k_\nu\rho)$, partial solutions of the coupled inhomogeneous equations are sought in the form,

$$\Phi_\nu(\rho,\zeta) = J_o(k_\nu\rho)f_\nu(\zeta) \ , \tag{21}$$

$$V_\nu(\rho,\zeta) = J_1(k_\nu\rho)g_\nu(\zeta) \ , \tag{22}$$

where $J_o'(k_\nu\rho) = -J_1(k_\nu\rho)$ and $J_1'(k_\nu\rho) + (k_\nu\rho)^{-1}J_1(k_\nu\rho) = J_o(k_\nu\rho)$. Substitution of Eqs. (21) - (22) into Eqs. (13) - (14) yields

$$\frac{d^2f_\nu}{d\zeta^2} - k_\nu^2 M^2 f_\nu = k_\nu M^2 g_\nu \ , \tag{23}$$

$$\frac{d^2g_\nu}{d\zeta^2} - (k_\nu^2 + H_\perp^2)N^2g_\nu = k_\nu H_\perp^2N^2f_\nu \ , \tag{24}$$

where the eigen-values $k_\nu > 0$ are determined by the boundary conditions (15) and (18) as the real roots of the transcendental equation,

$$J_1(k_\nu) = 0 \ , \quad \nu = 1,2,3,.... \tag{25}$$

Thus, the general solution of the coupled equations (13) - (14) obtains by linear superposition as:

$$\Phi(\rho,\zeta) = -2\zeta + \sum_{\nu=1}^{\infty} J_o(k_\nu\rho)f_\nu(\zeta) \ , \tag{26}$$

$$V(\rho,\zeta) = \sum_{\nu=1}^{\infty} J_1(k_\nu\rho)g_\nu(\zeta) \ . \tag{27}$$

In view of Eq. (25), Eq. (26) is a Fourier-Dini series in which a zero-order term, -2ζ, has to be included, in accordance with the Fourier-Dini expansion [Eq. (32)] of the boundary value in Eq. (17), whereas Eq. (27) is a Fourier-Bessel series. By decoupling Eqs. (23) - (24) one finds for $f_\nu(\zeta)$ and $g_\nu(\zeta)$ the differential equations of 4th order,

$$\frac{d^4 f_\nu}{d\zeta^4} - [k_\nu^2(M^2 + N^2) + N^2 H_\perp^2] \frac{d^2 f_\nu}{d\zeta^2} + k_\nu^4 M^2 N^2 f_\nu = 0, \tag{28}$$

$$\frac{d^4 g_\nu}{d\zeta^4} - [k_\nu^2(M^2 + N^2) + N^2 H_\perp^2] \frac{d^2 g_\nu}{d\zeta^2} + k_\nu^4 M^2 N^2 g_\nu = 0, \tag{29}$$

with

$$- [df_\nu(\zeta)/d\zeta]_{\zeta=\pm 1} = 2J_o(k_\nu \rho_{2,1})/J_o(k_\nu)^2 \quad , \tag{30}$$

$$g(\zeta)_{\zeta=\pm 1} = 0 \quad , \tag{31}$$

as boundary conditions by Eqs. (16) - (17). In deriving Eq. (30), the Dirac function in Eq. (17) has been expanded as the Fourier-Dini series,

$$\delta(\rho - \rho_{2,1})/\rho = 2 + 2\sum_{\nu=1}^{\infty} [J_o(k_\nu \rho_{2,1})/J_o^2(k_\nu)] J_o(k_\nu \rho) \ . \tag{32}$$

In addition to Eqs (28) - (31), $f_\nu(\zeta)$ and $g_\nu(\zeta)$ have to satisfy also the uncoupled Eqs. (23) - (24). With

$$\omega_{1\nu} \equiv \omega_{\nu+}, \ \omega_{2\nu} \equiv \omega_{\nu-}, \ \omega_{3\nu} \equiv -\omega_{\nu+}, \ \omega_{4\nu} \equiv -\omega_{\nu-}; \tag{33}$$

$$\omega_{\nu\pm} \equiv \left[\frac{1}{2}\{[k_\nu^2(M^2 + N^2) + N^2 H_\perp^2] \pm \{[k_\nu^2(M^2 + N^2) + N^2 H_\perp^2]^2 - 4k_\nu^4 M^2 N^2\}^{1/2}\}\right]^{1/2} \quad , \tag{34}$$

the general solutions for $f_\nu(\zeta) \sim e^{\omega\zeta}$ and $g_\nu(\zeta) \sim e^{\omega\zeta}$ of Eqs. (28) - (29), can be written as:

$$f_\nu(\zeta) = A_{1\nu} \frac{\sinh \omega_{1\nu}\zeta}{\sinh \omega_{1\nu}} + B_{1\nu} \frac{\cosh \omega_{1\nu}\zeta}{\cosh \omega_{1\nu}} + A_{2\nu} \frac{\sinh \omega_{2\nu}\zeta}{\sinh \omega_{2\nu}} + B_{2\nu} \frac{\cosh \omega_{2\nu}\zeta}{\cosh \omega_{2\nu}} \ , \tag{35}$$

$$g_\nu(\zeta) = C_{1\nu} \frac{\sinh \omega_{1\nu}\zeta}{\sinh \omega_{1\nu}} + D_{1\nu} \frac{\cosh \omega_{1\nu}\zeta}{\cosh \omega_{1\nu}} + C_{2\nu} \frac{\sinh \omega_{2\nu}\zeta}{\sinh \omega_{2\nu}} + D_{2\nu} \frac{\cosh \omega_{2\nu}\zeta}{\cosh \omega_{2\nu}} \ . \tag{36}$$

Only four of the eight integration constants $A_{1\nu},\ldots, D_{2\nu}$ for any $\nu \geq 1$ are independent; by Eqs (23) - (24),

$$\begin{aligned}
(\omega_{1\nu}^2 - k_\nu^2 M^2)A_{1\nu} &= k_\nu M^2 C_{1\nu} \\
(\omega_{2\nu}^2 - k_\nu^2 M^2)A_{2\nu} &= k_\nu M^2 C_{2\nu} \\
(\omega_{1\nu}^2 - k_\nu^2 M^2)B_{1\nu} &= k_\nu M^2 D_{1\nu} \\
(\omega_{2\nu}^2 - k_\nu^2 M^2)B_{2\nu} &= k_\nu M^2 D_{2\nu}
\end{aligned} \tag{37}$$

and

$$\begin{aligned}
[\omega_{1\nu}^2 - (k_\nu^2 + H_\perp^2)N^2]C_{1\nu} &= k_\nu N^2 H_\perp^2 A_{1\nu} \\
[\omega_{2\nu}^2 - (k_\nu^2 + H_\perp^2)N^2]C_{2\nu} &= k_\nu N^2 H_\perp^2 A_{2\nu} \\
[\omega_{1\nu}^2 - (k_\nu^2 + H_\perp^2)N^2]D_{1\nu} &= k_\nu N^2 H_\perp^2 B_{1\nu} \\
[\omega_{2\nu}^2 - (k_\nu^2 + H_\perp^2)N^2]D_{2\nu} &= k_\nu N^2 H_\perp^2 B_{2\nu}
\end{aligned} \tag{38}$$

where the coefficient determinants of the pairs of corresponding equations in Eqs. (37) and (38) vanish owing to Eqs. (33) - (34).

Upon application of the four relations in Eq. (38), which are equivalent to Eq. (37) by Eqs. (33) - (34), and the boundary conditions (31), which give

$$-C_{2\nu} = C_{1\nu} \equiv C_\nu \ , \quad -D_{2\nu} = D_{1\nu} \equiv D_\nu \ , \tag{39}$$

Equations (35) - (36) become:

$$\begin{aligned}
f_\nu(\zeta) = {} & \frac{C_\nu}{k_\nu N^2 H_\perp^2} \left\{ \Omega_{1\nu} \frac{\sinh \omega_{1\nu}\zeta}{\sinh \omega_{1\nu}} - \Omega_{2\nu} \frac{\sinh \omega_{2\nu}\zeta}{\sinh \omega_{2\nu}} \right\} \\
& + \frac{D_\nu}{k_\nu N^2 H_\perp^2} \left\{ \Omega_{1\nu} \frac{\cosh \omega_{1\nu}\zeta}{\cosh \omega_{1\nu}} - \Omega_{2\nu} \frac{\cosh \omega_{2\nu}\zeta}{\cosh \omega_{2\nu}} \right\} ,
\end{aligned} \tag{40}$$

$$g_\nu(\zeta) = C_\nu \left[\frac{\sinh \omega_{1\nu}\zeta}{\sinh \omega_{1\nu}} - \frac{\sinh \omega_{2\nu}\zeta}{\sinh \omega_{2\nu}}\right]$$

$$+ D_\nu \left[\frac{\cosh \omega_{1\nu}\zeta}{\cosh \omega_{1\nu}} - \frac{\cosh \omega_{2\nu}\zeta}{\cosh \omega_{2\nu}}\right] , \qquad (41)$$

where

$$\Omega_{i\nu} \equiv \omega_{i\nu}^2 - (k_\nu^2 + H_\perp^2)N^2 , \quad i = 1,2 . \qquad (42)$$

The boundary conditions (30) applied to Eq. (40) yield

$$C_\nu = - \frac{k_\nu N^2 H_\perp^2}{J_o^2(k_\nu)} \frac{[J_o(k_\nu\rho_1) + J_o(k_\nu\rho_2)]}{[\omega_{1\nu}\Omega_{1\nu}\mathrm{cth}\omega_{1\nu} - \omega_{2\nu}\Omega_{2\nu}\mathrm{cth}\omega_{2\nu}]} , \qquad (43)$$

$$D_\nu = + \frac{k_\nu N^2 H_\perp^2}{J_o^2(k_\nu)} \frac{[J_o(k_\nu\rho_1) - J_o(k_\nu\rho_2)]}{[\omega_{1\nu}\Omega_{1\nu}\mathrm{tgh}\omega_{1\nu} - \omega_{2\nu}\Omega_{2\nu}\mathrm{tgh}\omega_{2\nu}]} . \qquad (44)$$

Substitution of Eqs. (43) - (44) into Eqs. (40) - (41) gives as solutions for $f_\nu(\zeta)$ and $g_\nu(\zeta)$:

$$f_\nu(\zeta) \cdot J_o^2(k_\nu) = - \frac{[J_o(k_\nu\rho_1) + J_o(k_\nu\rho_2)]}{[\omega_{1\nu}\Omega_{1\nu}\mathrm{cth}\omega_{1\nu} - \omega_{2\nu}\Omega_{2\nu}\mathrm{cth}\omega_{2\nu}]} \times$$

$$\times \left[\Omega_{1\nu} \frac{\sinh \omega_{1\nu}\zeta}{\sinh \omega_{1\nu}} - \Omega_{2\nu} \frac{\sinh \omega_{2\nu}\zeta}{\sinh \omega_{2\nu}}\right] + \frac{[J_o(k_\nu\rho_1) - J_o(k_\nu\rho_2)]}{[\omega_{1\nu}\Omega_{1\nu}\mathrm{tgh}\omega_{1\nu} - \omega_{2\nu}\Omega_{2\nu}\mathrm{tgh}\omega_{2\nu}]} \times$$

$$\times \left[\Omega_{1\nu} \frac{\cosh \omega_{1\nu}\zeta}{\cosh \omega_{1\nu}} - \Omega_{2\nu} \frac{\cosh \omega_{2\nu}\zeta}{\cosh \omega_{2\nu}}\right] , \qquad (45)$$

and

$$g_\nu(\zeta) \cdot \frac{J_o^2(k_\nu)}{k_\nu N^2 H_\perp^2} = - \frac{[J_o(k_\nu\rho_1) + J_o(k_\nu\rho_2)]}{[\omega_{1\nu}\Omega_{1\nu}\mathrm{cth}\omega_{1\nu} - \omega_{2\nu}\Omega_{2\nu}\mathrm{cth}\omega_{2\nu}]} \times$$

$$\times \left[\frac{\sinh\,\omega_{1\nu}\zeta}{\sinh\,\omega_{1\nu}} - \frac{\sinh\,\omega_{2\nu}\zeta}{\sinh\,\omega_{2\nu}}\right] + \frac{[J_o(k_\nu\rho_1) - J_o(k_\nu\rho_2)]}{[\omega_{1\nu}\Omega_{1\nu}\mathrm{tgh}\omega_{1\nu} - \omega_{2\nu}\Omega_{2\nu}\mathrm{tgh}\omega_{2\nu}]} \times$$

$$\times \left[\frac{\cosh\,\omega_{1\nu}\zeta}{\cosh\,\omega_{1\nu}} - \frac{\cosh\,\omega_{2\nu}\zeta}{\cosh\,\omega_{2\nu}}\right] . \qquad (46)$$

Equations (45) - (46) form, together with Eqs. (26) - (27), the closed form solution of the problem of the rotating gas discharge in an axial magnetic field $\vec{B}_o$:

$$\Phi(\rho,\zeta) = - 2\zeta - \sum_{\nu=1}^{\infty} \frac{J_o(k_\nu\rho)}{J_o^2(k_\nu)} \left\{ \frac{[J_o(k_\nu\rho_1) + J_o(k_\nu\rho_2)]}{[\omega_{1\nu}\Omega_{1\nu}\mathrm{cth}\omega_{1\nu} - \omega_{2\nu}\Omega_{2\nu}\mathrm{cth}\omega_{2\nu}]} \times \right.$$

$$\times \left[\Omega_{1\nu} \frac{\sinh\,\omega_{1\nu}\zeta}{\sinh\,\omega_{1\nu}} - \Omega_{2\nu} \frac{\sinh\,\omega_{2\nu}\zeta}{\sinh\,\omega_{2\nu}}\right]$$

$$\left. - \frac{[J_o(k_\nu\rho_1) - J_o(k_\nu\rho_2)]}{[\omega_{1\nu}\Omega_{1\nu}\mathrm{tgh}\omega_{1\nu} - \omega_{2\nu}\Omega_{2\nu}\mathrm{tgh}\omega_{2\nu}]} \left[\Omega_{1\nu} \frac{\cosh\,\omega_{1\nu}\zeta}{\cosh\,\omega_{1\nu}} - \Omega_{2\nu} \frac{\cosh\,\omega_{2\nu}\zeta}{\cosh\,\omega_{2\nu}}\right] \right\} \qquad (47)$$

and

$$V(\rho,\zeta) = - N^2 H_\perp^2 \sum_{\nu=1}^{\infty} \frac{k_\nu J_1(k_\nu\rho)}{J_o^2(k_\nu)} \left\{ \frac{[J_o(k_\nu\rho_1) + J_o(k_\nu\rho_2)]}{[\omega_{1\nu}\Omega_{1\nu}\mathrm{cth}\omega_{1\nu} - \omega_{2\nu}\Omega_{2\nu}\mathrm{cth}\omega_{2\nu}]} \times \right.$$

$$\times \left[\frac{\sinh\,\omega_{1\nu}\zeta}{\sinh\,\omega_{1\nu}} - \frac{\sinh\,\omega_{2\nu}\zeta}{\sinh\,\omega_{2\nu}}\right]$$

$$\left. - \frac{[J_o(k_\nu\rho_1) - J_o(k_\nu\rho_2)]}{[\omega_{1\nu}\Omega_{1\nu}\mathrm{tgh}\omega_{1\nu} - \omega_{2\nu}\Omega_{2\nu}\mathrm{tgh}\omega_{2\nu}]} \left[\frac{\cosh\,\omega_{1\nu}\zeta}{\cosh\,\omega_{1\nu}} - \frac{\cosh\,\omega_{2\nu}\zeta}{\cosh\,\omega_{2\nu}}\right] \right\} . \qquad (48)$$

The remaining nondimensional discharge fields $\vec{E} = - \nabla\phi/E_o$ and $\vec{J} = \vec{j}/j_o$ are given in terms of the solutions for $\Phi(\rho,\zeta)$ and $V(\rho,\zeta)$:

$$E_r = -\frac{1}{\rho}\,\partial\Phi/\partial\rho \ , \quad E_\theta = 0 \ , \quad E_z = -N^{-1}\partial\Phi/\partial\zeta \qquad , \qquad (49)$$

$$J_r = \frac{1}{1+\omega^2\tau^2}\left(-\frac{\partial\Phi}{\partial\rho} + V\right),\quad J_\theta = \frac{\omega\tau}{1+\omega^2\tau^2}\left(-\frac{\partial\Phi}{\partial\rho} + V\right),\quad J_z = -\frac{1}{N}\frac{\partial\Phi}{\partial\zeta} \tag{50}$$

where $E_o = \phi_o/R_o$, $j_o = \sigma\phi_o/R_o$, and $N = c/R_o$ [Eq. (12)].

If the cathode is in the plane $z = -c(\zeta = -1)$ and the anode is in the plane $z = +c(\zeta = +1)$, then the reference fields v_o and ϕ_o [Eq. (12)] are negative, since $I < 0$. The results are also applicable to the case where the anode is in the plane $z = -c(\zeta = -1)$ and the cathode is in the plane $z = +c(\zeta = +1)$. In the latter situation, the reference fields v_o and ϕ_o [Eq. (12)] are positive, since $I > 0$. These explanations hold for magnetic fields pointing in the positive z- direction, $B_o > 0$; v_o changes its sign if $B_o < 0$ [Eq. (12)].

NUMERICAL ILLUSTRATIONS

As an illustration the radial (ρ) dependence of the nondimensional discharge fields $V(\rho,\zeta)$, $\Phi(\rho,\zeta)$, $E_r(\rho,\zeta)$, $E_z(\rho,\zeta)$, and $J_r(\rho,\zeta)$ has been calculated for $I < 0$ in the cross-sectional planes $\zeta = -0.99$ (cathode region), $\zeta = 0$ (central region), and $\zeta = +0.99$ (anode region) based on Eqs. (47)-(50). The remaining fields $J_\theta(\rho,\zeta)$ and $J_z(\rho,\zeta)$ are proportional to $J_r(\rho,\zeta)$ and $E_z(\rho,\zeta)$, respectively [Eq. (50)]. The characteristic (nondimensional) magnetic interaction numbers are treated as parameters:

$$\omega\tau = 1,\ 10\ ;\quad H = 1,\ 10,\ 100.$$

The geometry parameter N is taken to be $N = 1$ so that $M^{-2} = 1 + \omega^2\tau^2$, corresponding to $R_o = c$ [Eq. (20)]. The radial positions of the cathode and anode are assumed to be:

$$\rho_1 = 0.01\ (R_1 = 0.01\ R_o)\ ;\quad \rho_2 = 0.9\ (R_2 = 0.9\ R_o).$$

The dimensional fields are negative everywhere where the nondimensional fields are positive, and vice-versa [Eq. (11)] since $v_o < 0$ and $\phi_o < 0$ for $I < 0$ [Eq. (12)].

Central Region, $\zeta = 0$: In the Figs. 2-6, the azimuthal velocity field $V(\rho,0)$, the electric potential $\Phi(\rho,0)$, the radial and axial electric fields $E_r(\rho,0)$ and $E_z(\rho,0) \propto J_z(\rho,0)$, and the radial current density $J_r(\rho,0)$ are represented versus ρ, with $(\omega\tau,H) = (1,1)$, $(1,10)$, $(1,100)$, $(10,1)$, $(10,10)$, $(10,100)$ as parameters. It is seen that $|V|$ increases considerably at any point $0 < \rho < 1$ if either H or $\omega\tau$ are increased. In the region $\rho \gtrsim 0$ sufficiently close to the axis, $|\Phi|$, $|E_r|$, $|E_z - 2N^{-1}|$, and $|J_r|$ increase with increasing H or $\omega\tau$. The field distributions move towards the axis $\rho = 0$ as $\omega\tau$ becomes

larger. The "hump" developing at $\rho \tilde{=} 0.9$ (Figs. 4-6) with increasing $\omega\tau$ shows the influence of the ring anode ($\rho = 0.9$, $\zeta = +1$) in the plane $\zeta = 0$.

Cathode Region, $\zeta = -0.99$: The Figs. 7-11 show $V(\rho, -0.99)$, $\Phi(\rho, -0.99)$, $E_r(\rho, -0.99)$, $E_z(\rho, -0.99) \propto J_z(\rho, -0.99)$, and $J_r(\rho, -0.99)$ versus ρ with $(\omega\tau, H) = (1,1), \ldots (10,100)$ as parameters. These fields increase in intensity at any point $0 < \rho < 1$ if H or $\omega\tau$ is increased. Since the ring cathode is at $\rho_1 = 0.01$ ($\zeta = -1$), the field distributions are closer concentrated at the axis $\rho = 0$ than those in the plane $\zeta = 0$ (Figs. 2-6). Note that the plasma rotates only in the region $\rho \tilde{=} 0.1$ with a significant velocity, since the Lorentz force $-J_r B_o$ decreases rapidly with increasing $\rho \to 1$. A comparison of the corresponding fields in Figs. 2-6 and Figs. 7-11 indicates that the discharge spreads slightly in radial direction with increasing $-1 < \zeta \leq 0$. In particular, an increasing radial section of the plasma rotates with a significant speed as $-1 < \zeta \leq 0$ increases.

Anode Region, $\zeta = +0.99$: In the Figs. 12-16, $V(\rho, +0.99)$, $\Phi(\rho, +0.99)$, $E_r(\rho, +0.99)$, $E_z(\rho, +0.99) \propto J_z(\rho, +0.99)$, and $J_r(\rho, +0.99)$ are plotted versus ρ with $(\omega\tau, H) = (1,1), \ldots (10,100)$ as parameters. The dependence of these fields on H and $\omega\tau$ is as in the previous cases for $\zeta = 0$ and $\zeta = -0.99$. The velocity distributions are fully developed nearly through the entire chamber across section $0 < \rho \lesssim 0.9$, since the Lorentz force $-J_r B$ is strongest in the vicinity $\rho \tilde{=} 0.9$ of the ring anode, $\rho = 0.9 (\zeta = +1)$. As a result, a thin and steep boundary layer exists close to the

cylinder wall ($\rho = 1$) with backflows at sufficiently small $\omega\tau$-values (Fig.12). The radial distributions of Φ, E_r, $E_z \propto J_z$, and J_r (Figs. 13-16) clearly indicate that, in the plane $\zeta = +0.99$, the electrical discharge has shifted to the region $\rho \tilde{=} 0.9$ due to the influence of the nearby ring anode, $\rho = 0.9 (\zeta = +1)$. This shift occurs first slowly in the region $-1 < \zeta < +1 - \Delta\zeta$, and then rapidly in a relatively thin layer $\Delta\zeta << 1$ close to the anode plane $\zeta = +1$.

It is remarkable that the discharge remains concentrated in a radial region close to the cylinder axis with little radial spreading of the current density $\vec{J}$, except in a layer $\Delta\zeta$ close to the ring electrode of large radius ($R_2 >> R_1$) in which the radial current component J_r dominates the axial current component J_z. This spatial concentration of the discharge is the more pronounced the larger H and $\omega\tau$ are, since the axial magnetic field B_o reduces the radial current flow J_r for increasing $\omega\tau$. The speed of plasma rotation $V(\rho,\zeta)$ increases with increasing magnetic induction B_o by orders of magnitude over the reference speed v_o as the Figs. 2, 7, and 12 indicate which show $V(\rho,\zeta)$ for increasing $\omega\tau$ and H. The theoretical electric field and current density distributions are in qualitative agreement with experiments.[1)]

The graphs in Figs. 2-16 are based on the Fourier-series solutions, in which the first 100 terms were considered and the eigenvalues λ_ν were calculated up to the 10th decimal point. An even larger number of terms in the Fourier series solutions has to be taken into account if one wishes to compute (approximately) the discharge fields extremely close to the ring cathode ($\rho = 0.01$, $\zeta = -1$) and ring anode ($\rho = 0.9$, $\zeta = +1$) where $\partial\Phi(\rho,\zeta)/\partial\zeta$ changes discontinuously with ρ due to the electrode boundary conditions.

APPLICATION

The system analysis presented indicates that extremely high speeds of plasma rotation are obtainable already at moderate discharge currents I and magnetic inductions B_o, presumed the magnetic interaction numbers are not small, $H > 1$, $\omega\tau > 1$. As an example, consider a rotating arc discharge with:

$$|I| = 10^2 \text{ amp} \quad , \quad |B_o| = 10^0 \text{ Tesla},$$

$$\sigma = 10^2 \text{ mho m}^{-1}, \quad R_o = c = 10^{-1} \text{m}.$$

Hence, by Eq. (12)

$$v_o = Ic/2\pi\sigma B_o R_o^3 = (5/\pi) \times 10^1 \text{ m sec}^{-1},$$

and, by Fig. 2,

$$0[v] = 0[v_o V] = 10^4 \text{ m sec}^{-1}, \text{ for } \omega\tau = 10, H = 100.$$

Speeds of plasma rotation v, which are by orders of magnitude larger than 10^6 cm sec^{-1}, can be produced if the order of magnitude of the parameters $\omega\tau$ and H is increased. The viscous forces reduce, however, the speed of plasma rotation always in the layers close to the walls $(z = \pm c;\ r = R_o)$.

One recognizes that the torque of the Lorentz forces is a large physical effect which can be readily used to build an electrical "discharge-ultra-centrifuge" for isotope separation. If the working gas of the electrical discharge consists of two isotope gases, then the centrifugal forces would concentrate the lighter isotope ions and atoms in the central region and enrich the heavier isotope atoms and ions in the peripheral region of the discharge.

As an illustration to the plasma centrifuge, the isotope separation ratio is calculated. According to the equations of motion for two isotopes of masses m_i and m_j, the isotope density ratio at distances $0 \leq r \leq R_o - \delta$, where δ is the viscous boundary layer thickness, is approximately (T_o = temperature of the isotope ions)

$$\frac{\bar{n}_i(r)}{\bar{n}_j(r)} \tilde{=} \frac{\bar{n}_i(0)}{\bar{n}_j(0)} \, e^{+\frac{1}{2}\Delta m_{ij}\bar{v}(r)^2/kT_o}, \quad \Delta m_{ij} = m_i - m_j \ ,$$

where the bar designates a spatial average over the region $|z| < c$. As a specific example, consider an uranium plasma centrifuge containing the isotope ions (i) U^{237} and (j) U^{235} at a temperature $T_o = 10^3$ °K (and electrons at a temperature $T_e > T_o$). In this case, one has $\Delta m_{ij} = m(237) - m(235) = 3.320 \times 10^{-27}$ kg, $kT = 1.381 \times 10^{-20}$ Joule. Hence, the isotope separation ratio is:

$$\frac{\bar{n}_{237}(r)}{\bar{n}_{235}(r)} \Big/ \frac{\bar{n}_{237}(0)}{\bar{n}_{235}(0)} \tilde{=} 1.128 \times 10^0 \text{ for } \bar{v}(r) = 10^3 \text{ m sec}^{-1},$$

$$\tilde{=} 1.661 \times 10^5 \text{ for } \bar{v}(r) = 10^4 \text{ m sec}^{-1}.$$

It should be noted that the magnetogasdynamic considerations are only applicable to dense discharge plasmas, for which the mean free paths of the electrons, ions, and atoms are small compared to the characteristic chamber dimension, min (R_o;c). The evaluation of collisionless, rotating plasmas poses a rather different problem, since in this case the interactions through the selfconsistent electric magnetic fields play a dominant role.[9] The separation of isotopes by centrifugal forces in low density plasmas has been established experimentally.[10]

References

1. R. Schwenn, Z. Naturforsch. 25a, 1601 (1970).
2. A. A. Vedenov, E. P. Velikhov, and R. Z. Sagdeev, Sov. Phys. - Usp. 4, 332 (1961).
3. N. N. Komorov and V. M. Fodeev, Sov. Phys. JETP 14, 378 (1962).
4. M. V. Samakhin, Doklady Akad. Nank SSSR, Fizika, 155, 72 (1964).
5. C. C. Chang and T. S. Lundgren, Phys. Fluids 2, 627 (1959).
6. O. Okado and T. Dodo, J. Nucl. Sci. Technol. 10, 626 (1973).
7. H. Schlichting, Boundary Layer Theory (McGraw-Hill, New York, 1960).
8. L. E. Kalikhman, Magnetogasdynamics (W. B. Saunders, Philadelphia, 1967).
9. H. E. Wilhelm, unpublished (1976).
10. B. Bonnevier, Plasma Phys. 13, 763 (1971).

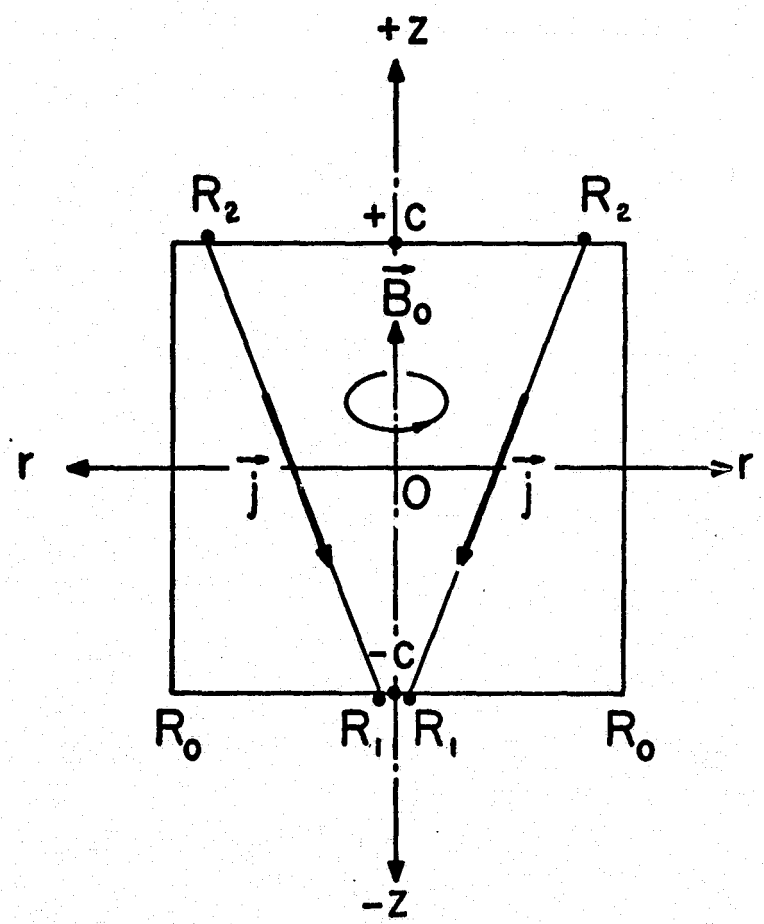

FIG. 1: Scheme of spatially diverging discharge between cathode (R_1) and anode (R_2) in a cylinder (R_o) of height 2c with axial magnetic field $\vec{B}_o$ ($R_2 >> R_1$).

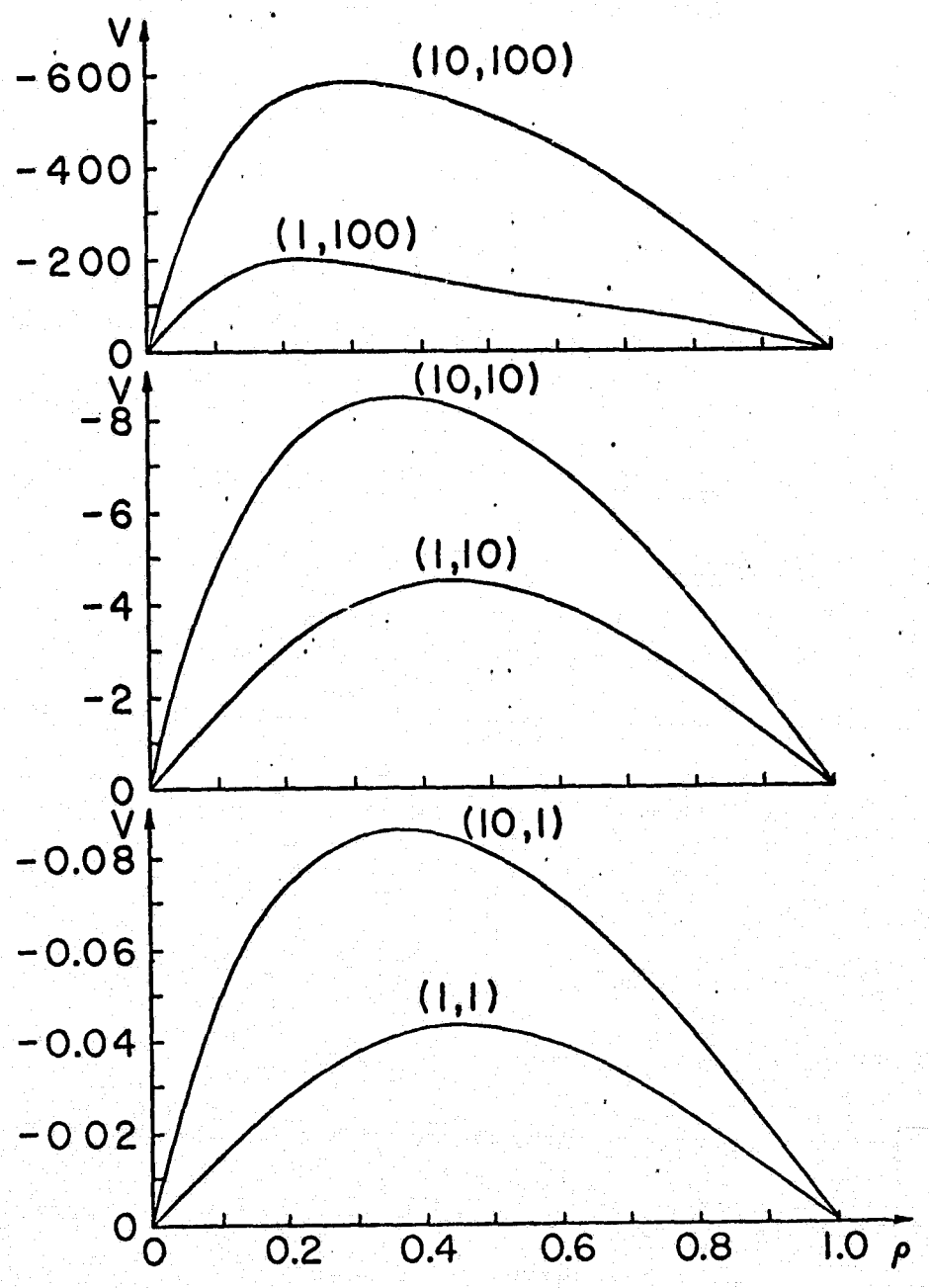

FIG. 2: $V(\rho,\zeta)$ versus ρ for $\zeta = 0$, and $(\omega\tau, H) = (1,1)$ to $(10,100)$.

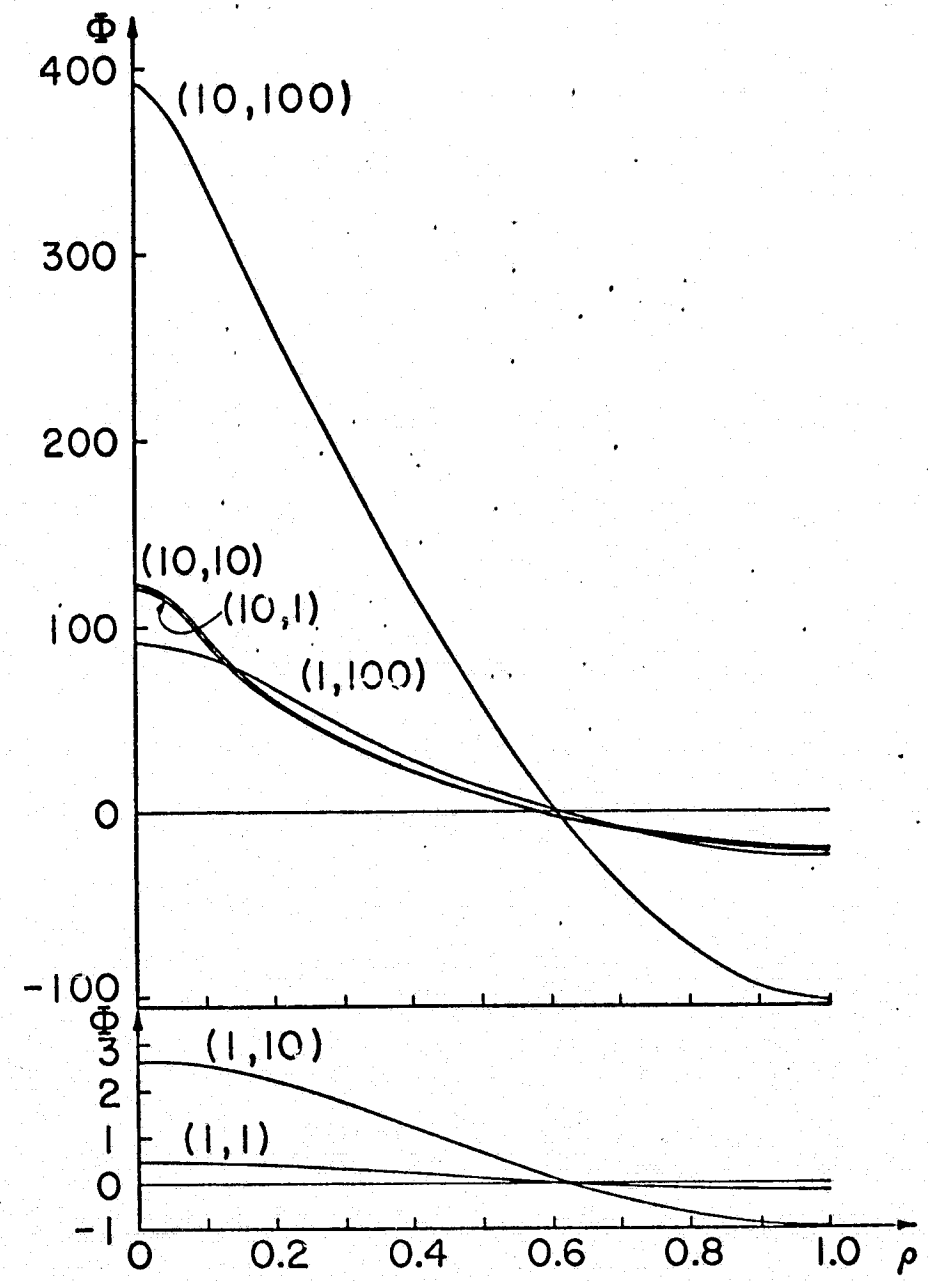

FIG. 3: $\Phi(\rho,\zeta)$ versus ρ for $\zeta = 0$, and $(\omega\tau, H) = (1,1)$ to $(10,100)$.

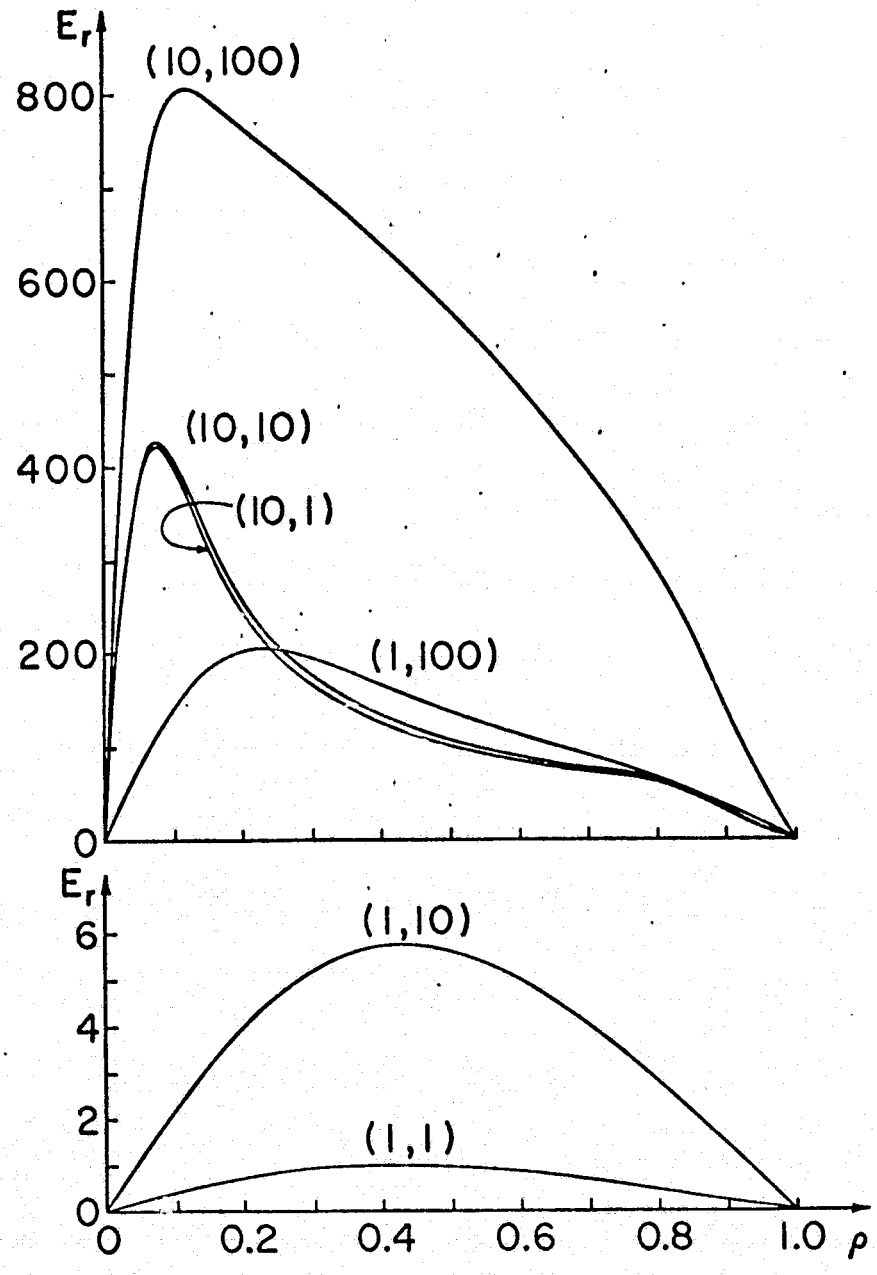

FIG. 4: $E_r(\rho,\zeta)$ versus ρ for $\zeta = 0$, and $(\omega\tau, H) = (1,1)$ to $(10,100)$.

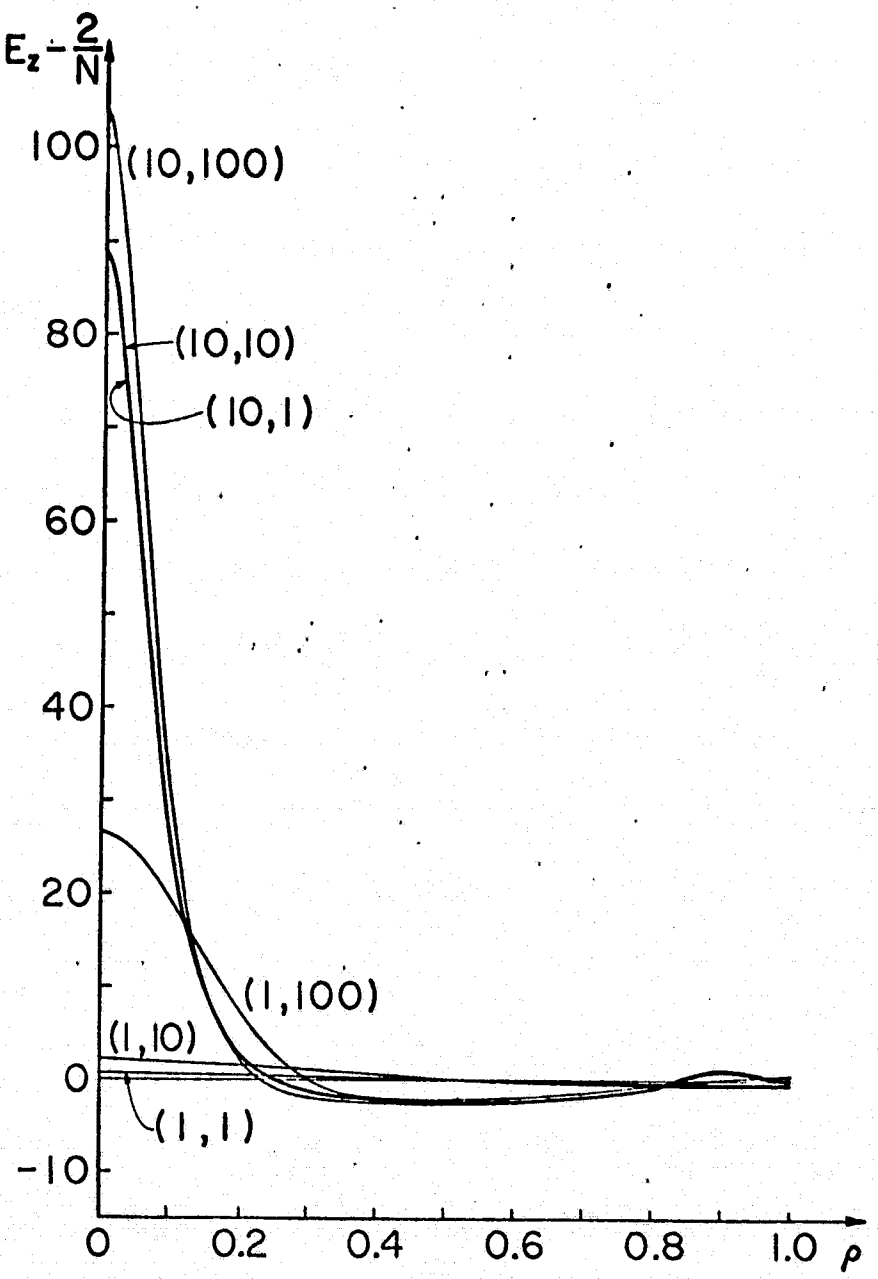

FIG. 5: $E_z(\rho,\zeta)$ versus ρ for $\zeta = 0$, and $(\omega\tau, H) = (1,1)$ to $(10,100)$.

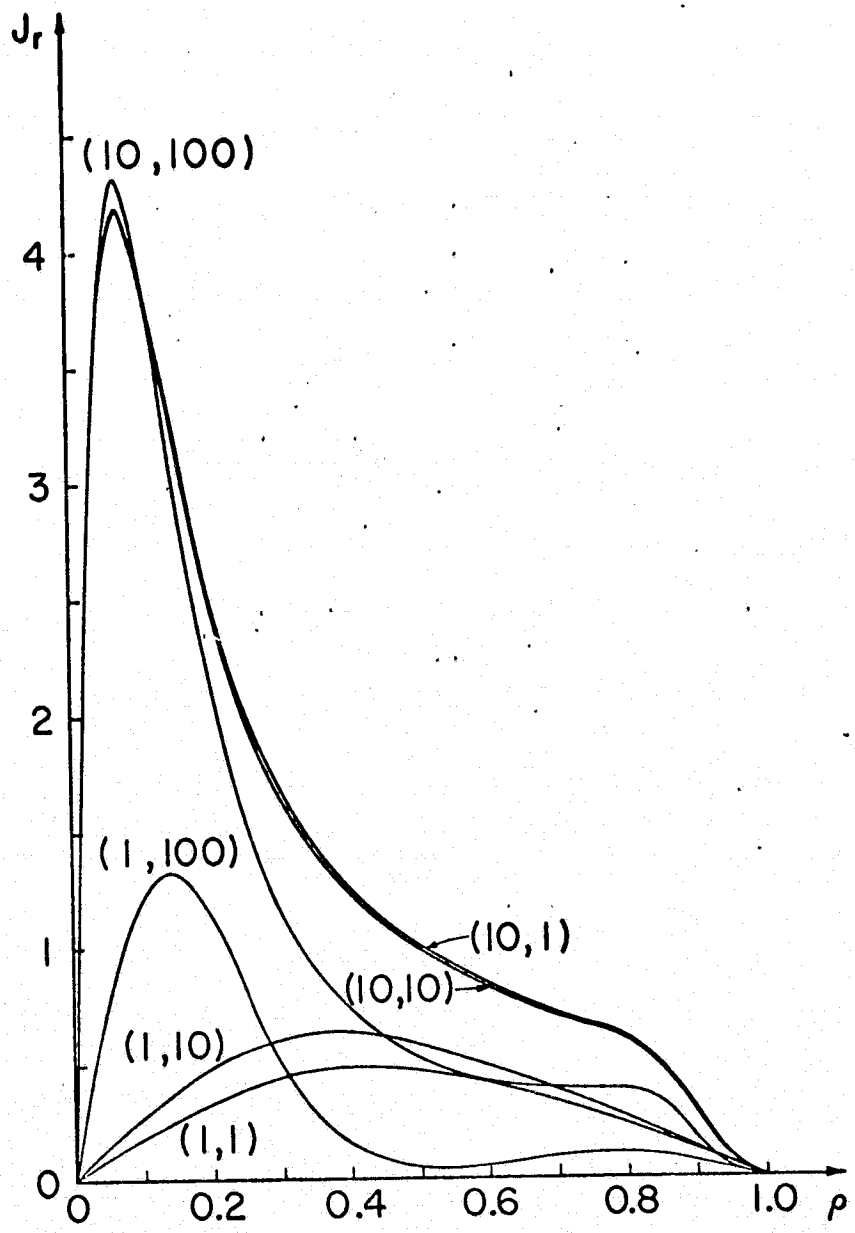

FIG. 6: $J_r(\rho,\zeta)$ versus ρ for $\zeta = 0$, and $(\omega\tau, H) = (1,1)$ to $(10,100)$.

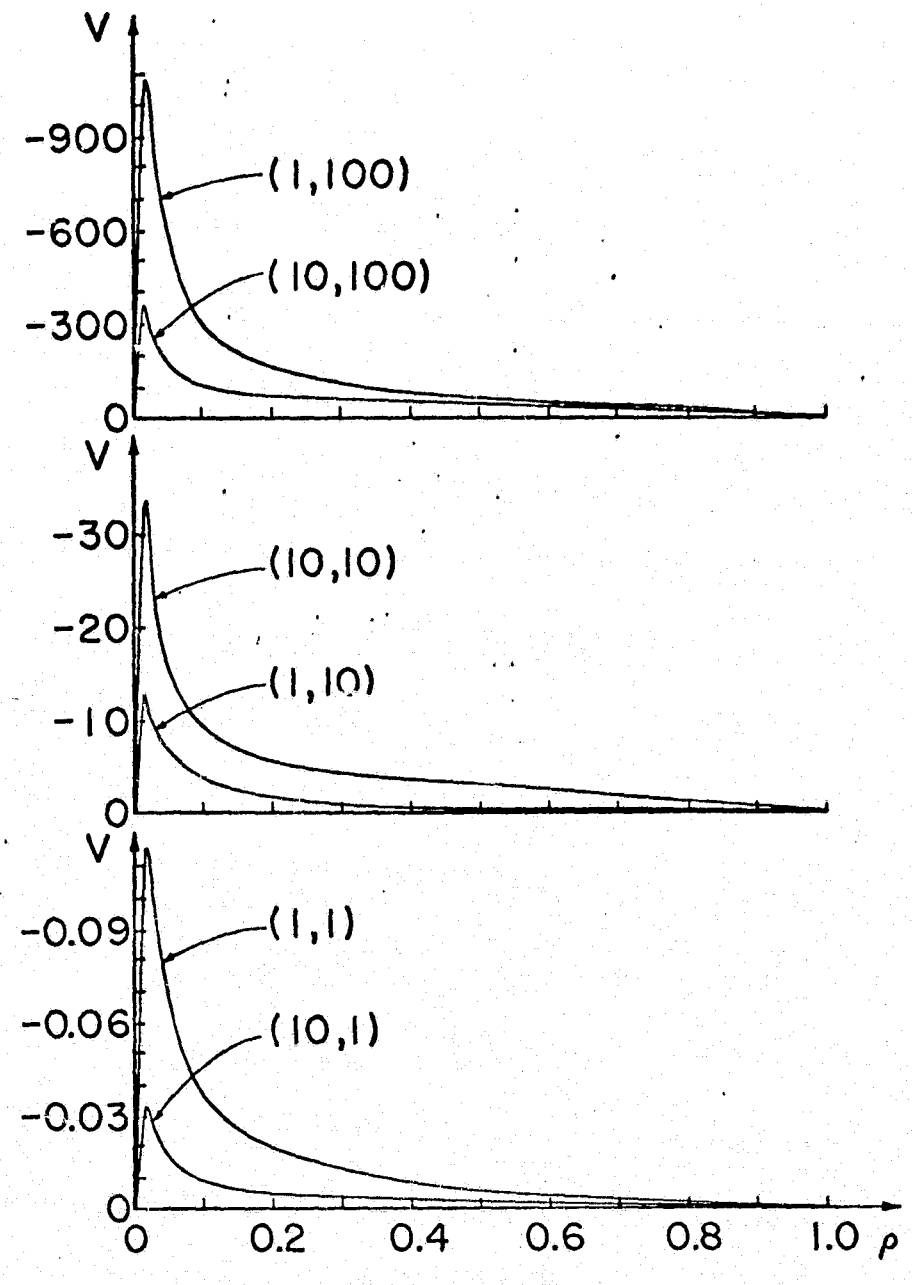

FIG. 7: $V(\rho,\zeta)$ versus ρ for $\zeta = -0.99$, and $(\omega\tau, H) = (1,1)$ to $(10,100)$.

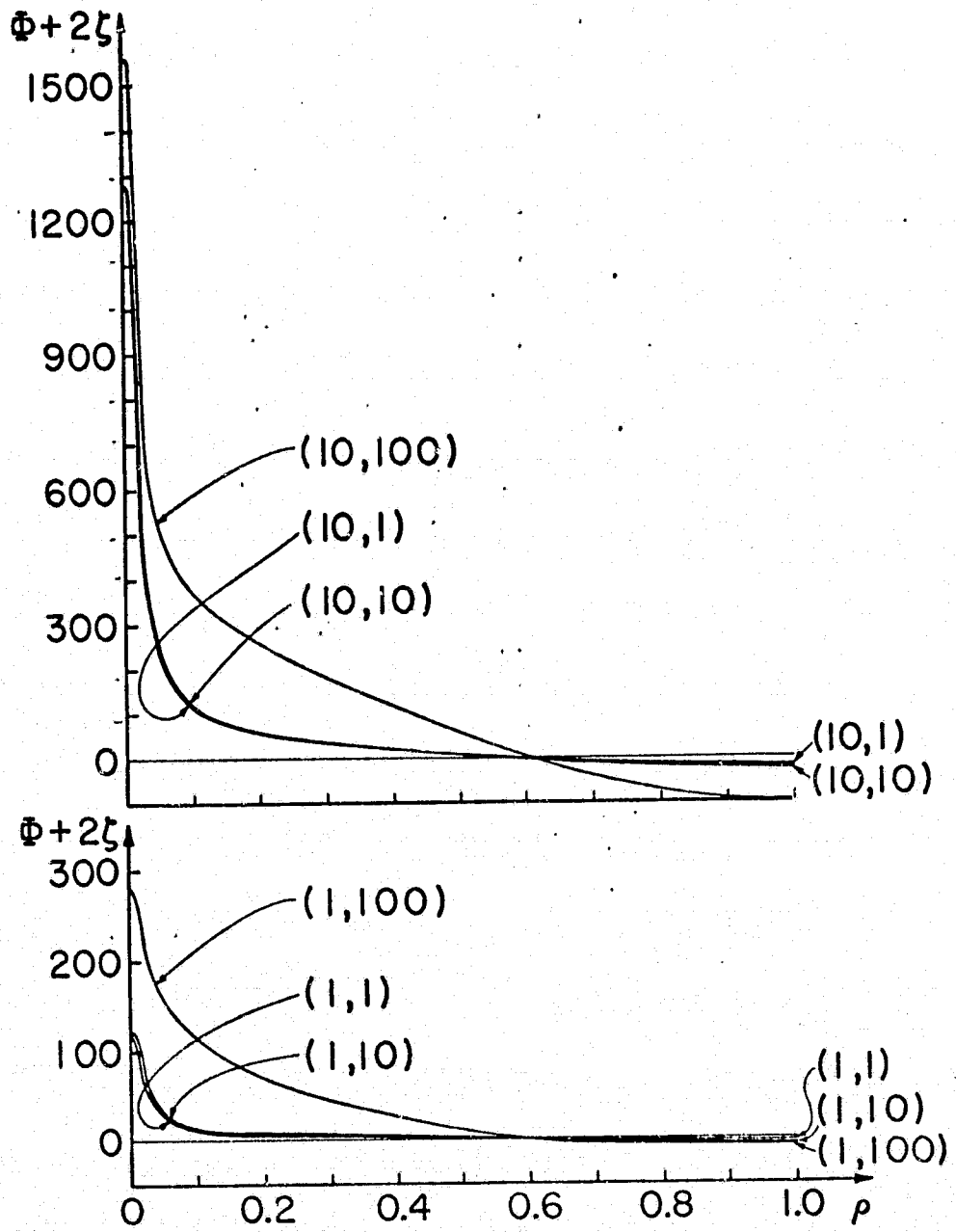

FIG. 8: $\Phi(\rho,\zeta)$ versus ρ for $\zeta = -0.99$, and $(\omega\tau, H) = (1,1)$ to $(10,100)$.

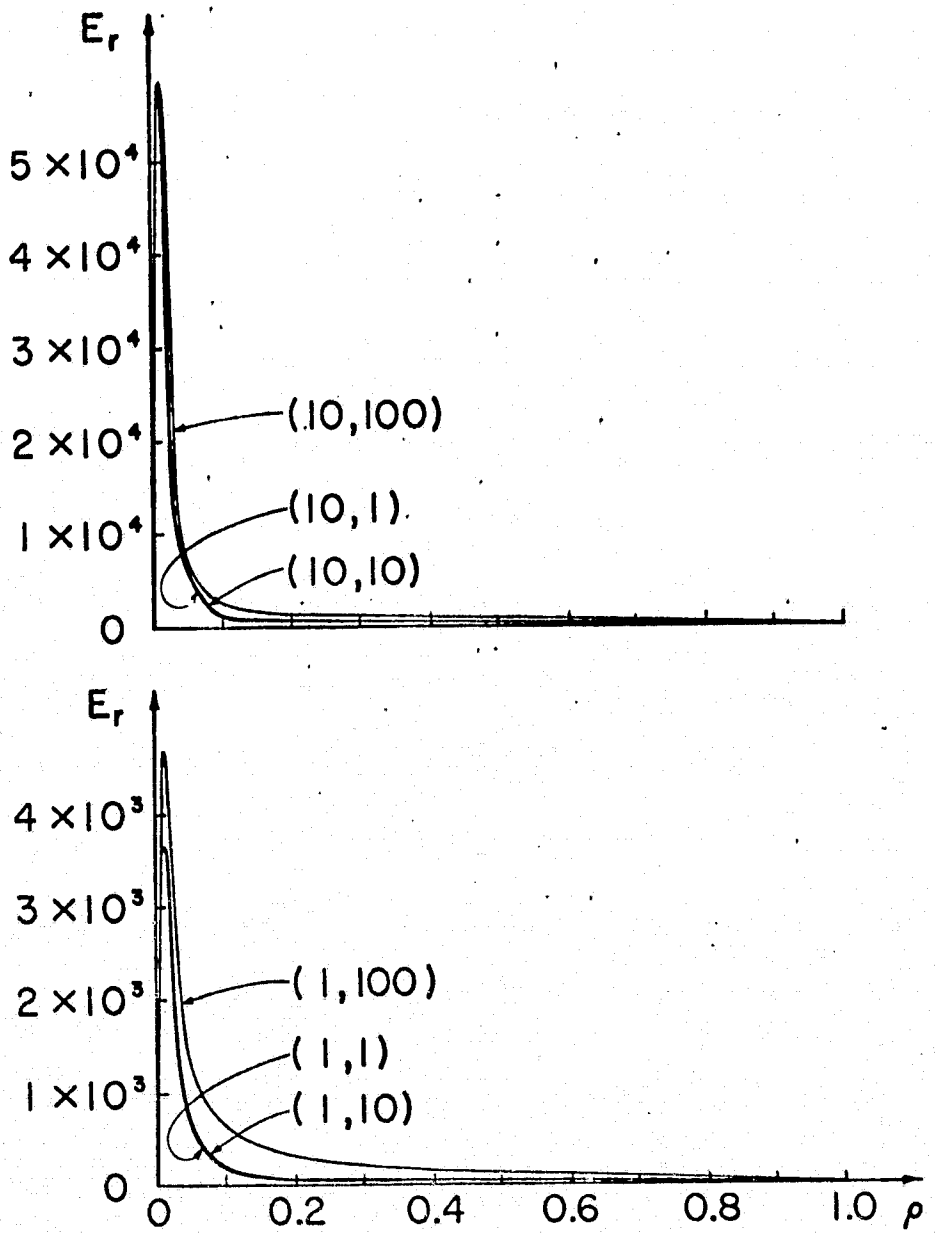

FIG. 9: $E_r(\rho,\zeta)$ versus ρ for $\zeta = -0.99$, and $(\omega\tau, H) = (1,1)$ to $(10,100)$.

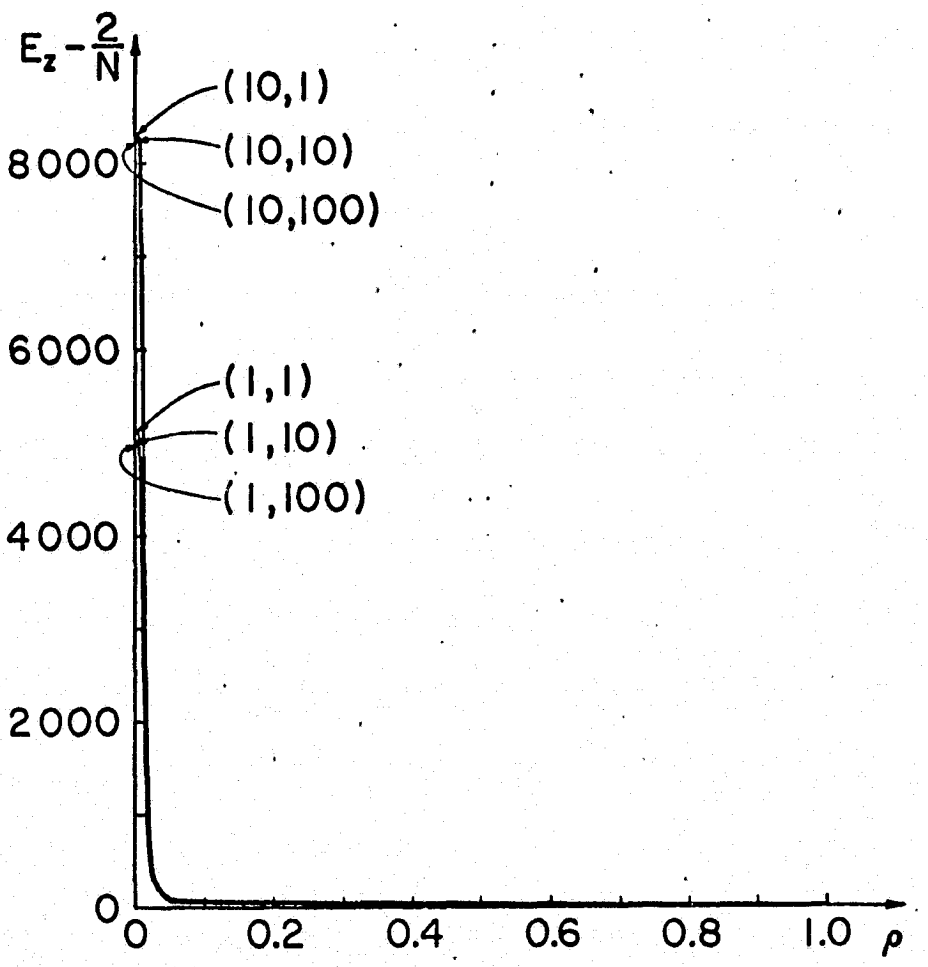

FIG. 10: $E_z(\rho,\zeta)$ versus ρ for $\zeta = -0.99$, and $(\omega\tau, H) = (1,1)$ to $(10,100)$.

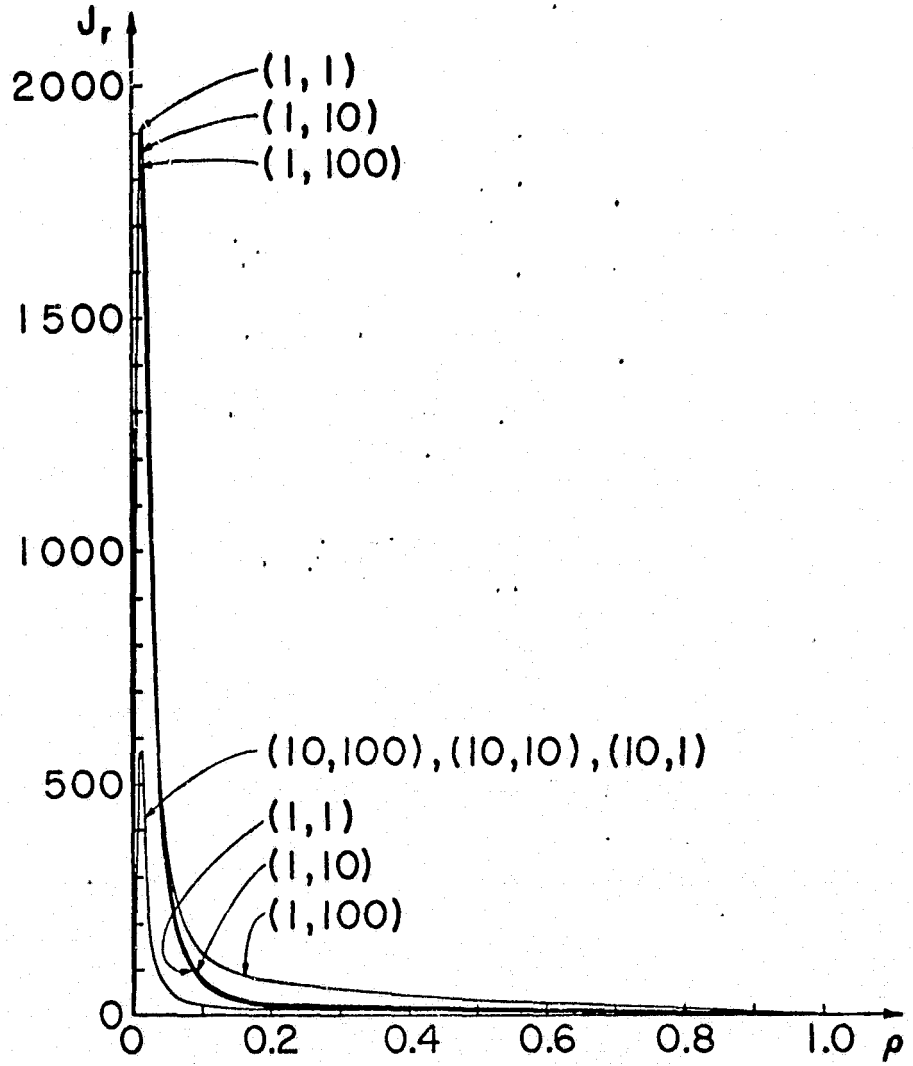

FIG. 11: $J_r(\rho,\zeta)$ versus ρ for $\zeta = -0.99$, and $(\omega\tau, H) = (1,1)$ to $(10,100)$.

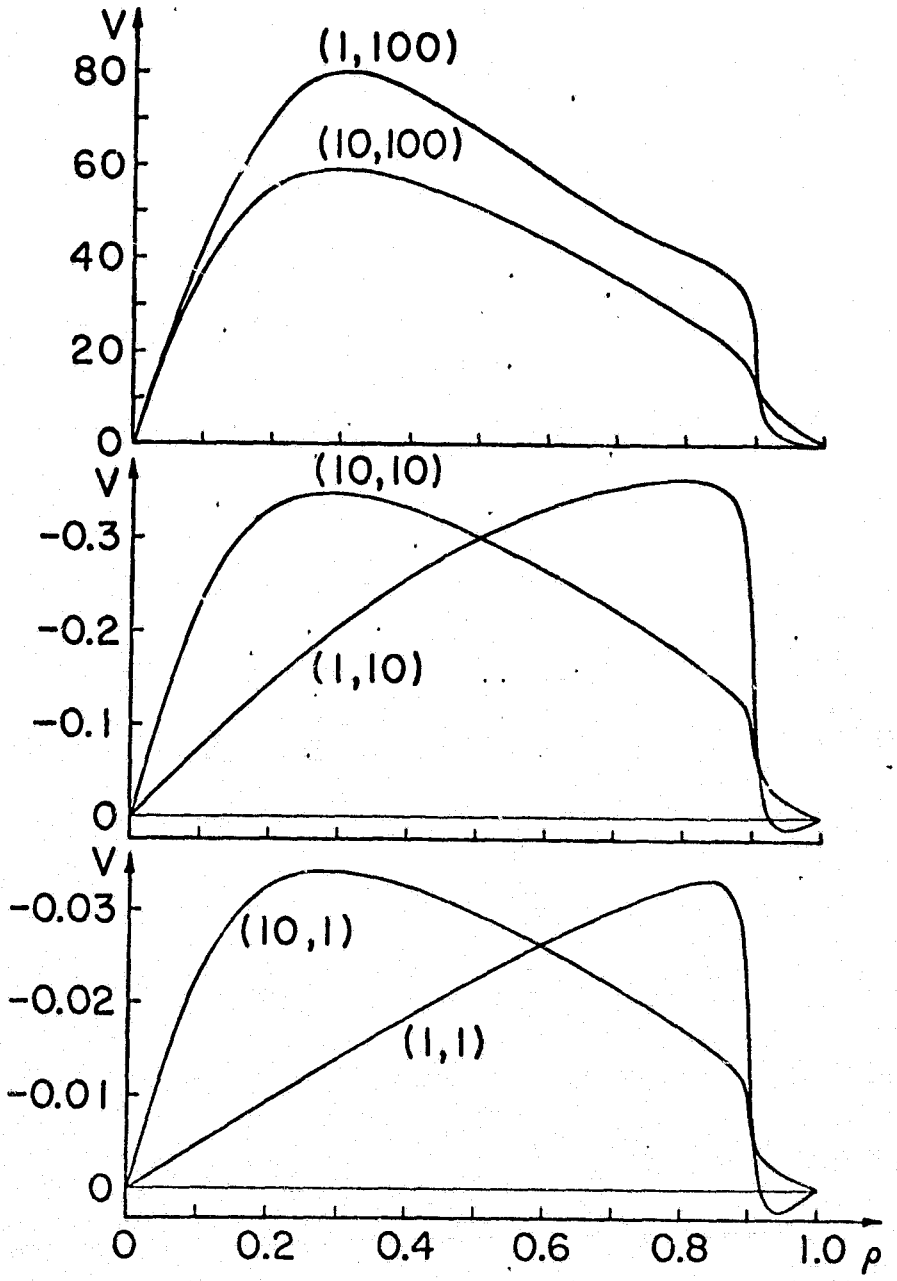

FIG. 12: $V(\rho,\zeta)$ versus ρ for $\zeta = +0.99$, and $(\omega\tau, H) = (1,1)$ to $(10,100)$.

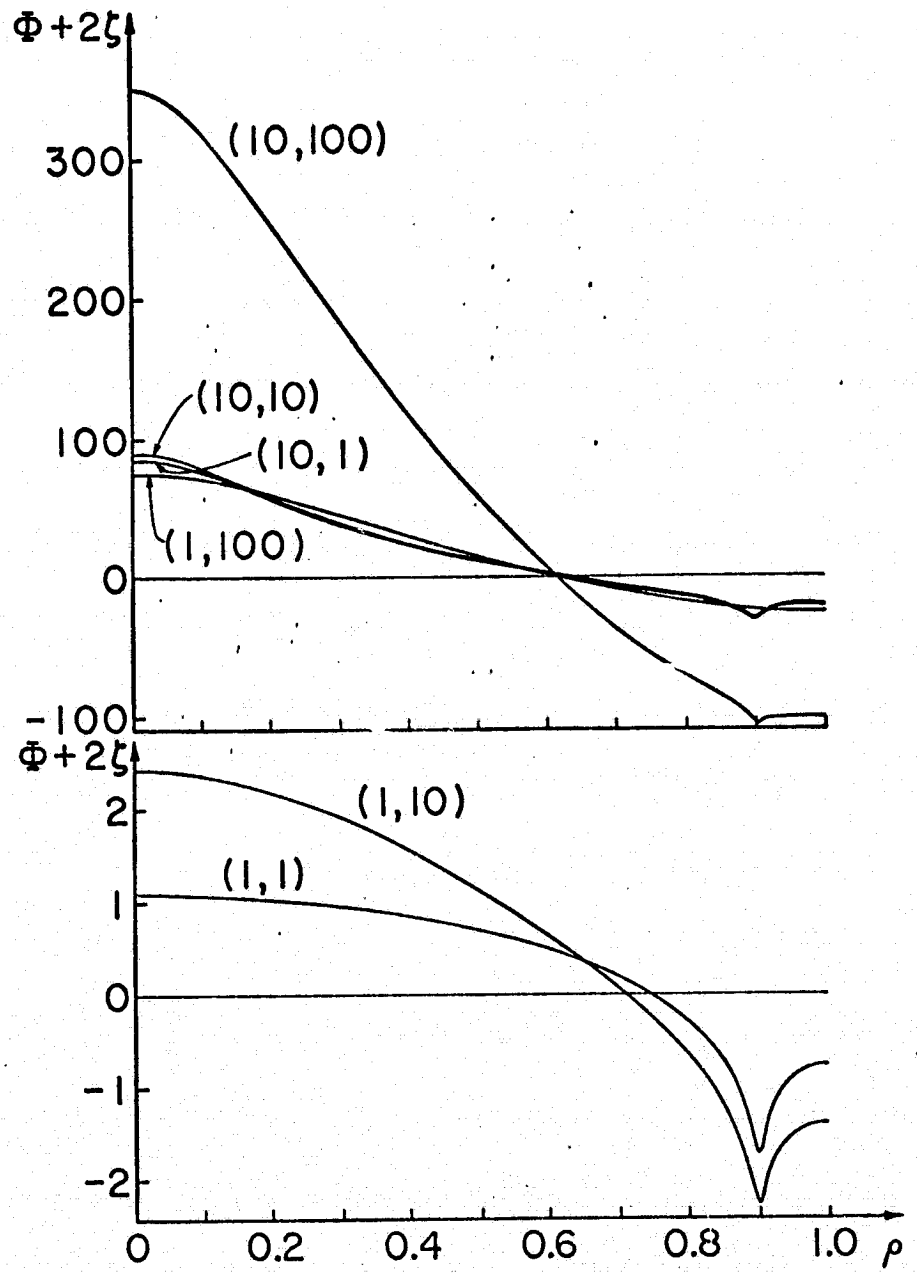

FIG. 13: $\Phi(\rho,\zeta)$ versus ρ for $\zeta = +0.99$, and $(\omega\tau, H) = (1,1)$ to $(10,100)$.

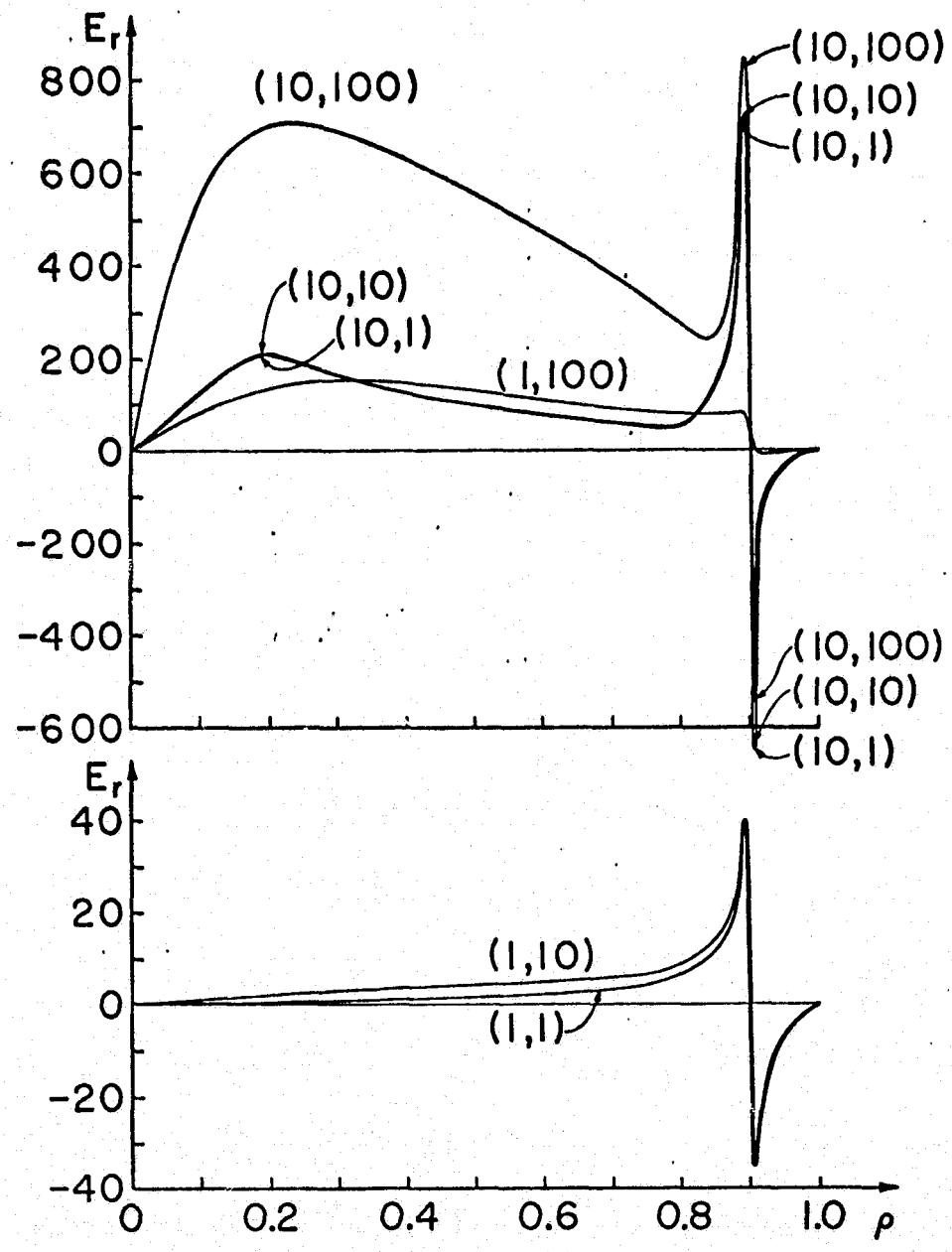

FIG: 14: $E_r(\rho,\zeta)$ versus ρ for ζ = +0.99, and ($\omega\tau$, H) = (1,1) to (10,100).

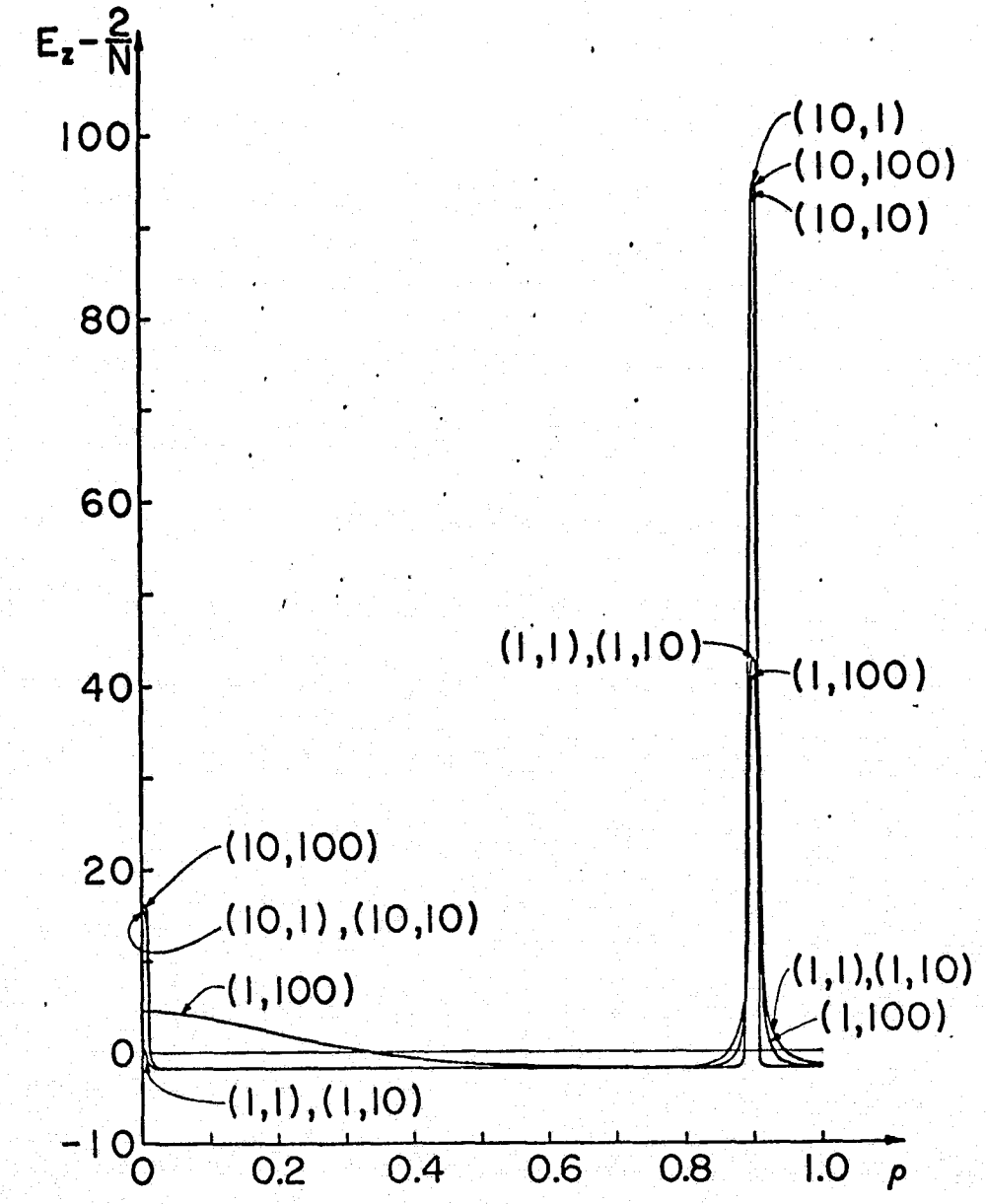

FIG. 15: $E_z(\rho,\zeta)$ versus ρ for ζ = +0.99, and ($\omega\tau$, H) = (1,1) to (10,100).

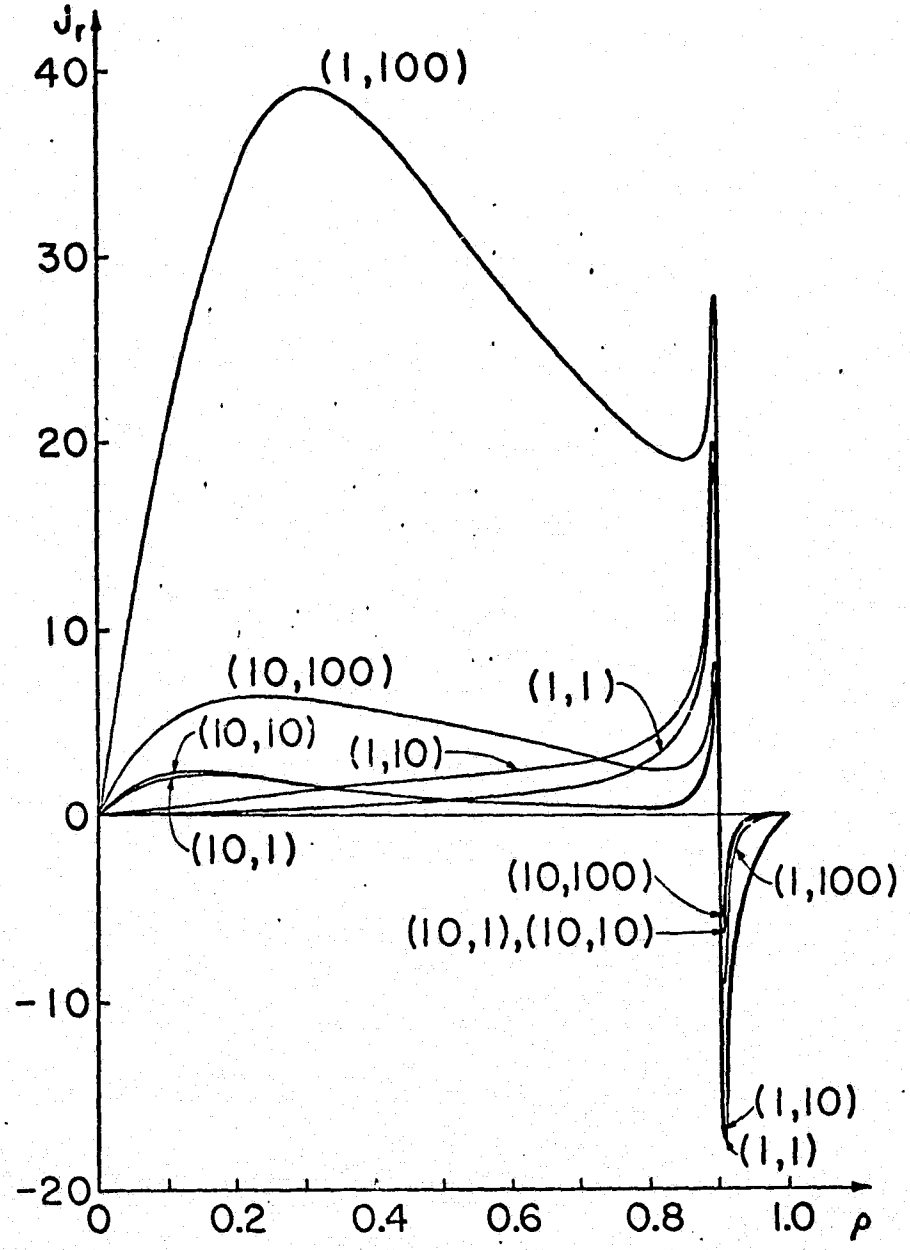

FIG. 16: $J_r(\rho,\zeta)$ versus ρ for $\zeta = +0.99$, and $(\omega\tau, H) = (1,1)$ to $(10,100)$.

DEPOSITION OF SPUTTERING PRODUCTS ON SYSTEM SURFACES*

H. E. Wilhelm and S. H. Hong
Department of Electrical Engineering
Colorado State University
Fort Collins, Colorado 80523

ABSTRACT

The boundary-value problem describing the diffusion of sputtered atoms and their deposition on the surfaces of ion propulsion systems is treated by means of a model of simple geometry. Based on an integral theorem of Weber for outer boundary-value problems with an inner cylindrical boundary, an analytical solution is derived for the density field of the sputtered atoms which involves a function which is determined by an inhomogeneous integral equation.

*) Supported by NASA

In an ideal vacuum, sputtered atoms travel undeflected along straight paths determined by their initial velocities at the point of emission. Within this free particle flow, a system surface is reached by the sputtered atoms only if it can be seen along a straight line from the emitting surface. In reality, ion propulsion systems are surrounded by a very rarefied plasma consisting of escaped beam ions, recombined ions, and electrons. For this reason, always some of the sputtered atoms will be deflected out of their initial paths by interacting through long-range forces (polarization forces) with the plasma particles so that they can reach system surfaces which are not seen along a straight line from the emitter.

Figure 1 depicts the geometry of an idealized propulsion system which exhibits an emitting plane $z = 0$, $0 \leq r \leq a$ (accelerating grid), the rocket surfaces $r = a$, $-c \leq z \leq 0$ and $z = -c$, $0 \leq r \leq a$, and the plane $z = -d$, $a \leq r \leq b$ of the solar energy collectors. All these system surfaces can be reached by the atoms sputtered from the emitter by diffusion through the rarefied plasma. The diffusion coefficient D is determined by the Vlasov equation[1] for the sputtered atoms interacting through weak long-range forces[1] with the plasma particles. In view of the mathematical difficulties associated with the solution of outer boundary-value problems for the geometry in Fig. 1, a somewhat simpler system is studied here consisting of an emitting plane ($z = 0$, $0 \leq r \leq a$), the upper rocket surface ($r = a$, $-c \leq z \leq 0$) and the plane ($z = -c$, $a \leq r \leq \infty$) of the solar energy collectors (Fig. 2). The latter is assumed to have infinite radial extension, $r_{max} = b \to \infty$, since in general $b \gg a$ and $b \gg c,d$ (Fig. 1). Within the model of Fig. 2, particle deposition on system surfaces in the space $z \leq -c$ cannot be analyzed.

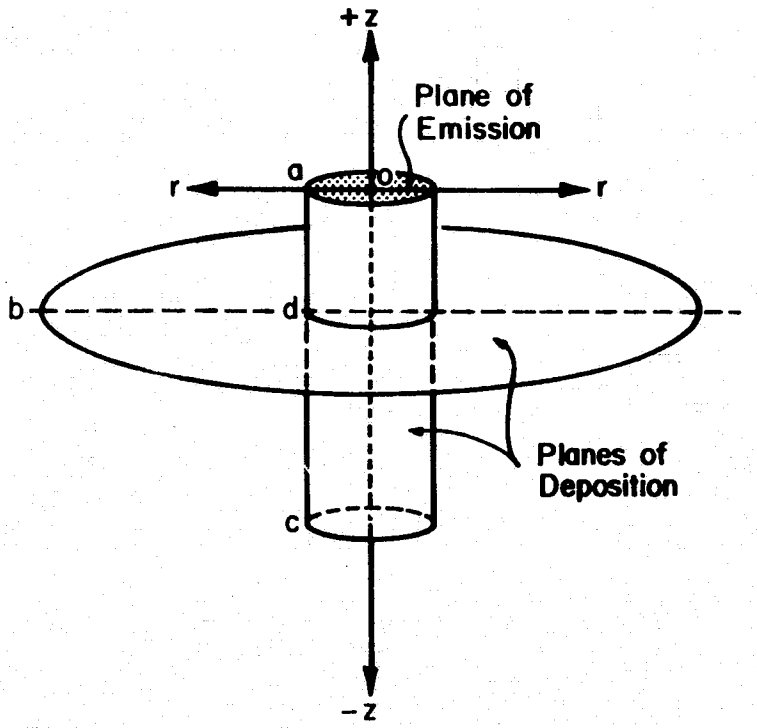

FIG.: 1

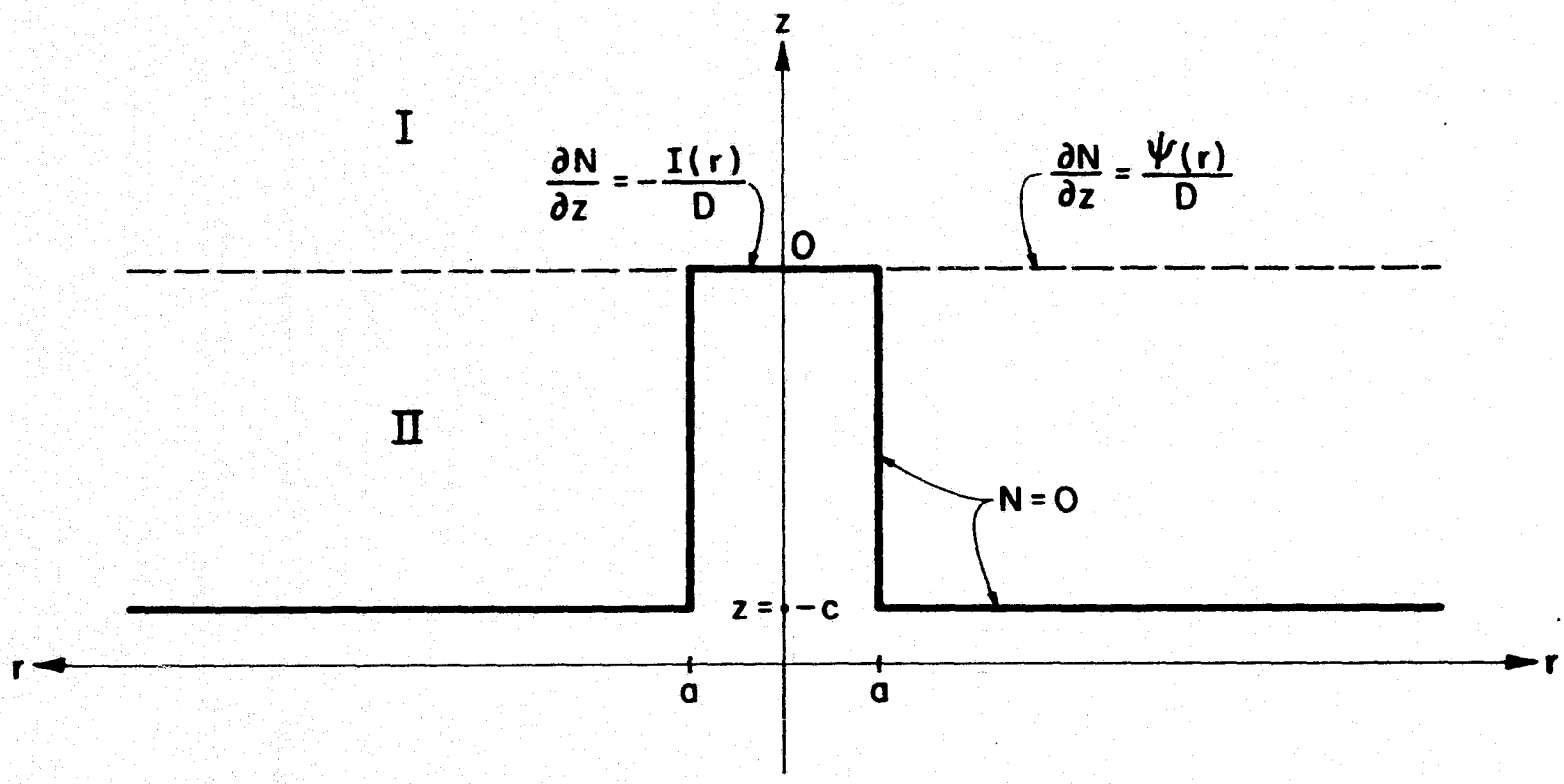
z
I
$\frac{\partial N}{\partial z} = -\frac{I(r)}{D}$
$\frac{\partial N}{\partial z} = \frac{\Psi(r)}{D}$
O
II
N = O
z = -c
r
r
a
a

Figure 2

BOUNDARY-VALUE PROBLEM

In the space $z \geq -c$, let the density of the sputtered atoms be designated by $n(r,z)$ [cm^{-3}] and the flux of emitted atoms at the emitter surface by $I(r)$ [$cm^{-3} \cdot cm\ sec^{-1}$]. In steady state, the spatial distribution $n = n(r,z)$ of sputtered atoms is determined by the boundary-value problem for the Laplace diffusion equation (Fig. 2):

$$\frac{\partial^2 n}{\partial r^2} + \frac{1}{r}\frac{\partial n}{\partial r} + \frac{\partial^2 n}{\partial z^2} = 0 \qquad (1)$$

where

$$[\partial n(r,z)/\partial z]_{z=0} = -I(r)D^{-1}, \qquad 0 \leq r \leq a \quad , \qquad (2)$$

$$n(r,z)_{r=a} = 0, \quad -c \leq z \leq 0 \quad , \qquad (3)$$

$$n(r,z)_{z=-c} = 0, \quad a \leq r \leq \infty \quad , \qquad (4)$$

and

$$n(r,z) \to 0, \qquad (r^2 + z^2) \to \infty \quad , \qquad (5)$$

are the proper and improper boundary conditions, respectively. D designates the diffusion coefficient of the sputtered atoms in the rarefied plasma which represents a spatial average, $D = \langle D(r,z) \rangle$.

The boundary conditions (3)-(4) imply that sputtered atoms arriving at the system surfaces are deposited there, i.e., do not return into the diffusion space. This assumption is at least approximately correct for nonheated surfaces as long as the number of atomic layers deposited is not too large. The fluxes $\Phi_i = -D\ \nabla_i n$ of atoms arriving at the system surfaces $r = a$, $-c \leq z \leq 0$ and $z = -c$, $a \leq r \leq \infty$ are given by (Fig. 2):

$$\Phi_r(r = a,z) = -D\ \partial n(r = a,z)/\partial r, \qquad -c \le z \le 0 \quad , \tag{6}$$

$$\Phi_z(z = -c,r) = -D\ \partial n(z = -c,r)/\partial z, \qquad a \le r \le \infty \quad , \tag{7}$$

Accordingly,

$$\dot{N}_{r=a} = -2\pi aD \int_{-c}^{0} [\partial n(r = a,z)/\partial r]dz \quad , \tag{8}$$

$$\dot{N}_{z=-c} = -2\pi D \int_{a}^{\infty} [\partial n(r,z = -c)/\partial z]rdr \quad , \tag{9}$$

are the numbers of sputtered atoms deposited per unit time on the system surfaces $r = a$, $-c \le z \le 0$ and $z = -c$, $a \le r \le \infty$, respectively. The above boundary-value problem cannot be solved directly, i.e., requires a decomposition of the space $z \ge -c$ into appropriate subregions for which the associated boundary-value problems are solvable. In this approach, the common boundary value $[\psi(r)]$ at the decomposition plane is determined by an integral equation.

Let nondimensional independent and dependent variables be introduced in accordance with:

$$\rho = r/a, \qquad 0 \le \rho \le \infty, \qquad \zeta = z/c, \qquad -1 \le \zeta \le \infty \quad , \tag{10}$$

and

$$N(\rho,\zeta) = n(r,z)/n_o, \qquad S(\rho) = I(r)/I_o \quad , \tag{11}$$

with

$$n_o \equiv cI_o/D, \qquad I_o \equiv I(r=0), \qquad \gamma \equiv c/a \quad . \tag{12}$$

The boundary-value problem defined in Eqs. (1)-(5) reads in nondimensional form:

$$\frac{\partial^2 N}{\partial \rho^2} + \frac{1}{\rho}\frac{\partial N}{\partial \rho} + \gamma^{-2}\frac{\partial^2 N}{\partial \zeta^2} = 0 \tag{13}$$

where

$$[\partial N(\rho,\zeta)/\partial\zeta]_{\zeta=0} = -S(\rho), \qquad 0 \leq \rho \leq 1 \quad , \tag{14}$$

$$N(\rho,\zeta)_{\rho=1} = 0, \qquad -1 \leq \zeta \leq 0 \quad , \tag{15}$$

$$N(\rho,\zeta)_{\zeta=-1} = 0, \qquad 1 \leq \rho \leq \infty \quad , \tag{16}$$

and

$$N(\rho,\zeta) \to 0, \qquad (\rho^2 + \zeta^2) \to \infty \quad . \tag{17}$$

In Fig. 2, the space is decomposed into the regions $I(0 \leq \rho \leq \infty,\ 0 \leq \zeta \leq \infty)$ and $II(1 \leq \rho \leq \infty,\ -1 \leq \zeta \leq 0)$. At the interface $\zeta = 0$, $1 \leq \rho \leq \infty$, the partial $\partial N(\rho,\zeta = 0)/\partial\zeta = \psi(\rho)H(\rho-1)$ is introduced as the common (unknown) boundary value $\psi(\rho)$ of the adjacent regions I and II, $1 \leq \rho \leq \infty$. Thus, the boundary-value problem in Eqs. (13)-(17) can be decomposed into boundary-value problems for the regions I and II.

I. In region I, $N \equiv N_I(\rho,\zeta)$ is described by the "regular" boundary-value problem:

$$\frac{\partial^2 N_I}{\partial\rho^2} + \frac{1}{\rho}\frac{\partial N_I}{\partial\rho} + \gamma^{-2}\frac{\partial^2 N}{\partial\zeta^2} = 0, \qquad 0 < \rho < \infty, \qquad 0 < \zeta < \infty \quad , \tag{18}$$

$$[\partial N_I(\rho,\zeta)/\partial\zeta]_{\zeta=0} = -S(\rho), \qquad 0 \leq \rho \leq 1 - 0,$$

$$= \Psi(\rho), \qquad 1 + 0 \leq \rho \leq \infty \quad , \tag{19}$$

$$N_I(\rho,\zeta) \to 0, \qquad (\rho^2 + \zeta^2) \to \infty \quad , \tag{20}$$

where

$$S(\rho=1) = \Psi(\rho=1) = 0 \tag{21}$$

for physical reasons. Since region I is the upper half of the infinite space ($0 \leq \zeta \leq \infty$), the general solution of Eqs. (18) and (20) is given by the Fourier integral,

$$N_I(\rho,\zeta) = \int_0^\infty A(k)e^{-\gamma k\zeta} J_o(k\rho)dk \quad , \qquad (22)$$

which satisfies the improper boundary condition for $\rho \to \infty$ and $\zeta \to \infty$. The Fourier amplitude $A(k)$ is determined by the boundary condition (19),

$$-\gamma \int_0^\infty A(k)\, J_o(k\rho)\, kdk = -\, S(\rho)H(1-\rho) + \Psi(\rho)H(\rho-1) \quad . \qquad (23)$$

Application of the inverse Hankel transform to Eq. (23) gives:

$$A(k) = \gamma^{-1} \int_0^1 S(\alpha)J_o(k\alpha)\alpha d\alpha - \gamma^{-1} \int_1^\infty \Psi(\alpha)J_o(k\alpha)\alpha d\alpha \quad , \qquad (24)$$

Substitution of Eq.(24) into Eq. (22) results in the solution for region I:

$$N_I(\rho,\zeta) = \gamma^{-1} \int_0^\infty dke^{-\gamma k\zeta} J_o(k\rho)\left[\int_0^1 S(\alpha)J_o(k\alpha)\alpha d\alpha - \int_1^\infty \Psi(\alpha)J_o(k\alpha)\alpha d\alpha\right],$$

$$0 \leq \rho \leq \infty, \quad 0 \leq \zeta \leq \infty \quad . \qquad (25)$$

II. In region II, $N \equiv N_{II}(\rho,\zeta)$ is described by the "outer" boundary-value problem:

$$\frac{\partial^2 N_{II}}{\partial \rho^2} + \frac{1}{\rho}\frac{\partial N_{II}}{\partial \rho} + \gamma^{-2}\frac{\partial^2 N_{II}}{\partial \zeta^2} = 0, \quad 0 < \rho < \infty, \quad -1 < \zeta < 0 \quad , \qquad (26)$$

$$[\partial N_{II}(\rho,\zeta)/\partial\zeta]_{\zeta=0} = \Psi(\rho), \qquad 1 \leq \rho \leq \infty \quad , \qquad (27)$$

$$N_{II}(\rho,\zeta)_{\rho=1} = 0, \qquad -1 < \zeta < 0 \quad , \qquad (28)$$

$$N_{II}(\rho,\zeta)_{\zeta=-1} = 0, \qquad 1 \leq \rho \leq \infty \qquad , \qquad (29)$$

$$N_{II}(\rho,\zeta) \to 0, \qquad \rho \to \infty, \qquad -1 \leq \zeta \leq 0 \qquad . \qquad (30)$$

According to Eq. (28), region II has an inner, cylindrical boundary at $\rho = 1$ where $N_{II}(\rho,\zeta)$ vanishes. For this reason, a Fourier integral representation of $N_{II}(\rho,\zeta)$ is needed for $1 \leq \rho \leq \infty$ which vanishes at $\rho = 1$. According to Weber's integral theorem, an arbitrary function $\psi(\rho)$, $a \leq \rho \leq \infty$, with $\psi(\rho = a, \infty) = 0$ satisfies the integral equation: [2,3]

$$\psi(\rho) = \int_0^\infty \frac{kdkW_k^\nu(\rho)}{J_\nu^2(ka) + Y_\nu^2(ka)} \int_a^\infty \psi(\alpha)W_k^\nu(\alpha)\alpha d\alpha, \qquad a \leq \rho \leq \infty \qquad , \qquad (31)$$

where

$$W_k^\nu(\rho) \equiv J_\nu(k\rho)Y_\nu(ka) - J_\nu(ka)Y_\nu(k\rho) \qquad , \qquad (32)$$

and $J_\nu(k\rho)$ and $Y_\nu(k\rho)$ are Bessel functions of order ν of the first and second kind, resepctively. In view of Eqs. (31)-(32), a Fourier integral solution of Eqs. (26)-(30), is sought in the form,

$$N_{II}(\rho,\zeta) = \int_0^\infty B(k)W_k(\rho)\ \sinh\gamma k(\zeta+1)\ dk \qquad , \qquad (33)$$

$$W_k(\rho) \equiv J_o(k\rho)Y_o(k) - J_o(k)Y_o(k\rho) \qquad , \qquad (34)$$

which obviously satisfies the boundary conditions (28)-(30). The Fourier amplitude $B(k)$ is determined by the boundary condition (27),

$$\gamma \int_0^\infty B(k)W_k(\rho)\ \cosh\gamma k\ kdk = \Psi(\rho), \qquad 1 \leq \rho \leq \infty \qquad , \qquad (35)$$

which gives

$$B(k) = \gamma^{-1}\cosh^{-1}\gamma k \int_1^\infty \Psi(\alpha)W_k(\alpha)\alpha d\alpha/[J_o^2(k) + Y_o^2(k)] \qquad , \qquad (36)$$

by Eq. (31). Substitution of Eq. (36) into Eq. (33) results in the solution for region II:

$$N_{II}(\rho,\zeta) = \gamma^{-1} \int_0^\infty dk \, \frac{\sinh\gamma k(\zeta+1)}{\cosh\gamma k} \cdot \frac{W_k(\rho)}{J_o^2(k)+Y_o^2(k)} \int_1^\infty \Psi(\alpha)W_k(\alpha)\alpha d\alpha,$$

$$1 \leq \rho \leq \infty, \qquad -1 \leq \zeta \leq 0 \qquad . \qquad (37)$$

The solutions $N_I(\rho,\zeta)$, Eq. (25), and $N_{II}(\rho,\zeta)$ Eq. (37), contain the yet unknown boundary-value $\Psi(\alpha)$, $1 \leq \alpha \leq \infty$. $\Psi(\alpha)$ is determined by the continuity condition at the interface of regions I and II,

$$N_I(\rho,\zeta)_{\zeta=0} = N_{II}(\rho,\zeta)_{\zeta=0}, \qquad 1 \leq \rho \leq \infty, \qquad , \qquad (38)$$

which gives

$$\int_0^\infty dk J_o(k\rho)\left[\int_0^1 S(\alpha)J_o(k\alpha)\alpha d\alpha - \int_1^\infty \Psi(\alpha)J_o(k\alpha)\alpha d\alpha\right]$$

$$= \int_0^\infty dk \, tgh\gamma k \, \frac{W_k(\rho)}{J_o^2(k)+Y_o^2(k)} \int_1^\infty \Psi(\alpha)W_k(\alpha)\alpha d\alpha, \qquad 1 \leq \rho \leq \infty \qquad . \qquad (39)$$

Eq.(39) indicates that $\Psi(\alpha)$ is determined by an inhomogeneous integral equation.[4)]

Because of the boundary conditions (19) and (27), the remaining continuity condition at the interface of regions I and II,

$$[\partial N_I(\rho,\zeta)/\partial\zeta]_{\zeta=0} = [\partial N_{II}(\rho,\zeta)/\partial\zeta]_{\zeta=0}, \qquad 1 \leq \rho \leq \infty \qquad , \qquad (40)$$

has already been satisfied. Indeed, substitution of Eqs. (25) and (37) into Eq. (40) yields

$$-\int_0^\infty kdkJ_o(k\rho)\left[\int_0^1 S(\alpha)J_o(k\alpha)\alpha d\alpha - \int_1^\infty \Psi(\alpha)J_o(k\alpha)\alpha d\alpha\right]$$

$$= \int_0^\infty kdk \frac{W_k(\rho)}{J_o^2(k)+Y_o^2(k)} \int_1^\infty \Psi(\alpha)W_k(\alpha)\alpha d\alpha, \qquad 1 \le \rho \le \infty \quad . \qquad (41)$$

Since,

$$\int_0^\infty J_o(k\rho)J_o(k\alpha)\, kdk = \delta(\alpha-\rho)/\alpha \quad , \qquad (42)$$

$$\int_0^\infty \frac{W_k(\rho)W_k(\alpha)}{J_o^2(k)+Y_o^2(k)}\, kdk = \delta(\alpha-\rho)/\alpha \quad , \qquad (43)$$

Equation (41) reduces to the expression [$\delta(\alpha-\rho)$ = Dirac function]

$$-\int_0^1 S(\alpha)\delta(\alpha-\rho)\, d\alpha + \int_1^\infty \Psi(\alpha)\delta(\alpha-\rho)d\alpha$$

$$= \int_1^\infty \Psi(\alpha)\delta(\alpha-\rho)d\alpha, \qquad 1 \le \rho \le \infty \quad , \qquad (44)$$

which gives the expected identity, $\Psi(\rho) = \Psi(\rho)$.

INTEGRAL EQUATION

By introducing the kernel $K(\alpha,\rho)$ and the source $Q(\rho)$, the integral equation in Eq. (39) can be rewritten in the convenient form:

$$\int_1^\infty \Psi(\alpha)K(\alpha,\rho)\alpha d\alpha = Q(\rho), \qquad 1 \le \rho \le \infty \quad , \qquad (45)$$

where

$$K(\alpha,\rho) \equiv \int_0^\infty \left[J_o(k\alpha)J_o(k\rho) + tgh\gamma k \frac{W_k(\alpha)W_k(\rho)}{J_o^2(k)+Y_o^2(k)}\right]dk \quad , \qquad (46)$$

$$Q(\rho) = \int_0^\infty dkJ_o(k\rho)\int_0^1 S(\alpha)J_o(k\alpha)\alpha d\alpha \quad . \qquad (47)$$

For simple particle emission distributions $S(\alpha)$, e.g., in the case of a homogeneous and a parabolic emission distributions, respectively, the source integral $Q(\rho)$ is readily evaluated,

$$Q(\rho) = \frac{2}{\pi}\,\rho\left[E\left(\frac{1}{\rho}\right) - \left(1 - \frac{1}{\rho^2}\right)K\left(\frac{1}{\rho}\right)\right], \qquad 1 \leq \rho < \infty \quad ,$$

$$\text{for } S(\alpha) = 1, \qquad 0 \leq \alpha \leq 1 \quad , \qquad (48)$$

and

$$Q(\rho) = \frac{2}{\pi}\,\rho\left\{E\left(\frac{1}{\rho}\right) - \left(1 - \frac{1}{\rho^2}\right)K\left(\frac{1}{\rho}\right) - \frac{1}{9}\left[(1 + 4\rho^2)E\left(\frac{1}{\rho}\right) - (3 + 4\rho^2)\left(1 - \frac{1}{\rho^2}\right)K\left(\frac{1}{\rho}\right)\right]\right\}$$

$$\text{for } S(\alpha) = 1 - \alpha^2, \qquad 0 \leq \alpha \leq 1 \quad , \qquad (49)$$

where $K(\frac{1}{\rho})$ and $E(\frac{1}{\rho})$ are the complete elliptic integrals of the first and second kind, respectively.

Eq. (45) reduces the deposition problem to the resolution of an integral equation for the unknown boundary-value $\Psi(\rho)$, $1 \leq \rho \leq \infty$. Once $\Psi(\rho)$ is determined, the particle distributions $N_I(\rho,\zeta)$ and $N_{II}(\rho,\zeta)$ are given by Eqs. (25) and (37), respectively. From the solutions for $N_I(\rho,\zeta)$ and $N_{II}(\rho,\zeta)$ follow then the deposition rates at the system surfaces in accordance with Eqs. (8) - (9).

Unfortunately, the resolution of the integral equation leads to considerable mathematical difficulties. Both analytical and numerical methods for solving Eq. (45) have not produced final results because of convergence and uniqueness problems, which are typical for integral equations of this type.

Citations

1. A. A. Valsov, Many-Particle Theory and its Application to Plasma Gordon & Breach, New York, 1961.

2. H. Weber, Math. Annalen 6, 154 (1973).

3. E. C. Titchmarsh, Proc. Lond. Math. Soc. 22, 15 (1923).

4. N. I. Musckelischwili, Singular Integral Equations, Akademie - Verlag, Berlin, 1965.